POLARIMETRIC SCATTERING MODEL FOR MULTILAYERED VEGETATION IN TROPICAL FOREST

CHARLES D RICHARDSON
April, 2011

SUPERVISORS:
Mr. Shashi Kumar
Dr. Y.A.Yousif Hussin

POLARIMETRIC SCATTERING MODEL FOR MULTILAYERED VEGETATION IN TROPICAL FOREST

CHARLES D RICHARDSON
Enschede, The Netherlands, April, 2011

Thesis submitted to the Faculty of Geo-Information Science and Earth Observation of the University of Twente in partial fulfilment of the requirements for the degree of Master of Science in Geo-information Science and Earth Observation.
Specialization: Geoinformatics

SUPERVISORS:
Mr. Shashi Kumar
Dr. Y.A.Yousif Hussin

THESIS ASSESSMENT BOARD:
Prof. Dr. Ir. A. Alfred Stein (Chair)
Mr. P.L.N. Raju
Dr. A. Senthil Kumar (External Examiner, National Remote Sensing Centre)

Dedicated to my loving mom and dad

ABSTRACT

This research concentrates on understanding and analyzing polarization orientation angle shift and its influence in Freeman-II model based decomposition of fully-polarimetric synthetic aperture radar data. The radar transmits and receives backscatter information from Earth objects with respect to different polarizations. These backscatter responses are assumed to have polarization information from different scattering mechanism. Covariance matrix is the sum of these different scattering mechanisms. The random orientation of objects produces a shift in polarization orientation angle which leads to miscalculation of power in different polarization and there by covariance matrix. The circular polarization method of calculating orientation angle shift utilize coherency matrix. Similarity transformation matrix has been used to convert covariance matrix into coherency matrix for application of this method. The calculated orientation shift angles were used in unitary rotation matrix for the shift compensation. This compensation results in reduction in volume scattering power and increase in double bounce power with equal amounts and invariant surface return power in covariance matrix. The equal amount of reduction and increase in power leads to unchanged total power after compensation. Freeman-II decomposition techniques utilize covariance matrix to model the information from different scatter and it preserve total power. This decomposition technique assumes polarimetric backscatter response contains information from canopy scatter as volume scattering, double bounce and surface scattering. With the help of three different components it models these responses. The reduction in volume scattering power of covariance matrix leads to reduction in modelled contribution from canopy return and increase in surface return power in different amounts. The compensation of polarization orientation angle shift takes the total modelled power close to total power of covariance matrix. ALOS PALSAR fully-polarimetric data was used for this purpose. The data supply format was single look complex and it was used to generate Multilook images. The influence of noise in Multilook images was analyzed using statistical method.

Keywords: Fully-polarimetric data, Multilook images, covariance matrix, coherency matrix, decomposition, polarization orientation angle.

ACKNOWLEDGEMENTS

First and foremost, I thank God the almighty who provided me good heath and knowledge to work for this thesis.

I am extremely thankful to my IIRS supervisor, Mr. Shashi Kumar who remained a best scientist for me with his encouraging word at times, knowledge for guiding and constant support throughout. Because of whom I am able to start this work and finish it in time.

Also I am equally thankful to my ITC supervisor, Dr. Yousif Hussin for his knowledge in guiding, patience on my English and valid suggestion in needed times.

I wish to thank Dr. Nicholas Hamm for his right help at times when I needed it the most. From times during my proposal defence his constant encouraging words and monitoring which made me to work for thesis.

I wish to thank my Head Mr. P.L.N. Raju who was happy with my performances and remains as a constant support whenever I failed.

I wish to thank the administration which provides such a nice infrastructure to work and a handy place to stay and carry forward my work.

I am very much thankful to all my friends who remain a wonderful mechanism to stir my thoughts and accept me as what I am.

I remind my bank manager Mr. Ramasamy who provided me loan with kind word to continue my study and excel in life.

A heartfelt thanks to my loving mom and dad whom send me far from home, afford my expenditure and accepts what all I told.

TABLE OF CONTENTS

LIST OF FIGURES

LIST OF TABLES

1. INTRODUCTION

The need for monitoring the forests is increasing day by day in order to understand the impacts of global climate changes on such sources. To identify forest cover changes, parameters such as biomass, basal area, tree density, tree height and stem diameter needed to be parameterized for the application of remote sensing. Many researchers have identified several techniques to estimate forest parameters using Polarimetric Synthetic Aperture Radar (PolSAR) data. These techniques cannot be applied directly on any PolSAR data since it is sensitive to environmental condition, incidence angle and under lying terrain. The increase in forest parameters such as biomass and the tree height saturates the backscatter cross section [1].

The optical portion of electromagnetic spectrum which covers the range of 0.3 to 15 Micrometer, includes both reflective and emissive portion of the spectrum and can be focused on the lens. The non-optical wavelengths often called as microwave portion encompasses wavelength from 1mm to 1.3m of the electromagnetic spectrum. These wavelengths need to be focused by the antenna rather than a lens [2]. The idea of utilizing the microwave backscatter values for understanding the terrain and use of imaging radars for estimating the above ground biomass is due to its property of imaging day and night and all weather capacity especially in case of Tropical forests where the cloud cover is continuously present.

The penetration capability of Radar waves, which is a function of wavelength, can provide information about the underlying ground structures. The level to which the radar waves are depolarized can be used to study the underlying media [3]. To understand how microwave signals interact with the forest parameters and there by assist forest parameter retrieval several scattering models have already been developed. Typically two layered models are used to model the canopy including the branches and leaves as a top layer and stem as the lower layer [4]. The Polarimetric radar uses single signal frequency with different polarization which stores more information without complexity in the construction of radar. The meaningful data or information generated by this method is more when compared to conventional SAR which operates in single, fixed–polarization for both transmitting and receiving the radio waves.

In order to preserve all the scattering data and information, polarimetric form of storing information is needed. In this regard the measured information is vector measurements which are stored in the form of scattering matrix. This scattering matrix can then be used to develop the second order derivative known as coherency or covariance matrix. These matrices can then be decomposed using various decomposition techniques to understand the power return from various layers of the forest.

But above all, improvements has to be achieved on two key parameters: resolution, which depends on the wavelength of the system, and most importantly discriminating the power return due to different media present on the under lying ground. For this purpose models based on physical concepts utilizes main propagation phenomena and substance-radiation interactions can provides information on how radar and receiving platform works. At the same time, Mathematical models can statistically describe radar character and the expected properties from them [3].

Polarimetric SAR data can also be used for generating profile of the terrain and elevations in the azimuth direction and it can be measured using the shift in the orientation angle of the polarized wave due to the azimuth tilts of the scattering plane [5], [6]. Since SAR data is sensitive to the terrain slope variation,

calibration of the acquired data for the purpose attaining improved information is needed [7]. The polarization orientation angle is the angle of rotation about the line of sight. For horizontal medium these shifts are zero and for objects which are not horizontal to the line of sight, the orientation angle produces some shift [8]. These shifts reduce the size of the physical scattering area leading to error in the power gained by the receiver [7].

Polarimetric target decomposition techniques were developed for the purpose of separating the polarimetric radar measurements into basic scattering mechanisms for the purpose of geophysical parameter inversion, terrain and target classification [8].The most popular decomposition techniques are Pauli coherent decomposition, eigenvector based decomposition developed by Cloude and Pottier [9] and an incoherent decomposition technique was developed by Freeman and Durden which utilizes three basic scattering models to model volume scattering , double bounce and surface returns [10].Later Freeman modified his model to fit the data into two basic components namely volume scattering and surface return often called as Freeman-II model [11]. In this research the main focus is on studying Freeman-II model and improving it for polarization orientation angle shift caused by the terrain which affects the model output for volume scattering power.

1.1. Motivation and problem statment

Polarimetric form of storing information is needed in order to preserve all the information from the target. Here, the scattering matrix is being stored which can be decomposed into coherency or covariance matrix with process enabling amplitude and phase. The review of decomposition theorems were explained in [9]. The classification of dominant scatterer was explained in [12].

The objective of this current study is to improve the forward scattering model developed in [11] called as Freeman-II model. This model is developed to understand the geophysical parameter present in the polarimetric radar backscatter. The Freeman-II model contains two component scattering mechanism namely volume scattering which is modelled as randomly oriented prolate spheroid and double-bounce which represent ground-trunk (stem) interaction or surface scattering modelled by a pair of orthogonal surfaces with different dielectric constants, thus derived models are shown in methodology section. The output parameters from this model are the backscatter coefficients from each of the two components and two parameters which are describing them. The backscatter contributions estimated from the model can be used to estimate the contribution of each HH, VV and HV backscatter terms and HH-VV phase difference. Without using any ground truth, Freeman-II model fits the two component scattering mechanism to the polarimetric SAR backscatter data. This model is justified as a simple model when compared with other models for forward scattering as developed in [13] , [14] where model inputs are more than outputs. This model was developed with the assumption reflection symmetry media which compensates for polarization orientation angle that yields covariance matrix reflection symmetry. This reflection symmetry condition also proves that, in scattering matrix the coefficients correlating the co-polarized and cross-polarized terms are zero [15].

The orientation angle and the ellipticity represent the polarization state of an electromagnetic wave. The orientation angle is the angle between major axis of the ellipse and the horizontal axis. The polarization orientation angle shift is the angle of rotation about the line of sight. For horizontal medium these shifts are zero and for objects which are not horizontal to the line of sight, the orientation angle produces some shift [16], [17]. These shifts results in increased cross-polarized intensity. This leads to increase in the volume scattering power and misinterpretation on the observed information [8], [18]. So these shifts must be considered when modelling scatterer. The problem with Freeman-II model is that it explicitly assumes

reflection symmetry for canopy model. The specification of Freeman for further improvement also states incorporating orientation angle consideration in canopy scattering model [11].

The problem of orientation angle was generalized by adding a new component and also modified the canopy model for different distribution of tree trunk and branches in [19] .Previous studies have revealed that Freeman-II model have been applied in airborne sensors [8], [20], [21] but no research have been done on space borne data by considering the polarization orientation angle shift. The current study aims at utilising Freeman-II decomposition technique on space borne polarimetric data.

1.2. Research Identification

1.2.1. Research Objectives

The prime focus of this study is to decompose the fully polarimetric SAR data using Freeman-II model for multilayered vegetation in tropical forest and analyze the effect of orientation of Earth objects in identifying different scattering mechanism.

1.2.2. Sub Objectives

1. To understand the influence of orientation angle shift compensation in the matrix elements for the improvement in identifying different scatterers.
2. To investigate the improvement in the result produced after orientation shift compensation by Freeman-II model.

1.3. Research Questions

1. Which polarimetric SAR element is used to represent the polarization orientation shift of tree trunks and surface scatterer?
2. What could be the effect of Signal to noise (SNR) in identifying different scatter?
3. What could be the improvement in the results produced by Freeman-II model after orientation angle shift compensation?
4. What will be the effect of de-orientation in volume scattering?
5. How to validate the improvement in the result after modification in Freeman-II model?

1.4. Background

1.4.1. Radar remote sensing

The microwave remote sensing uses 1mm to 1.3m wavelength portion of the electromagnetic spectrum. These wavelengths are needed to be focused with an antenna rather than a lens. So remote sensing done on this portion of the electromagnetic spectrum is called as radar remote sensing. Microwave remote sensing is superior over the other forms of the remote sensing techniques since they are governed by different physical parameters which basically control the other forms of electromagnetic radiations. The amount of energy backscattered from a leaf is proportional to the size shape and water content rather than the greenness [2], [22].

Electromagnetic radiations are described in terms of waves and in other as flow of small particles of energy called as photons. In the case of microwave remote sensing it is described with the concept of wave theory: frequency, wavelength, refraction, diffraction, interference, polarization and scattering. The term electromagnetic originated from the apparent property of radiation. There are different mathematical ways to represent a wave. In simplest from, using a sine or cosine curve, waves can be better explained with shape and these waves are commonly called as sinusoidal waves [22].

If we consider the z- axis as direction of propagation of the waves , x and y are used to describe the polarization, the simple wave function will be as given in [22]

$$\psi\,(z) = A\,sinkz \tag{1-1}$$

Where k is positive constant known as wave number, and kz is in units of radians and maximum value of $\psi\,(z)$ is A.

This equation only describes the shape of the wave, and the waves change in time and so it needs to be described as a function of $\psi\,(z\,,t)$. With t = 0 and position z = 0, the wave may start at any angle. Thus, additional parameter Φ_o called as initial phase needs to be added. With the angular frequency ω also added which tells about the rate of change of phase angle, the complete description of the wave as given in [22] will be

$$\psi\,(z\,,t) = A\,\sin(kz - \omega t + \Phi_o) \tag{1-2}$$

1.4.2. Complex wave description

In the context of microwave remote sensing, the wave is represented using properties of complex number. The relationship that links the sinusoidal wave and complex numbers as given in [22]

$$e^{i\theta} = \cos\theta + i\sin\theta \tag{1-3}$$

Where , $i = \sqrt{-1}$, e is Euler's constant, and θ is phase angle. The right hand side of the above equation simply relates to the vector of length A, and θ then corresponds to phase Φ, and A the amplitude. So the wave using a complex number can be represented as given in [22]

$$\psi\,(z\,,t) = A\,e^{i(\omega t - kz + \Phi_o)} = Ae^{i\Phi} = A(\cos\theta + i\,sin\theta\,) \tag{1-4}$$

1.4.3. Polarization

The electromagnetic waves have two components namely electric and magnetic waves. Polarization generally refers to the orientation of the electrical field either it could be horizontally or vertically and in microwave remote sensing it can be controlled, and the magnetic field remains always at right angle to the electrical field. Only horizontal and vertical polarization of the wave is used for remote sensing though any angle of orientation can also be possible. Hence these combination yields four possibilities of radar system HH, VV, HV, VH (H and V – represents Horizontal and vertical transmitting and receiving of the waves) [2], [22]. The wave propagation along the z –axis, with the e-vector oscillates in one perpendicular axis, either $\hat{x}$ or $\hat{y}$ as given in [23], [24]

$$E = \hat{x}E_x\cos(\mathrm{kz} - \mathrm{vt} - \Phi_1\,(r,t)) + \hat{y}E_y\,\cos(\mathrm{kz} - \mathrm{vt} - \Phi_2\,(r,t)) \tag{1-5}$$

Where E_x *and* E_y are the magnitude of $\hat{x}$ *and* $\hat{y}$ components and Φ is the phase. By substituting ψ for $(\mathrm{kz} - \mathrm{vt})$ and droping the (r,t) temporarily we get,

$$E_x = E_x\cos(\psi - \Phi_1\,) \tag{1-6}$$

$$E_y = E_y\cos(\psi + \Phi_2\,) \tag{1-7}$$

The ellipticity and orientation of the ellipse depends on the parameters$\{E_x, E_y$ and $\Phi\}$. This mode is said to be elliptically polarized. With the condition $E_x = E_y$ and $\Phi_1 - \Phi_2 = \pi/2$ makes the electromagnetic wave vector traces out circular shape and often called circularly polarization. When $\Phi_1 - \Phi_2 = 0$ the ellipse degrades into line and this polarization is called linear polarization. If there is no deterministic relationship between $\Phi_1 - \Phi_2$ then it is called unpolarized.

1.4.4. Stokes Formalism:

In the year 1852 Stokes introduced parameters to characterize the polarization form of a wave. The parameters I_o,Q,U,V are stokes parameters Figure 1-1. The Stokes parameters are then written as Stokes vector,g, such that from

$$g = \begin{bmatrix} I_o \\ Q \\ U \\ V \end{bmatrix} = \begin{bmatrix} \langle E_y^2 \rangle & + \langle E_x^2 \rangle \\ \langle E_y^2 \rangle & - \langle E_x^2 \rangle \\ 2R_e & \langle E_y E_x^* \rangle \\ 2I_m & \langle E_y E_x^* \rangle \end{bmatrix} = I_o \begin{bmatrix} 1 \\ \cos 2\psi \cos 2\chi \\ \sin 2\psi \cos 2\chi \\ \sin 2\chi \end{bmatrix} \tag{1-8}$$

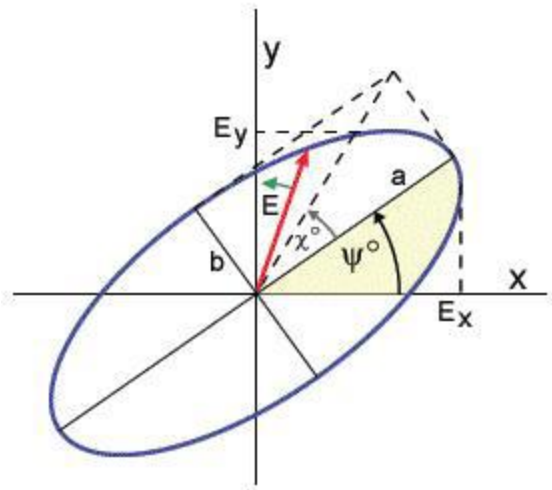

Figure 1-1: Polarization Ellipse [25]

Where ψ is orientation angle and it ranges between 0° to 180°, the χ is ellipticity angle and it ranges between -45° to 45°.The degree of ellipticity can be calculated using the angle as given in [22]

$$\chi = tan^{-1}\left(\frac{b}{a}\right) \tag{1-9}$$

Where a and b are major and minor axes respectively. Using the stokes parameters Q, U, V polarization state of any point can be represented on a Poincaré sphere of radius I_o . The Stokes vector can also be represented with other set of symbols $[I_o \quad Q \quad U \quad V]$ or $[S1 \quad S2 \quad S3 \quad S4]$ [23], [25].

In *completely polarized waves* only three parameters of stokes vector are independent and it satisfy

$$I_o^2 = \quad Q^2 + \quad U^2 + \quad V^2 \tag{1-10}$$

In *completely unpolarized waves* the magnitude of the E_x and E_y are equal and the phase angle will be random therefore,

$$Q = \quad U = \quad V = 0 \tag{1-11}$$

One important term that can be used to represent the polarization of the wave is *degree of polarization m* as given in [22],[24], [25]

$$m = \frac{\sqrt{Q^2 + U^2 + V^2}}{I_o} \tag{1-12}$$

The *degree of polarization* for a *completely polarized* wave is 1 and that for a *completely unpolarized* wave is 0 [22]. There are two measurements for a polarization to quantify, so stokes representation of polarization is not

efficient for characterizing the radar data. The alternative method used for such characterization of radar response is the Scattering matrix.

1.5. Thesis structure

The whole thesis has been organised into six chapters. The ***first chapter*** includes the major aspects of the research topic, motivation and problem statement, research objective and research questions. In the ***second chapter*** relevant topics has been reviewed. The ***third chapter*** includes the information on the materials used and the methodology followed. The ***fourth chapter*** contains the modelling theory of the decomposition technique used and the de-orientation theory. Results and discussions have been presented in the ***fifth chapter***. Finally in ***sixth chapter*** the thesis has been concluded with recommendations.

2. LITERATURE REVIEW

2.1. Introduction

The development of radar system has evolved operating from the single frequency single polarization and restricted incidence angle and low resolution to multi frequency polarimetric radar system. Due to which the investigation of radar waves with the ground features has been increased [26]. The polarization is an important property of the electromagnetic wave which influences the scattering. The polarization of an electromagnetic wave can be described using the vector form of the electromagnetic field. The electromagnetic field has two components namely the electric and magnetic fields. The electric field vibrates in the direction perpendicular to the direction of propagation of the wave and the magnetic field vibrates perpendicular to the electric field. A non fully-polarimetric radar only measures the amplitude for any arbitrary fixed polarization. Where as a fully polarimetric SAR system transmits and receives data in two orthogonal states at the same time they measures the relative phase also. In vegetation studies the choice of wavelength being chosen according to the dimension of the observed scatterers [27].

The modelling of forest mapping in matured conifers has shown that ,the backscatter values are dominated by the crown backscatter at short wavelengths, and at long wavelengths the back scatter values depends on polarization by the trunk-ground interaction dominated VV , the direct surface return dominated by HH, and the canopy backscatter dominated by HV polarization where HH, VV and HV refers to polarization of transmit and received wave [28]. The result of [29] shows that the correlation between sensitivity of the backscatter value to the biomass decreases as increase in frequency.

Frequency is an important property of radar signal since it influences the depth of penetration. The fully polarimetric radar system measures the information in the form of a scattering matrix. The scattering matrix helps in computing information about the target at any polarization since it measures the complete information of target. The scattering matrix can be expressed in two basic forms lexicographic scattering vector and Pauli basis scattering vector [29].The fundamental quantity measured by polarimetric radar can be expressed as a scattering matrix which is a 2x2 complex element, which contains the co-pol information as diagonal element and cross-pol information as off diagonal elements [22]. The scattering matrix can be used to represent the relationship between the incident and the scattered wave field [25].In general the scattering matrix can be used to represent the state of interaction of the electromagnetic wave with the target. The target can either be pure or mixed and in most cases the targets are mixed. The causes for mixed state can be the motion of the target of radar platform. Mostly the response will be in mixed state only .The polarization response created by the pure target is completely polarized wave and that of by the mixed targets are partially polarized wave [30]. Generally the scattering matrix contains seven independent parameters out of which four are amplitude and three are phase. If the reciprocity assumption is applied, $S_{HV} = S_{VH}$ then only five independent parameters will be present namely three amplitude and two phase elements [24].

2.2. Coherent decomposition

The scattering matrix can be effectively decomposed to understand the pure target (Coherent targets). But in the real scenario the radar cross section which is the effective area of reflectance contains coherent sum of scatterers since the radar resolution cell size always greater than the wavelength of the radar system [25].Partially polarized waves cannot be characterized using a scattering matrix. Thus the second order derivatives of the scattering matrix namely covariance matrix or the coherency matrix can be used to characterize it [24].

The covariance matrix represents the average properties of a group of resolution cells. It can be generated by multiplying the lexicographic scattering vector form of scattering matrix with its transpose. The coherency matrix can be generated by multiplying the Pauli basis scattering vector to its transpose [31]. However, the covariance and coherency matrices are having similar properties as both are hermitian positive semi definite and have same Eigen values. These two matrices are related to each other by unitary similarity transformation matrix [9]. The mathematical description of the mixed target state is given by these matrices. These matrices provide the information about the geometrical characteristics of the object that is sensed by radar. Therefore these matrices can be decomposed into different components which actually represent the underlying scatter type [30].

The polarimetric information from a target can have the geometrical structure or physical characteristics of target. The polarimetric target decomposition theorem expresses the average mechanism as a sum of independent mechanism. These theorems explore the phase information contained in the data and can be used for classification or target recognition. The polarimetric SAR data are coherent by their operating principle, but the incoherent method is chosen for the purpose of decomposition and applying statistical methods. There are two main types of decomposition techniques available currently. They are coherent and incoherent decomposition. The method which deals with the scattering matrix is called coherent decomposition and the method which deals the covariance or coherency matrices is called incoherent decomposition [32].

The polarimetric decomposition and target identification are widely used for image interpretation, classification and there by understanding the polarimetric signature present in the data. The targets under consideration require multivariate statistical descriptors to differentiate the combination of coherent speckle noise and random vector scattering effects from surface, double bounce or volume. For such targets we need to generate a dominant scattering mechanism in order to classify or inversion of scattering data [9].Polarimetric Decomposition is a method to parameterize the contents of a polarimetric data. The idea behind the decomposition is that the polarimetric responses are composed of idealized scatterers. Based on this idea using different scatters, different researchers have developed techniques to decompose the data into responses from different media. A physical based approach was developed by Freeman and Durden which characterize the response in a polarimetric data using three simple scattering mechanisms using varying combination of dihedral for double bounce, spherical scattering for direct surface returns and depolarized signals that corresponds to volume scattering from vegetation [22].

Various theoretical models have been developed for the purpose of characterising the electromagnetic wave scattering properties of forest canopy. The radiative transfer theory has been applied to study the scattering from the vegetation. The radiative transfer theory assumes that the particles scatter independently. A model was developed in [33] which modelled the canopy as a two layer component above rough surface. The leaves are modelled as randomly oriented and distributed discs and needles for deciduous forest and coniferous forest respectively. The branches are then modelled using finite length dielectric cylinders. The lower layer is modelled as randomly positioned vertical cylinders above a rough

surface. A complete model including the leaves, branches and the trunks was developed. Only one polarization (HH) has been considered in this model. The backscatter coefficient from such model is obtained by applying first order solution of the radiative transfer equation. However such equations can be proved invalid where the randomness of the relative positions is less than the radar wavelength [34].The resolution cell is an addition of response from dominant scatterer and the clutter. In case if there is no dominant scatter, the response will be simply speckle noise (clutter) in (Figure 2-1).

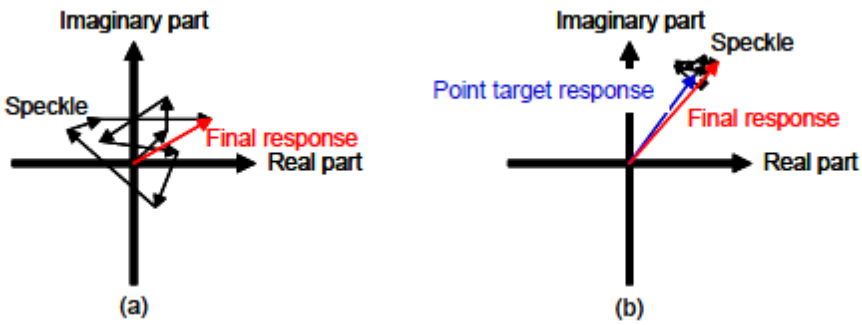

Figure 2-1: Coherent response of a given resolution cell (a) Without a dominant scatterer, (b) With a dominant scatterer [37]

The coherent decomposition techniques will preserve the amplitude and phase. Pauli format of decomposing the radar data is known widely as coherent decomposition since it can decompose only the coherent scatterers [9], [35] . In this method it decomposes the data using the complex quantity representing the single bounce, double bounce and the volume scattering component [32]. Krogager decomposition is another type of coherent decomposition, which models the scattering matrix with combination of sphere, helix and a diplane. It uses the circular polarization basis [36].

Normally coherent decomposition theorem can be exposed due to the presence of speckle. It cannot be effectively applied in the case of natural random targets like vegetation [25], [37]. In addition to this, targets with significant natural variability need incoherent way of decomposition [9], [38].

2.3. Incoherent decomposition

Among certain decomposition techniques Eigen value based technique has gained more popularity since it additionally provides entropy and average target scattering mechanism. This decomposition position technique works on the basis of Eigen value analysis of the coherency matrix. The Eigen value is basis invariant and also these values provide statistical independence between target vectors. The advantage of using this decomposition technique is that, it provides a formal connection between the signal processing theory and the noise can be estimated from the covariance matrix [9],[39].

The coherency matrix itself contains enough statistical independence between scattering mechanism for natural target SAR images. Thus any additional information through the Eigen value analysis is not necessary and also implementation of this technique using software is difficult and the processing is time consuming. The analysis using the additional information of entropy and alpha images shows no better performances to show the values of buildings not aligned along the track as double bounces [40].

New method has been developed to idealize the scattering vector model for the representation of coherent target scattering, which is generated by projecting the kennaugh-Huynen scattering matrix into Pauli basis, there by developing a concept of polarization basis invariant in terms of five independent

target scattering parameters. This new method leads to a unique way of decomposing the partially coherent target scattering [38]. However the presence of speckle leads to biased parameterization. The advantages of using roll invariant decomposition will stand valid only for targets of same scattering mechanism but with different orientation angle, and it can also have the problem of misclassifying the objects in other classes [40].

2.4. Durden Model:

L-band microwave scattering model was developed for understanding microwave scattering from forests, to simulate the microwave backscatter value, assumes uniform distribution of scatterers. The branches as upper layer are modelled using randomly oriented finite dielectric cylinders. The lower layer was modelled as layer containing only tree trunks using randomly oriented vertical dielectric cylinders and extended into the upper layer. The ground was considered as brag rough surface with first order small perturbation model. The contribution from ground, double bounce was also included [13].

A modified model of Durden was developed using two layers over a rough surface. The upper layer was modelled using vertical dielectric cylinders, randomly oriented cylinders and needles to model the trunks, branches and leaves respectively [14].Various other models were developed for the purpose of decomposition or simulation of microwave backscatter data [41], [42].Basic disadvantages of these models are some of the models needs more input parameters than the output by itself [13], [14], [43]. Some more models are mathematically based that cannot be used to relate physical scattering models. In physical models the scattering is based on the interaction of electromagnetic wave with the forest parameters [10], [44].

2.5. Freeman and Durden Model:

It is a physically based, three component scattering mechanism based model developed to fit the PolSAR data without utilizing any ground data. The three components included in the model are canopy using randomly oriented dipoles, Bragg surface scatter and double-bounce scattering mechanism. This model fit approach has equal number of inputs as basic scattering mechanisms and their contribution as output. Linking of these parameters to the biomass was analyzed in [45], [28]. This model was used in a classification scheme and it has been shown that this model is generic enough to apply for any sought of terrain when compared with models using Eigen value decomposition and Roll invariant parameters [10], [40].

2.6. Freeman-II Model:

Freeman-II model is basically an extension of Freeman and Durden model. Two simple scattering mechanisms namely canopy scatter from a reciprocal medium with azimuthal symmetry and double bounce scatter from a pair of orthogonal surfaces with different dielectric constants or a Bragg scatter from a moderately rough surface which is seen through vertically oriented scatter layer, is used to model the data. This model is developed to analyze the response from the tropical forest. This model is a simplification of more complicated scattering models.

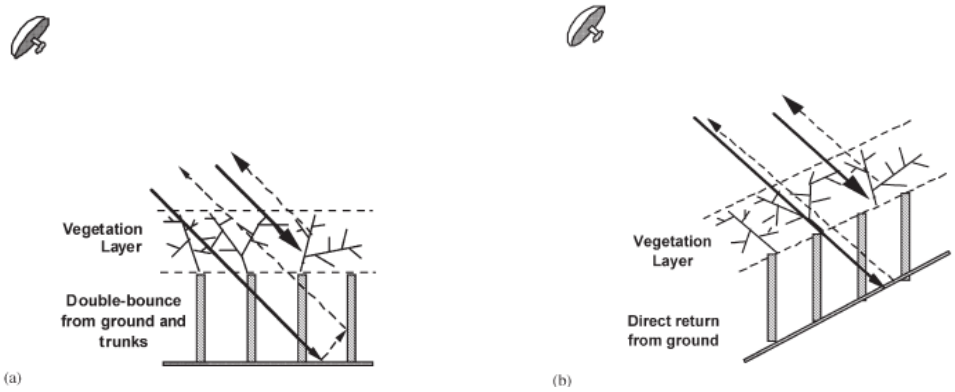

Figure 2-2: Two component scattering from the forest showing the main contributors as (a) vegetation layer scattering and double-bounce from ground-trunk interaction (b) vegetation layer scattering and direct ground return [11]

The scattering mechanism components included in this model is randomly oriented prolate spheroids and a surface scatter from the ground or double-bounce from ground trunk interaction. The Freeman-II model canopy scatter mechanism has the freedom to model large variety of canopy over the Freeman and Durden model [11]. (Figure 2-2) shows the two main contributors for the Freeman-II model.

2.6.1. Demerits in Freeman model:

The important application of the polarimetric decomposition is to extract physical information about the underlying object and these values can also be used for successful scattering parameter inversion [9]. The penetration capability of SAR signals was studied and raises with the results of certain scattering contribution could carry details about environmental evolution. The studies concluded that possible effect of topographic shift could play a role in the information gained [46], [47].The model based Freeman-II model which deals with the statistical independence of the obtained component cross-polarization generated by depolarization and the model, does not account for the terrain induced depolarization and wrongly interprets the power as volume scattering power [18].This terrain shift can also reduce the effective area of the backscatter and results in low backscattered power [7],[48].

2.7. Yamaguchi Decomposition technique:

In an attempt to extend the three components of decomposition technique developed by Freeman and Durden, the study was carried out by including Helix component as a fourth component in addition to three component scattering mechanism. This decomposition technique employs helix as the fourth component provided the PolSAR image include urban area information, whereas the Helix component is negligible in the case of naturally occurring scatterers. The Freeman-II model uses the assumption of reflection symmetry and calculates the contribution from each scattering mechanism, by adding the helical component the reflection symmetry assumption of the covariance matrix is omitted in Yamaguchi model and it makes the reflection symmetry matrix reflection asymmetry and calculates the contribution from each mechanism [19] ,[49].

2.8. MultiLooking:

The Multilooksetup generally reduces the effect of speckle in radar images. Multilooksetup generally shows the degree of averaging of SAR measurements during data formatting. The process of Multilook is done in the frequency domain. It is a process of compressing range or azimuth resolution leading to better

visibility for features in the images. Multilook helps not only in reducing the effect of the speckle but it also makes the computation easy [50], [51].

2.9. Orientation angle

The radar cross section is an effective measure in imaging radar since the backscattered energy is calculated from the effective scattering pixel area. The scattering matrices are generated by the backscattered power from a unit area. In imaging radar system the orientation of the effective backscattering area is an important property to consider. The polarization orientation angle shift affects the radar cross section which accounts for effective scattering pixel area [7]. The analysis for the effect of orientation angle shift of the polarization due to terrain azimuth and range slopes was carried in [5], [20], [52],[53]. The polarization orientation shift can be due to radar look angle and also by range and azimuth slope and the diagram shows the radar imaging geometry in Figure 2-3 [16], [17].

New technique has been adopted for the compensation of the terrain slopes which induces the polarization orientation angle shift. The circular polarization algorithm for the calculation of shift in orientation angle, also utilizes the Digital Elevation Model (DEM) generated from the interferogram and conclude that, the circular polarization algorithm is computationally efficient [20]. In the advent of developing a reliable technique for the estimation of polarization orientation angle shift in PolSAR data due to terrain slopes, a method using circular polarization covariance matrix has been generated. The robustness of the algorithm has been shown with assumption of reflection symmetry [52].

A technique has been developed for directly sensing terrain surface slopes, using the origin shift in orientation angle in the signature. The L and P-band radar data were used for the analysis of the terrain. Since the PolSAR data is effective to terrain slopes, the study concludes that, topographic slopes could affect the geophysical parameters extraction. The shift in signature of the polarization orientation angle has been utilized for the calculation of polarization orientation angle shift in [54].

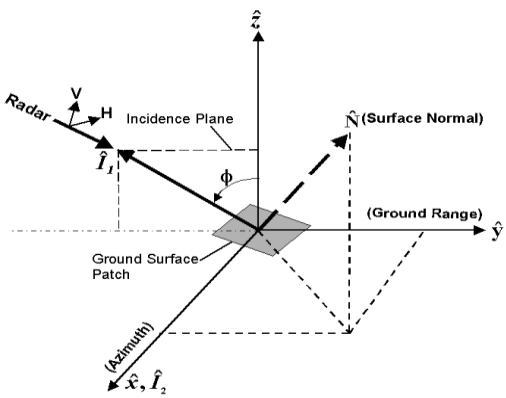

Figure 2-3: A schematic diagram of the radar imaging geometry which relates the orientation angle to ground slopes [20] .

In an effort to remove the terrain slope induced polarimetric shift an algorithm was proposed which rotates the covariance matrix until it achieves the maximum azimuthal symmetry condition. The method shows that the terms which are associated with the asymmetry are reduced to near-zero. Any additional data such as digital elevation model to make corrections is not required [55]. The effects of azimuthal slope related orientation angle change in covariance matrix has been analyzed. The estimation of orientation angle was carried out using circular polarization covariance matrix elements [56].

The circular polarization algorithm for calculating the orientation angle adopted in. [8],[16], [20], [52] for calculation of polarization orientation angle shift induced by the terrain slopes is

$$\eta = \frac{1}{4}\left[\tan^{-1}\left(\frac{-4\mathrm{Re}(\langle(S_{HH} - S_{vv})S^{*}{}_{HV}\rangle)}{-\langle|S_{HH} - S_{VV}|^{2}\rangle + 4\langle|S_{HV}|^{2}\rangle}\right) + \Pi\right]$$

$$\theta = \begin{cases} \eta & if\ \eta \leq \frac{\pi}{4} \\ \eta - \frac{\pi}{2} & if\ \eta > \frac{\pi}{4} \end{cases}$$

For the purpose of compensation of the data after the effective analysis of the shift in orientation angle the unitary rotation matrix given in [8],[20], [52], [57] has to be used for compensation of the shift.

$$U = \begin{bmatrix} 1 & 0 & 0 \\ 0 & \cos 2\theta & sin2\theta \\ 0 & -sin2\theta & cos2\theta \end{bmatrix}$$

The process of rotation of target to the negative of the obtained orientation angle is indirectly means by rotation of polarization base along the line of sight for the shift [57]. The orientation angle compensation on the image can be validated through a simple assumption; the polarization orientation response from different parts of the image should be same. This method has been adopted for the purpose of orientation compensation validation for Faraday rotation which is not accounted in this study [58], [59].

3. MATERIALS AND METHODOLOGY:

This section is divided into two parts, the first explaining with the data source and followed by the detailed research method which has been adopted in this study. The method include the data supply format and the projection of data in lexicographic and the Pauli format for the purpose of generation of coherency and covariance matrix generation. The coherency matrix elements have been utilized for the purpose of calculation of polarization orientation angle shift induced by the terrain. The covariance matrix has been used an input parameter for the Freeman-II model for the purpose of generating volume scattering and surface scattering power. The calculated polarization orientation angle shift has been utilized to compensate the data for the effect of terrain induced polarization orientation angle shifts.

3.1. Data Used

Table 1: Details of data used in the study

Description	Data 1	Data 2	Data 3
Mission/Sensor	ALOS/PALSAR	ALOS/PALSAR	ALOS/PALSAR
Date	5/22/2009	11/22/2009	5/25/2010
Polarization	HH+HV+VV+VH	HH+HV+VV+VH	HH+HV+VV+VH
Orbit number	17718	20402	23086
Path number	519	519	519
Row number	60	60	60
Mode	Ascending	Ascending	Ascending
Centre latitude	30.135531	30.13654	30.137188
Centre longitude	78.128464	78.143318	78.153453
Incidence angle	25.8	25.8	25.8

3.1.1. Characteristics of the ALOS PALSAR data used

The characteristics of ALOS PALSAR data used are detailed below. The supply format of the data was in single look complex (SLC) fully polarimetric. Later the data has been converted into Multilooksetup (MLC) by adding pixels from the range direction and azimuth direction to make a square pixel.

Product Name	Phased Array L-band synthetic Aperture Radar
Pixel Spacing in range direction (m) of SLC	9.368514
Pixel Spacing Azimuth direction (m) of SLC	3.792661
Ground resolution (m)	25
Range Ground pixel resolution (m)	21.525378
Azimuth Ground pixel resolution (m)	3.792661
Swath width (Km)	30
Wavelength (cm)	23.5
Range Pixel Spacing (m) of MLC	21.525378
Azimuth Pixel Spacing (m) of MLC	22.755966

3.2. Study area

The location of the data obtained is shown with Google image which was accessed on 17th march 2011.

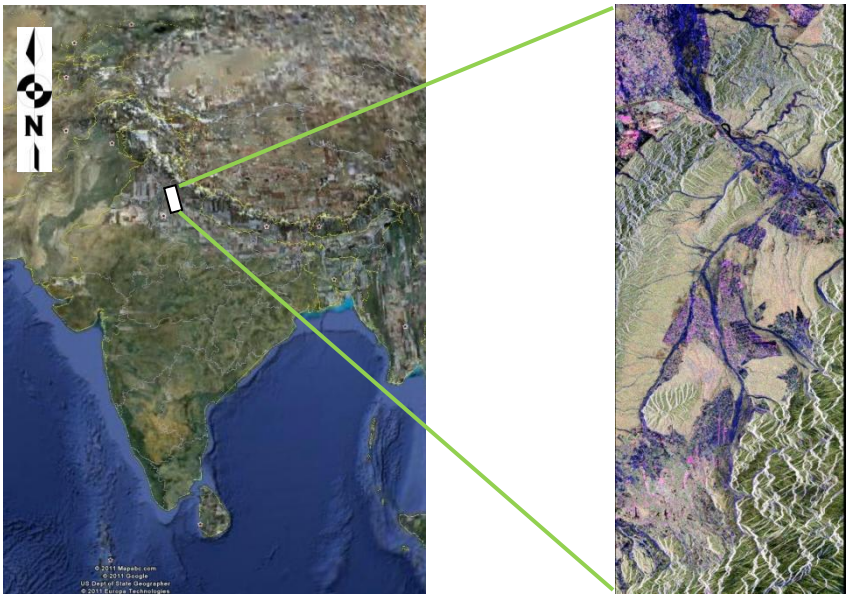

(a) (b)

Figure 3-1: Google image showing location of data site (b) The image of data in Multilooksetup

The data used in this thesis is captured over Uttarkhand state which is in the northern part of India. In terms of geographic lat/long the area extends from 30.4148920 N to 30.4597220 N and 77.9407350 E to 78.2013470 E. It includes dense forests from those regions. The dense forest consists of mixed tree species. The main types of trees species are *Eucalyptus hybrid* locally called as *Eucalyptus, Mallotus philippensis* locally called as *Rohini*, *Trewia nudifloralocally* locally called as *Gutel, Tectona grandislocally* locally called as *Teak* and *Dalbergia sissoolocally* locally called as *Sheesham*. The data includes information from foot hills of Himalayan ranges. Thus the data captured over this region helps this study by containing information from forest as well as the rugged terrain.

3.3. Method adopted

The following section explains the steps adopted in the method in this research. It also includes the data supply format and the creation of Multilooksetup which is the first two steps in the methodology Figure 3-1.

3.3.1. Multilook setup

The supply format of ALOS PALSAR is in single look complex mode fully polarimetric data. The single look complex image includes information for all the polarizations. The radar antenna receives the transmitted pulses backscattered from the ground. For a transmitted signal, if the antenna receives two responses from different objects on the ground, then the time difference will be used to determine the distance between objects. This distance in the sensor look direction is called as slant range. Due to the slant range distortion the objects in the near range appears compressive. The data compression also results in different resolution in azimuth and range direction. The effect of slant range can be removed by converting the slant range into ground range. The ground range is the horizontal distance measured along the ground for each corresponding points measured in the slant range. The conversion of slant range to ground range is done with the help of trigonometry. The process of Multilooksetup enables the creation of ground range images by adding number of looks from the azimuth direction. The data provided contains a range resolution of 21m and azimuth resolution of 3m approximately as shown in

characteristics. After the conversion of slant range to ground range the single look complex image is used to generate the Multilooksetup. The number of looks considered in the azimuth direction to make it a square pixel is 6 with keeping number of pixels in the range direction 1. By doing so, the resolution in the azimuth direction increases from 3m to 22m approximately and enables the creation of multi look image with equal range and azimuth resolution.

3.3.2. Covariance Matrix

The scattering matrix is the form in which the PolSAR data is stored. The scattering matrix can be expressed in lexicographic basis or Pauli basis. One of the second order derivatives of this matrix is covariance matrix which is created by expressing the scattering matrix in lexicographic format. The data has been expressed in this basis for the creation of the covariance matrix is given in equation (3-2). The resultant covariance matrix is a 3x3 matrix with the reciprocal assumption.

3.3.3. Decomposition

The created covariance matrix was used as input for Freeman-II model to decompose the data for different scattering mechanism. The Freeman-II decomposition assumes reflection symmetry condition and it use only five elements out of nine elements in the covariance matrix. Hundred (100) random samples have been selected in order to identify the difference after compensation from the model output.

3.3.4. Orientation angle calculation and conversion of covariance matrix to coherency matrix

The coherency matrix has been generated for the calculation of polarization orientation angle shift. The coherency matrix is another second order derivative of the scattering matrix provided the scattering matrix being expressed in the Pauli basis. In this study, since the covariance matrix and coherency matrix are related to each other, a similarity transformation matrix was used to generate the coherency matrix from covariance matrix as shown in equation (3-18). The generated coherency matrix is also a 3x3 matrix. The coherency matrix elements were used for the calculation of polarization orientation angle shift as give in equation (3-15). The same similarity transformation matrix has been used for the conversion of coherency matrix into covariance matrix.

3.3.5. Compensation for orientation angle shift

The negative of the calculated orientation angle has been used in a unitary rotation matrix for data compensation as given in equation (3-19). The data has been validated for the compensation by applying the equation (3-15) assuming it should not yield any shift.

3.3.6. Analysis of roll-invariant element

Hundred (100) random samples from the each matrix elements before and after compensation will be selected. The selected samples need to be plotted to identify the changes in the matrix elements. Though the Freeman-II decomposition uses only five elements for decomposition with reflection symmetry assumption out of total nine matrix elements all the elements are considered in order to analyse the effect of orientation angle compensation. The coherency matrix elements have also been considered for this analysis since the calculation of orientation angle and compensation is being done on the coherency matrix.

After the analysis for the changes in the matrix elements, the effect of these changes in the Freeman-II model will be analysed by applying this decomposition technique in the compensated matrix. Hundred (100) random samples will be selected and plots between those selected samples before and after compensation will be generated. The results of these plots will be analysed in results and discussion section. The methodological work flow has been shown in Figure 3-1.

3.3.7. Methodological work flow

The Figures 3-2 shows the procedure to generate different scattering products, to calculate polarisation orientation angle shift of electromagnetic wave. It also shows the procedure to compensate the data for the shift and analysis of compensation in the generated scattering products.

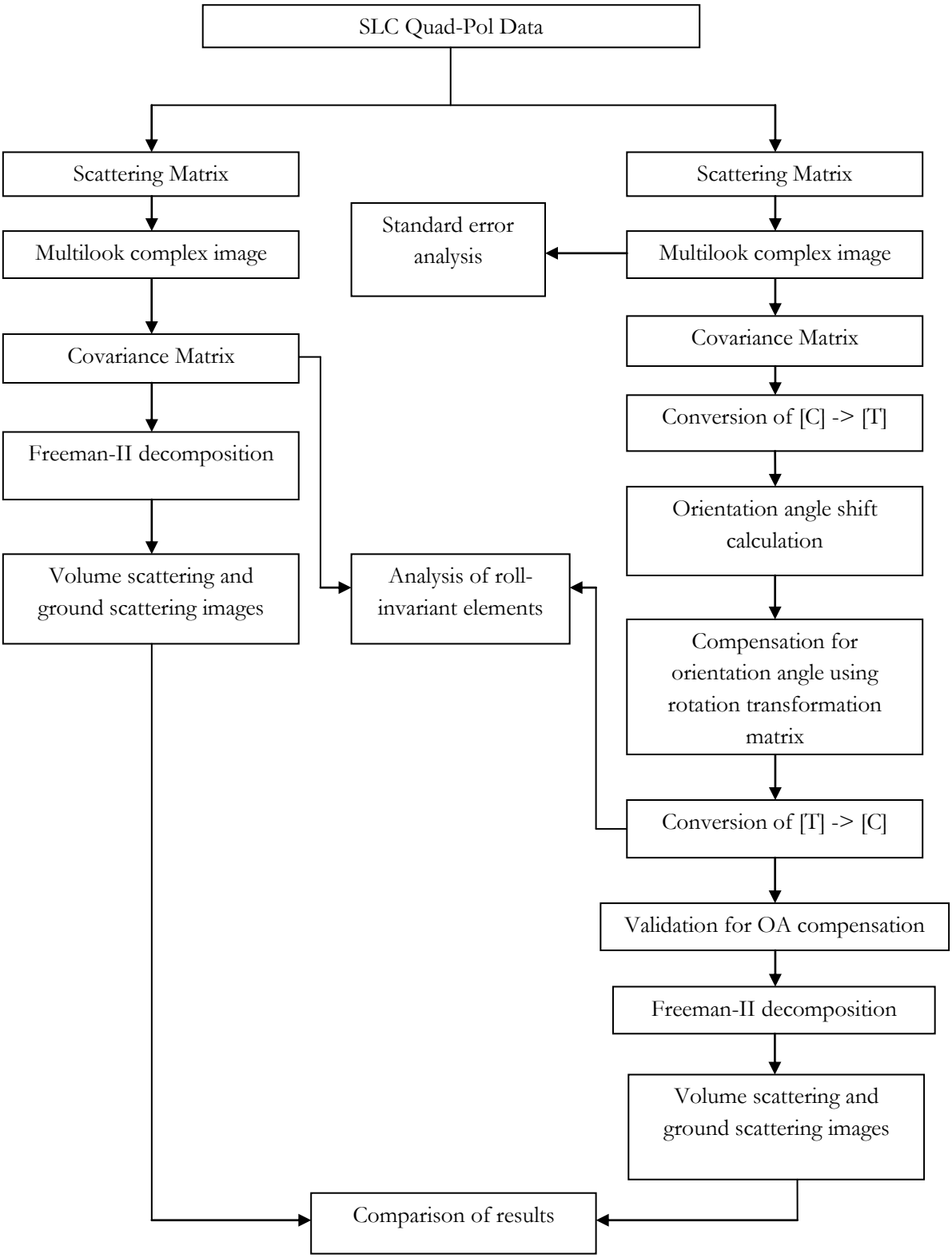

Figure 3-2 : Research method flow diagram

3.4. Approach:

The data obtained contains a single look complex image of quad-polarimetric mode which contains HH, VV, HV and VH information and a parameter file to describe it. These files are used for the purpose of generation of scattering matrices. The scattering matrix is a 2x2 complex element, which contains the co-pol information as diagonal element and cross-pol information as off diagonal elements.

$$S = \begin{pmatrix} S_{VV} & S_{VH} \\ S_{HV} & S_{HH} \end{pmatrix} \tag{3-1}$$

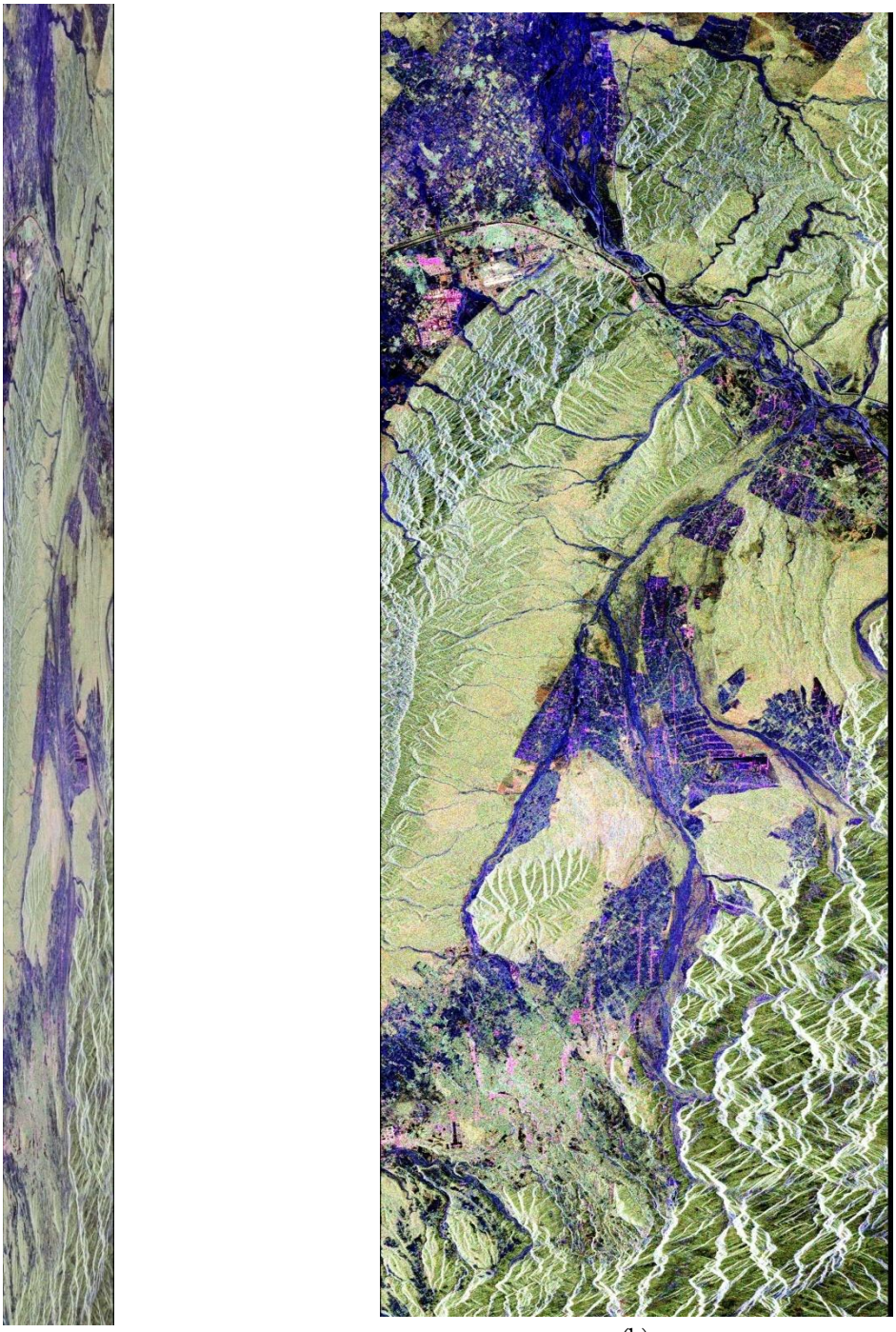

(a) (b)

Figure 3-3: (a) Single look complex image (b) Multi look complex image

The Multilook complex image has been generated for the purpose of easy visualization of the ground features. From Figure 3-3: (a) Single look complex image (b) Multi look complex image Multilook complex (MLC) image has better appearance than single look complex (SLC) image. Colour combination for the image has been created by expressing the HH+VV through blue, HV+VH through green, and HH-VV through red gun. This form of expressing is otherwise called as Pauli composition, where vegetation takes green colour, built up area takes blue and corner reflectors or areas with double bounces takes pink colour. The vectorized form of the scattering matrix can be expressed in lexicographic basis and the Pauli basis. The lexicographic format will represent the data with the reciprocal assumption leading to $S_{VH} = S_{HV}$ in

$$K_L = \begin{bmatrix} S_{HH} \\ \sqrt{2}\, S_{HV} \\ S_{VV} \end{bmatrix} \tag{3-2}$$

The product of this vector with its conjugate transpose yields the covariance matrix. Usually the covariance matrix will be represented using C. Covariance matrix $C = K_L . K_L^{*T}$, where * represents the conjugate and T represents transpose.

$$C = \begin{pmatrix} S_{HH} S^*{}_{HH} & \sqrt{2} S_{HH} S^*{}_{HV} & S_{HH} S^*{}_{VV} \\ \sqrt{2} S_{HV} S^*{}_{HH} & 2 S_{HV} S^*{}_{HV} & \sqrt{2} S_{HV} S^*{}_{VV} \\ S_{VV} S^*{}_{HH} & \sqrt{2} S_{VV} S^*{}_{HV} & S_{VV} S^*{}_{VV} \end{pmatrix} \tag{3-3}$$

3.4.1. Amplitude of Correlation coefficient: HHVV

The amplitude of correlation between the co-polarized terms was calculated using the expression as given in [60]. The amplitude of correlation coefficient values varies from 0 to 1 and the direct surface return will take up values close to 1 and the volume scattering will occupy the lower values [61].

$$\rho_{HH-VV} = \left| \frac{\langle S_{HH} S_{VV}^* \rangle}{\sqrt{|S_{HH}|^2 |S_{VV}|^2}} \right| \tag{3-4}$$

3.4.2. Standard error

Based on the assumption that the noise in the PolSAR images are exponential distribution as given in [11] the formula for the calculation of the standard error is

$$\text{Standard error} = \frac{SD(\, span)}{\sqrt{n}} \tag{3-5}$$

3.4.3. Freeman-II model:

The Freeman-II decomposition models the covariance matrix as two different scattering mechanisms to estimate the return power due to volume scattering and ground return.

$$C = P_c C_{\ volume} + P_g C_{\ surface} \tag{3-6}$$

The component for volume scattering in Freeman-II model is [11]

Volume Scattering = $$f_c\begin{pmatrix}1 & 0 & \rho\\ 0 & (1-\rho) & 0\\ \rho^* & 0 & 1\end{pmatrix} \qquad 0 \le \rho \le 1;\ arg(\rho) = 0 \tag{3-7}$$

Double-bounce from ground-trunk interaction = $$f_c\begin{pmatrix}1 & 0 & \alpha\\ 0 & 0 & 0\\ \alpha^* & 0 & |\alpha|^2\end{pmatrix} \qquad |\alpha| \le 1; \arg(\alpha) \approx \pm\pi \tag{3-8}$$

Surface scatterer = $$f_g\begin{pmatrix}1 & 0 & e^{-2j\emptyset}b\\ 0 & 0 & 0\\ e^{2j\emptyset}b & 0 & |b|^2\end{pmatrix} \qquad |b| \ge 1; \arg(b) = 0 \tag{3-9}$$

The surface scattering component has the same form as double bounce component, except the variation in α and b modulus and argument, and it can be shown as given in [11]

$$\alpha = e^{2j\emptyset}b \tag{3-10}$$

Using the above the model output parameters of volume scattering and ground return power output will be

$$P_c = f_c(3-\rho) \tag{3-11}$$

And

$$P_g = f_g(1+|\alpha|^2) \tag{3-12}$$

3.4.4. Orientation angle calculation:

The orientation angle calculation was performed using the coherency matrix, which can be generated by multiplying the transpose of the scattering vector expressed in the Pauli form of vectorization.

$$K_p = \frac{1}{\sqrt{2}}\begin{bmatrix}S_{HH}+S_{VV}\\ S_{HH}-S_{VV}\\ 2S_{HV}\end{bmatrix} \tag{3-13}$$

Coherency matrix T = $K_p . K_P^{*T}$ where, * represents the conjugate and ^{T} represents transpose.

T

$$= \frac{1}{2}\begin{pmatrix}\langle|S_{HH}+S_{VV}|^2\rangle & \langle(S_{HH}+S_{VV})(S_{HH}-S_{VV})^*\rangle & 2\langle(S_{HH}+S_{VV})S^*{}_{HV}\rangle\\ \langle(S_{HH}-S_{VV})(S_{HH}+S_{VV})^*\rangle & \langle|S_{HH}-S_{VV}|^2\rangle & 2\langle(S_{HH}-S_{VV})S^*{}_{HV}\rangle\\ 2\langle S_{HV}\begin{pmatrix}S_{HH}+\\ S_{VV}\end{pmatrix}^*\rangle & 2\langle S_{HV}\begin{pmatrix}S_{HH}-\\ S_{VV}\end{pmatrix}^*\rangle & 4\langle|S_{HV}|^2\rangle\end{pmatrix} \tag{3-14}$$

The formula for calculating polarization orientation angle shift induced by the terrain slopes as given in [8],[16], [20], [52] is

$$\eta = \frac{1}{4}\left[\tan^{-1}\left(\frac{-4\mathrm{Re}(\langle(S_{HH}-S_{vv})S^*{}_{HV}\rangle)}{-\langle|S_{HH}-S_{VV}|^2\rangle + 4\langle|S_{HV}|^2\rangle}\right)+\pi\right] \tag{3-15}$$

$$\theta = \begin{cases}\eta & if\ \eta \le \frac{\pi}{4}\\ \eta - \frac{\pi}{2} & if\ \eta > \frac{\pi}{4}\end{cases} \tag{3-16}$$

Since the formula for the calculation of polarization orientation angle shift was derived using the coherency matrix, the similarity transformation matrix was utilized for the conversion of covariance matrix into coherency matrix and the same was used again to convert it back to the covariance matrix for the purpose of decomposition using Freeman-II decomposition [37].

$$[T] = [A]\,[C][A^T] \tag{3-17}$$

$$[A] = \begin{bmatrix} \frac{1}{\sqrt{2}} & \frac{1}{\sqrt{2}} & 0 \\ 0 & 0 & 1 \\ \frac{1}{\sqrt{2}} & -\frac{1}{\sqrt{2}} & 0 \end{bmatrix} \tag{3-18}$$

3.4.5. Compensation for the shift in orientation angle:

For the purpose of compensation of the data after the effective analysis of the shift in orientation angle the unitary rotation matrix given in [8],[20], [52], [57] has to be used for compensation of the shift.

$$[U] = \begin{bmatrix} 1 & 0 & 0 \\ 0 & \cos 2\theta & sin2\theta \\ 0 & -sin2\theta & cos2\theta \end{bmatrix} \tag{3-19}$$

The above shown matrix is a unitary rotation operator [8]. The rotation is obtained by,

$$[\tilde{T}] = [U]\,[T][U^T] \tag{3-20}$$

$[\tilde{T}]$ Will be the rotated or compensated matrix generated using the θ angle shift in orientation. In this case $[\tilde{T}]$ has been compensated and converted back as used as $[\tilde{C}]$ and used as input for the Freeman-II model after rotation in order to identify compensated effect on the model output.

3.4.6. Validation for the compensation of the shift in orientation angle:

The orientation angle compensation on the data was analyzed by applying the same equation for the calculation of orientation angle. By doing so the equation should not produce any result and this has been explained in the results and discussion chapter.

3.4.7. Comparison of Values:

For the purpose of comparison of results produced before and after compensation for polarization orientation angle shift, randomly selected points throughout the image were plotted. The changes that can happen in a valid location in the output images will be compared with the high resolution Google image. The detailed explanation about this will be explained in the results and discussion chapter.

4. MODELLING THEORY OF FREEMAN-II DECOMPOSITION AND DE-ORIENTATION

4.1. Freeman-II Decomposition

The Freeman-II decomposition model is used to decompose PolSAR image. The scattering mechanisms are canopy scatterer mechanism and a ground scatterer term. The model fit approach assumes that either double bounce term or direct ground return can be set to zero and models the other remaining two components. The canopy scattering term has an advantage of allowing wide range of canopies to be modelled.

The model fit will reveal which mechanism is present by examining the HH/VV amplitude and phase ratio. The model for total backscatter with the composite scattering matrix M_{hv} where h, v represents the polarization as given in [11].

$$\langle M_{hh} M_{hh}^* \rangle = f_c + f_g \tag{4-1}$$

$$\langle M_{hv} M_{hv}^* \rangle = \frac{1-\rho}{2} f_c \tag{4-2}$$

$$\langle M_{vv} M_{vv}^* \rangle = f_c + |\alpha|^2 f_g \tag{4-3}$$

$$\langle M_{hh} M_{vv}^* \rangle = \rho f_c + \alpha f_g \tag{4-4}$$

Where f_c and f_g are the contributions of canopy and ground scattering in HH cross section. The solution to solve for α from above equation,

$$z_1 = \langle M_{hh} M_{hh}^* \rangle = \langle M_{vv} M_{vv}^* \rangle = f_g\,(1 - |\alpha|^2) \tag{4-5}$$

$$z_2 = 2\langle M_{hv} M_{hv}^* \rangle + \langle M_{hh} M_{vv}^* \rangle - \langle M_{hh} M_{hh}^* \rangle = (\alpha - 1)\, f_g \tag{4-6}$$

The ratio was taken to eliminate f_g and will fetch,

$$z_3 = \frac{z_2}{z_1} = \frac{(\alpha - 1)}{(1 - |\alpha|^2)} = 0 \tag{4-7}$$

By taking the real and imaginary parts,

$$\left(1 - (x^2 + y^2)\right) R_e(z_3) + 1 - x = 0 \tag{4-8}$$

And

$$\left(1 - (x^2 + y^2)\right) I_m(z_3) - y = 0 \tag{4-9}$$

Where,

$$x = \left(\frac{R_e(z_3) y}{I_m(z_3)} + 1\right) \tag{4-10}$$

By substituting the value of x in above equation, we get,

$$\left(\frac{{R_e}^2(z_3)}{I_m z_3} + I_m(z_3)\right) y^2 + (2R_e(z_3) + 1)y = 0 \tag{4-11}$$

Solution of the equation is

$$y = 0 \text{ or } y = \frac{-I_m(z_3)(2R_e(z_3)+1)}{|z_3|^2} \tag{4-12}$$

Using this equation (4-12) y ,the imaginary part of α can be solved. The real part of α, x can be solved from the equation (4-10). Once α is known we can recover f_g from (4-5) and f_c from (4-1) and the value of ρ can be solved from (4-1) . The contribution of each mechanism to the span P can be measured by,

$$P = P_c + P_g \equiv (|M_{hh}|^2 + 2|M_{hv}|^2 + |M_{vv}|^2) \tag{4-13}$$

The value of P_c and P_g can be solved using,

$$P_c = f_c(3 - \rho) \tag{4-14}$$

And

$$P_g = f_g(1 + |\alpha|^2) \tag{4-15}$$

α represents the relative phase and amplitude difference between the HH and VV backscatter for both double-bounce and ground return. The propagation term was modeled to represent propagation through canopy and only of trunks, the reflection term for direct surface and ground-trunk was included and α can be represented as,

$$\alpha = e^{[-2(\beta_h - \beta_v)h/cos\theta_i]} \cdot \left[e^{j2(\gamma_h - \gamma_v)} \right]_{canopy} \cdot \left[e^{j2(\gamma_h - \gamma_v)} \right]_{trunk} \cdot (R_{gh}/R_{gv}) \tag{4-16}$$

or

$$\alpha = e^{[-2(\beta_h - \beta_v)h/cos\theta_i]} \cdot \left[e^{j2(\gamma_h - \gamma_v)} \right]_{canopy} \cdot \left[e^{j2(\gamma_h - \gamma_v)} \right]_{trunk} \cdot (\frac{R_{gh}}{R_{gv}})(\frac{R_{th}}{R_{tv}}) \tag{4-17}$$

Where, β is an attenuation coefficient, γ determine the phase delay as waves propagates through canopy and trunk, and h is the height of the forest. The model outputs are image showing the volume scattering power and the ground return power due to double bounce or direct ground return.

$z_1 = 0$ occurs when HH and VV backscatter measure is equal. This leads to division by zero when calculating the equation (4-7). The solution adopted was to make z_1a very small positive number. $z_3 = 0$ This cause division by zero when calculating the equation (4-12) the solution to avoid such situation is to assume a very small positive value for real part of equation (4-7) and the negative value of f_c can be avoided by averaging many pixels ensures the importance of Multilooksetup.

4.2. Reflection symmetry condition

The components of Freeman-II model in section (3.4.3) are under the assumption of condition reflection symmetry. This symmetry condition was shown to equalise the measured scattering coefficients in two linear polarization bases. The correlation between co-polarization and cross-polarisation scattering coefficients will be zero under this condition and it is shown in [15] as

$$\begin{aligned} \mathrm{Re}\,\sigma_{\mathrm{hhhv}} &= \mathrm{Re}\,\sigma_{\mathrm{vhvv}} = \mathrm{Re}\,\sigma_{\mathrm{hhvh}} = \mathrm{Re}\,\sigma_{\mathrm{hvvv}} = 0 \\ \mathrm{Im}\,\sigma_{\mathrm{hhhv}} &= \mathrm{Im}\,\sigma_{\mathrm{vhvv}} = 0 \end{aligned} \tag{4-18}$$

Under the reflection symmetry condition the covariance matrix will take up the form as given in [15]

$$C = \begin{bmatrix} \sigma_{\mathrm{hhhh}} & 0 & \sigma_{\mathrm{hhvv}} \\ 0 & \sigma_{\mathrm{hvhv}} & 0 \\ \sigma^*_{\mathrm{hhvv}} & 0 & \sigma_{\mathrm{vvvv}} \end{bmatrix} \tag{4-19}$$

Which show the values of in [15]

$$\sigma_{\mathrm{hhhv}} = \sigma_{\mathrm{hvhh}} = \sigma_{\mathrm{vvvh}} = \sigma_{\mathrm{vhvv}} = 0 \tag{4-20}$$

The covariance matrix expressed using element numbers will take the form and is same in the case of coherency matrix also with C replaced by T

$$C = \begin{bmatrix} C11 & C12 & C13 \\ C^*12 & C22 & C23 \\ C^*13 & C^*13 & C33 \end{bmatrix} \tag{4-21}$$

The element numbers which take the zero as value are

$$C12 = C^*12 = C23 = C^*13 = 0 \tag{4-22}$$

4.3. De-orientation Theory

The purpose of de-orientation is to reduce the influence of randomly oriented target in the polarimetric scattering. The de-orientation technique can reduce the influence of the cross-polarized power which leads to power concentrated on co-polarized channels. The Pauli form of representation of the scattering matrix will take the form [57]

$$K_p = \frac{1}{\sqrt{2}} \begin{bmatrix} S_{HH} + S_{VV} \\ S_{HH} - S_{VV} \\ 2S_{HV} \end{bmatrix} \tag{4-23}$$

The parameterization of Pauli form of scattering matrix was explained in [9], [62] using the parameters α and β as

$$K_p = \|K_p\| \left[\cos\alpha\, e^{j\Phi_1} \quad \sin\alpha\cos\beta\, e^{j\Phi_2} \quad \sin\alpha\sin\beta\, e^{j\Phi_3}\right]^T \tag{4-24}$$

Where, the $\|K_P\|$ means vector norm and α, β represents the scale of each complex elements and Φ_1, Φ_2 and Φ_3 are the phase angles of each element. The parameterization of scattering matrix in lexicographic form is defined as [57]

$$K_L = \begin{bmatrix} S_{VV} \\ \sqrt{2}\, S_{HV} \\ S_{VV} \end{bmatrix} \tag{4-25}$$

$$K_L = \|K_L\| \left[\sin c \cos a \,.\, e^{j\Phi_0} \quad \cos c \,.\, e^{j\Phi_x} \quad \sin c \sin a \,.\, e^{j(\Phi_0 + 2b)}\right]^T \tag{4-26}$$

From equations (19) and (20) it can been shown that in [57]

$$a = tan^{-1}\left(\frac{|S_{vv}|}{|S_{hh}|}\right) \tag{4-27}$$

$$b = \frac{1}{2}\arg\left(\frac{S_{vv}}{S_{hh}}\right) \tag{4-28}$$

$$c = cos^{-1}\left(\frac{\sqrt{2}|S_x|}{\|K_L\|}\right) \tag{4-29}$$

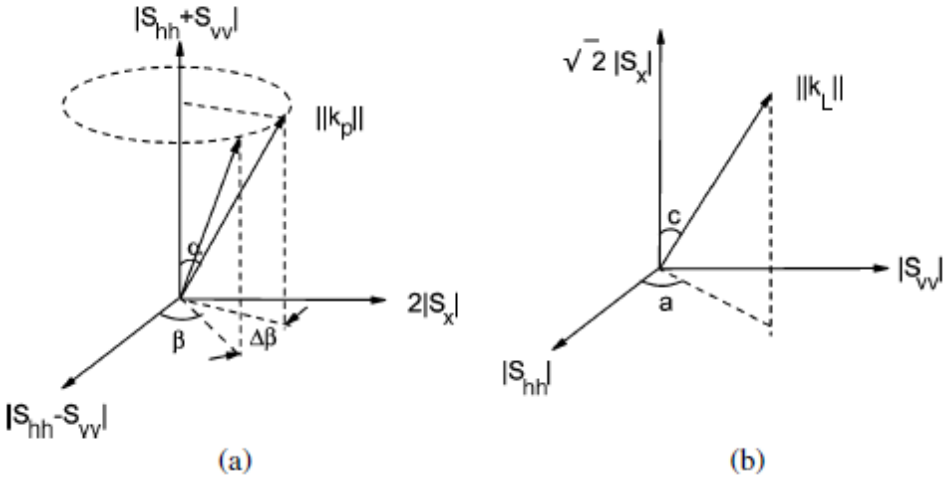

Figure 4-1: Parameterization of target scattering vector, (a) Pauli format vectorization (b) Lexicographic format vectorization [58]

As shown in the Figure 4-1 the orthogonality of K_L might not be good as K_p but it has been shown that vectorization is more intuitive and easier to process. The equations (4-27), (4-28), (4-29) show that the parameter 'a' represents the co-polarized amplitude ratio, the parameter 'b' represents co-polarization phase difference, and 'c' indicates the cross-polarization scattering. The two sets of parameters α, β and a, b, c can be related to each other by as given in [57]

$$\cos\alpha = \sqrt{\frac{1+\sin 2a\cos 2b}{2+\frac{2}{tan^2 c}}} \tag{4-30}$$

$$\cos\beta = \sqrt{\frac{1-sin2a\cos 2b}{1-sin2a\cos 2b+\frac{2}{tan^2 c}}} \tag{4-31}$$

When the cross-pol scattering is small, it makes $c \approx 90^0$ and $\beta \approx 0^0$, then the parameter α can be determined using a and b only as given in [57]

$$\cos 2\alpha = \sin 2a\cos 2b \tag{4-32}$$

4.3.1. Target orientation information extraction

The parameter β in Pauli vectorization represents the target orientation [9] The rotation transformation as discussed in [20] yields new polarization base for the ψ angle rotation along the line of sight [57]. The relationship between K_p and $K_P^{'}$ as given in [57]

$$K_P^{'} = K_p.[U] \tag{4-33}$$

Where

$$[U] = \begin{bmatrix} 1 & 0 & 0 \\ 0 & \cos 2\psi & sin2\psi \\ 0 & -sin2\psi & cos2\psi \end{bmatrix} \tag{4-34}$$

$$K_P^{'} = \begin{bmatrix} 1 & 0 & 0 \\ 0 & \cos 2\psi & sin2\psi \\ 0 & -sin2\psi & cos2\psi \end{bmatrix} . \frac{1}{\sqrt{2}} \begin{bmatrix} S_{HH} + S_{VV} \\ S_{HH} - S_{VV} \\ 2S_{HV} \end{bmatrix} \tag{4-35}$$

In order to rotate the polarization along the line of sight, it is equal to rotate the target to the negative of the angle [57], from (18) and (29) parameters of K_p and $K_P^{'}$ relationship as shown in [57]under the condition of $\Phi_3 - \Phi_2 \approx 0, \pi$

$$\begin{bmatrix} \cos\alpha^{'} e^{j\Phi_1^{'}} \\ \sin\alpha^{'} \cos\beta^{'} e^{j\Phi_2^{'}} \\ \sin\alpha^{'} \sin\beta^{'} e^{j\Phi_3^{'}} \end{bmatrix} = \begin{bmatrix} \cos\alpha\, e^{j\Phi_1} \\ \sin\alpha \cos(\beta \mp 2\psi). e^{j\Phi_2} \\ \sin\alpha \sin(\pm\, \beta - 2\psi). e^{j\Phi_2} \end{bmatrix} \tag{4-36}$$

From this relationship it has been shown that $\alpha^{'} = \alpha$, $\beta^{'} = \beta - 2\psi$ or $-\beta - 2\psi$, means α remains roll invariant and β changes by 2ψ after ψ angle rotation along the line of sight, and $\Phi_3 - \Phi_2 \approx 0, \pi$ show the condition for symmetry target [57].

4.4. Minimization of Cross-polarization power

The de-orientation purpose is to reduce the fluctuating influence of the randomly oriented target scattering and the influence of the terrain slope to preserve important information from intrinsic scatters [57]. The ψ_m rotation yields the minimization of the cross-polarization scattering contribution was shows under the condition as $\Phi_3 - \Phi_2 \approx 0, \pi$ [57]

$$\psi_m = \left[sgn\{\cos(\Phi_2 - \Phi_3)\} \, . \, \frac{\beta}{2} \right]_{\pi/2} \tag{4-37}$$

The ψ_m satisfy (30) and it shows min cross-polarization equals to 0, and volume scattering can always satisfies the condition$\Phi_3 - \Phi_2 \approx 0, \pi$. The value of $\Phi_3 - \Phi_2$ can be taken as a indicator for the degree of non-symmetry [57].

$$K_P^d = K_p . [U_m] \tag{4-38}$$

Where ^{d} denotes the de-oriented vector the $[U_m]$ transform matrix and the value of ψ is replaced by ψ_m which is the calculated angle of orientation. The same way the lexicographic form vectorization de-oriented scattering matrix can also be obtained. In de-orientation technique after compensation there will be reduction in cross-polarized power representing volume scattering. The increase in the double bounce power and the surface return power can then be used for important information extraction from the features.

5. RESULTS AND DISCUSSION

This chapter presents the results from the method discussed in section 3.3. This chapter is outlined to answer for the research question in this thesis. The following analysis is from dataset two followed by dataset one and three. The dataset two is used to analyse changes from matrix elements since it covers objects which fall short in other two dataset which were considered for analysing the effect of orientation angle shift compensation.

5.1. Analysis for the signal to noise ratio

The amount of standard error in calculating the values of matrix elements has been analysed by the span of the single look complex image and the multi look complex image with the assumption that the standard error in the image is of exponential distribution.

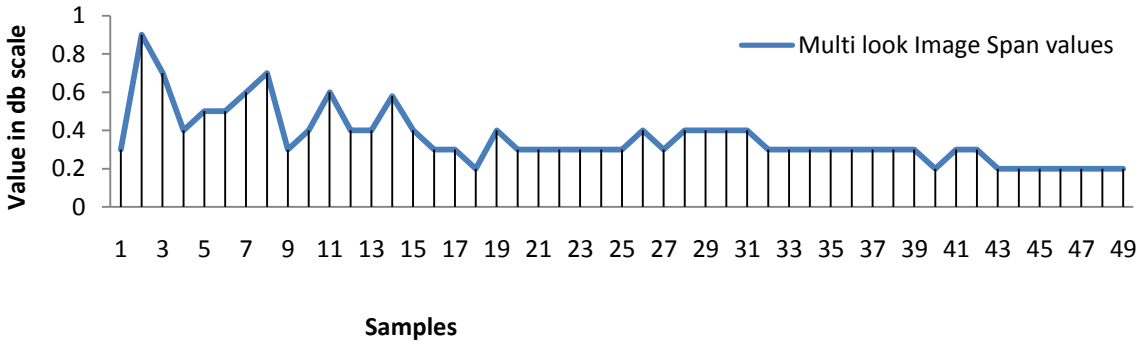

Figure 5-1: standard error in the multi look complex image span values

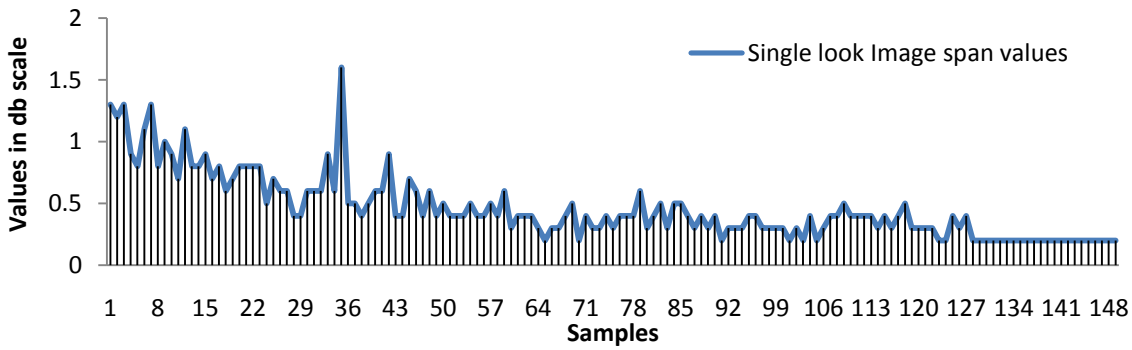

Figure 5-2: standard error in the single look complex image span values

The effect of signal to noise ratio needs to be analyzed since the multi look complex images contains lesser noise than the single look images as it considers the average of many pixels. Based on the assumption that noise is exponentially distributed, the derived total power from a single look image (total power image which is the addition of diagonal elements of the covariance or coherency matrices) and the multi look image has been plotted in Figure 5-1 and Figure 5-2. The graphs plotted for calculating the standard error in the pixel values showed that, in a multi look image, the error drops below 0.2 decibel(a level used in [11]) after averaging 40 samples due to lesser noise. Whereas in the case of Single look images the speckle is more dominant hence it is required to average more number of pixels (i.e. 130) for the standard error to drop below 0.2 decibel. From these analysis it was found that the multi look images are better not only for visualization purposes but it also reduces the effect of noise for the calculation of coherence between the like and cross-polarized term when compared with the single look images and shows coarser resolution which is needed for accurate estimation of degree of coherence [63].

5.2. Analysis of orientation angle shift

The transmitted signals from the radar are oriented along the line of sight. Due to alignment of objects from Earth orientation of the signals will not be same as transmitted. It experiences shift due to reasons discussed in section 0. The model based decomposition technique mostly depends on the polarization property of the received signal to identify different scatter. Thus resulting shift can possibly increase the magnitude of the cross-polarization and leads the model based decomposition technique to miscalculation. Hence, calculation of polarization orientation angle shift and compensation may helps the model based decomposition techniques to overcome miscalculation. The results in the Figure 5-3(a) is showing image of orientation angle shift and Figure5-3(b) showing corresponding image histogram. This result was produced using equation (3-15). The histogram of the image showing shift ranges between -45° and 45°. The output of image is very clear that the data is containing orientation angle shift.

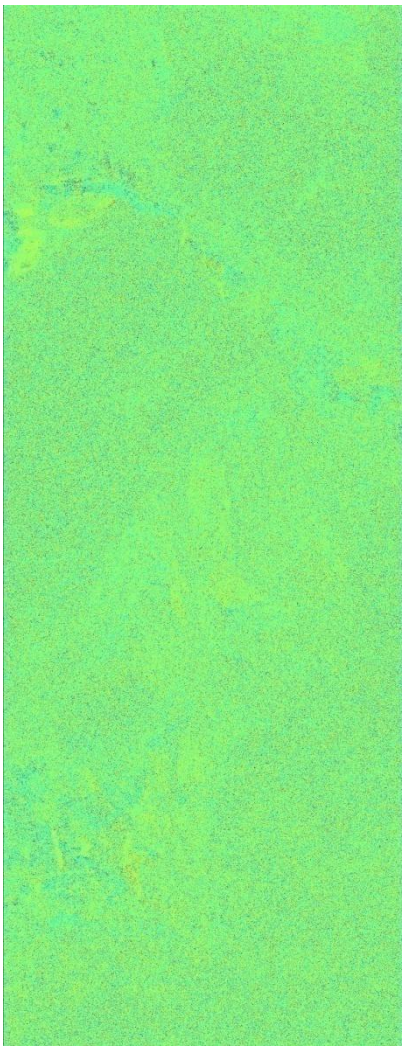

(a)

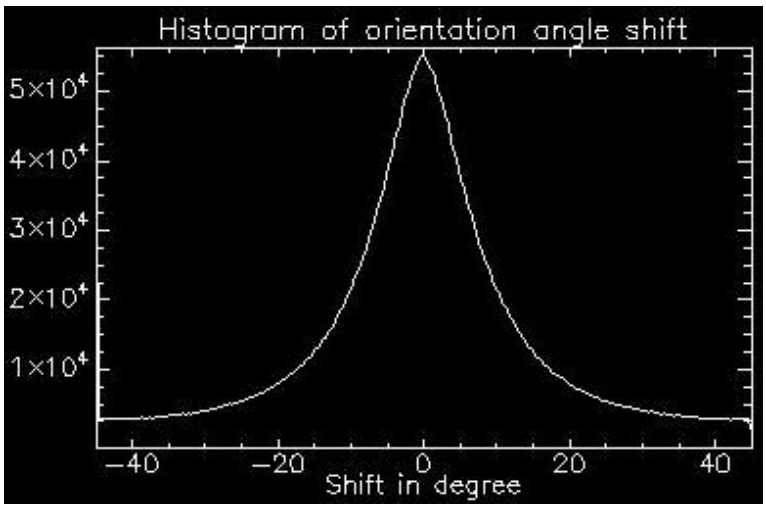

(b)

Figure 5-3: (a) Orientation angle shift image and (b) corresponding image histogram

The data needs to be compensated for polarization orientation angle shift. The equation (3-19) used for compensation. This equation utilises the calculated orientation shift angle and compensate it by rotating to the negative of calculated angle. The rotation compensates data for shift. The data compensation was analysed by applying equation (3-15) on compensated data with assumption it should not produce any

shift. Figure 5-4(a), (b) are showing the resultant image and histogram of image after compensation. The histogram of the image shows a clear cluster of pixels around 0° indicates a valid application of the equation (3-19) for compensation. The minimum and maximum shift after compensation was -0.000086^{o} and 0.000109^{o}.

(a)

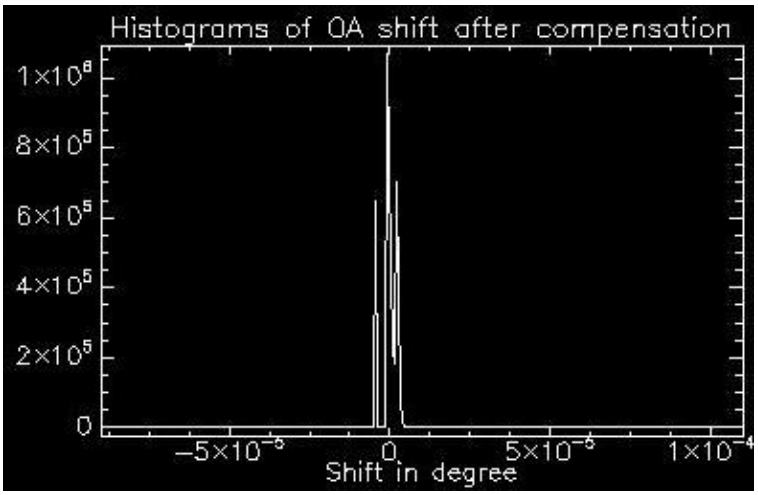

(b)

Figure 5-4: (a) Orientation angle shift image after compensation (b) corresponding image histogram.

5.3. Analysis of OA shift compensation on covariance matrix diagonal elements

The compensated data was used for the purpose of analysing effect of orientation angle compensation on various covariance matrix elements along with data without compensation. The diagonal elements are first considered since the addition of all elements holds the total power and each element separately holds information from different polarization. 100 random samples pixels were selected throughout the image and analysed for the changes in values among those selected pixels.

The Figures in 5-5 (a) (b) (c) are diagonal matrix elements of covariance matrix. The covariance matrix element $C11 = S_{HH} S^{*}{}_{HH}$ holds the information of the horizontal polarization which is sensitive to surface return. The location selected on the Figure 5-5 (a) is zoomed in Figure 5-6 (a) shows clear bright information from a road surface which confirms the C11 element of the covariance matrix contains horizontal polarization information. The matrix element $C22 = 2S_{HV} S^{*}{}_{HV}$ holds information of cross polarization which is sensitive to volume scattering. The location selected was a dense forest area and it

shows bright patches compared with the other elements of the matrix for that location in Figure 5-6 (b). The matrix element $C33 = S_{VV} S^*_{VV}$ contains the information of the vertical polarization which is sensitive to corner reflectors. The selected area in Figure 5-5 (c) shows some bright patches from the corners of the buildings in Figure 5-6(c) confirm it.

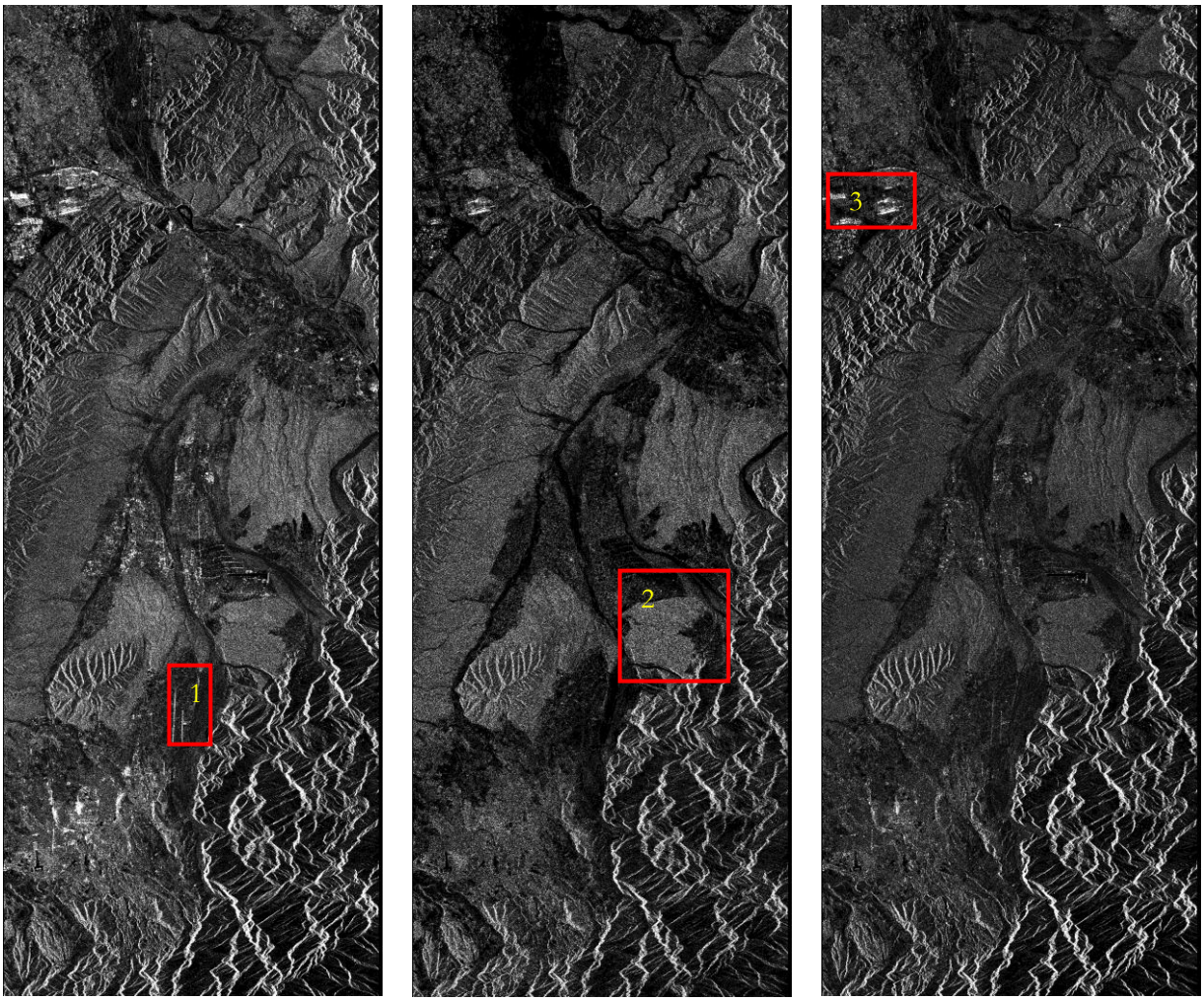

(a) (b) (c)

Figure 5-5: (a) Matrix element C11 (b) matrix element C22 (c) matrix element C33

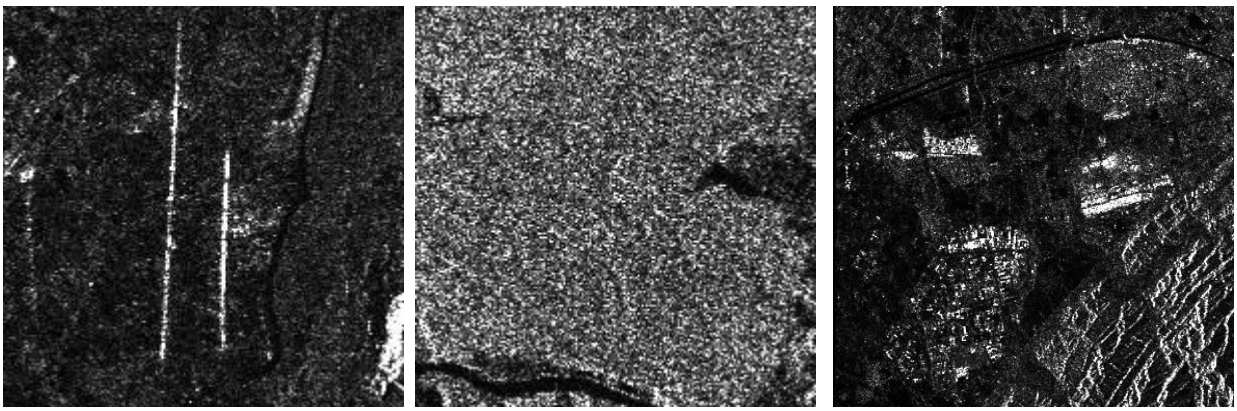

(a) (b) (c)

Figure 5-6: (a) Zoomed area of location1,(b) zoomed area of location 2 , (c) zoomed area of location 3

5.3.1. Results of analysis on diagonal elements of matrix

In order to identify changes caused by compensation for orientation angle shift 100 samples has been selected from each diagonal element C11, C22 and C33 of covariance matrix created before and after compensation. The selected samples from the element C11 is plotted in Figure 5-7 with blue and red colour lines representing values of element before and after polarization orientation angle shift compensation respectively. No change has happened in red line with respect to blue line. This shows that element C11 is roll invariant and remains constant to angle of rotation as discussed in the equation (4-36). This graph shows all values in this element are positive.

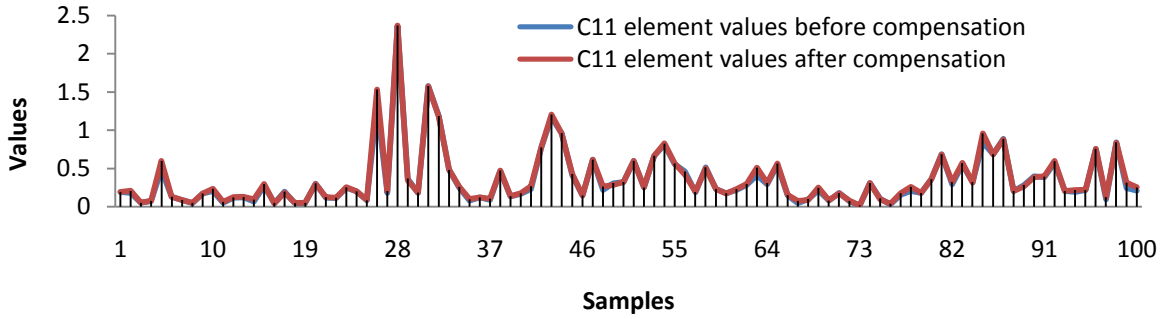

Figure 5-7: Samples plot of element C11

The Figure 5-8 is showing plot of values from selected 100 samples of element C22 before and after the compensation. The blue colour and red colour line representing values from this element before and after polarization orientation angle shift compensation respectively. As discussed in the chapter 4, the compensation will reduce the cross-polarized power, the element C22 which represent the cross polarized power showing reduction in values by red lines taking lower values with respect to blue lines in (Figure 5-8).

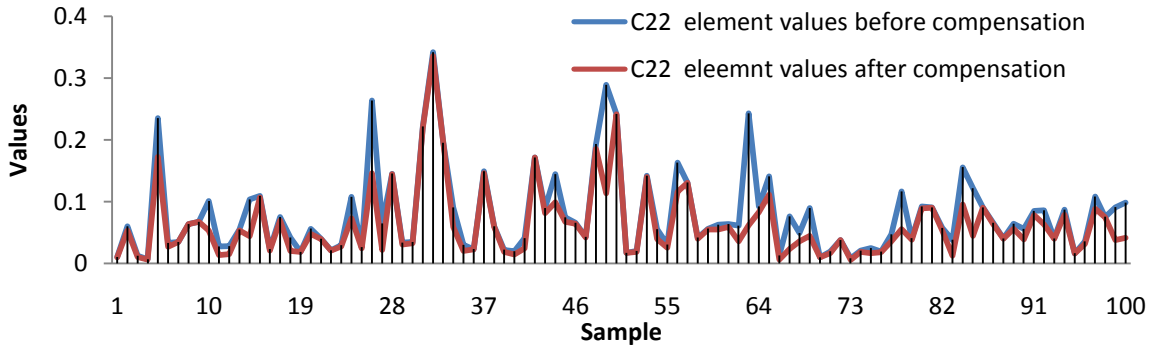

Figure 5-8: Samples plot of element C22

The Figure 5-9 represents plot between 100 samples of element C33. This element holds the information from the vertical polarisation is sensitive to corner reflectors The selected samples has been plotted using blue colour and red colour lines representing values before and after polarization orientation angle shift compensation respectively in Figure 5-9. The values increase in some points and remain same at some points. This is with respect to red lines when compared to blue lines.

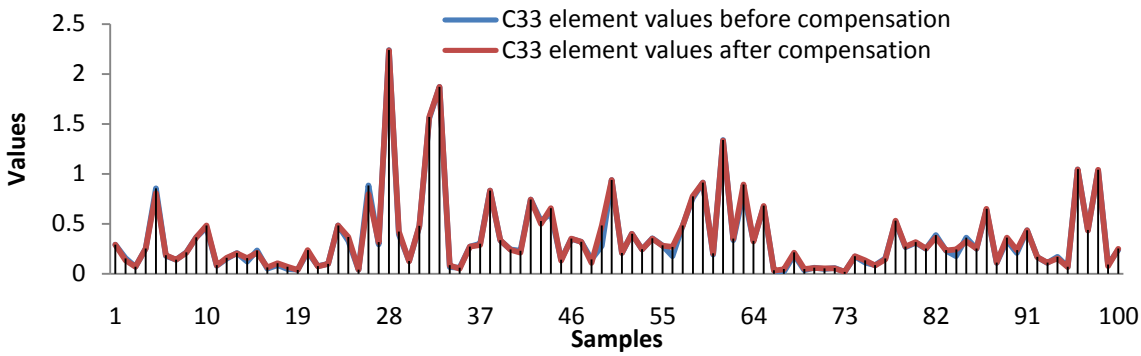

Figure 5-9: Samples plot of element C33

As a concluding remark for changes in diagonal elements of covariance matrix, element C11represention horizontal polarization remains same after the polarization orientation angle shift compensation, element C22 representing cross polarization shows decrease in values after compensation. Element C33 which represents vertical polarization remains same or shows some increase in values at points after compensation. These conclusions are made with changes in red lines of plots with respect to blue lines in Figure 5-7, 5-8 and 5-9.

5.3.2. Span of covariance matrix

The sum of diagonal elements of covariance matrix represents total power and it often called as span. The analysis on total power is considered in order to identify power change pattern. For this analysis 100 samples were selected from the span of the matrix created before and after compensation. Figure 5-10 shows sample values plotted from span. Blue colour and red colour line in the same figure is showing the span values before and after compensation of the matrix for polarization orientation angle shift respectively. With the plot remains constant by no change in red line with respect to blue line, it shows that the total power remains unchanged after compensation.

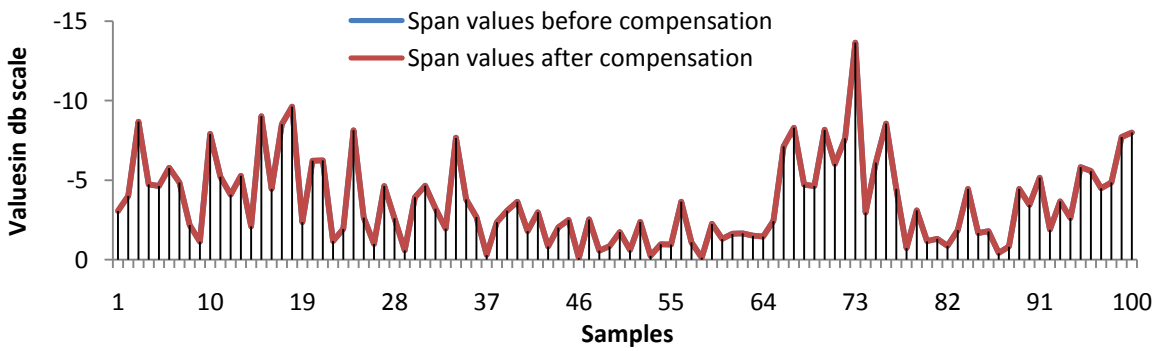

Figure 5-10: Span of the matrix

With the total power and C11 remains unchanged, changes are happening only between elements C22 and C33. The relationship between these changes is analyzed with difference in values from each element. The values selected before and after polarization orientation angle shift compensation from the element C22 was subtracted. The subtracted values from the element C22 is plotted (Figure 5-11) in blue colour line. The same procedure was carried out for the samples of element C33 also and is shown in red colour in the same figure. From Figure 5-11, relationship between the reduction and increase in power is that it is happening with equal amount.

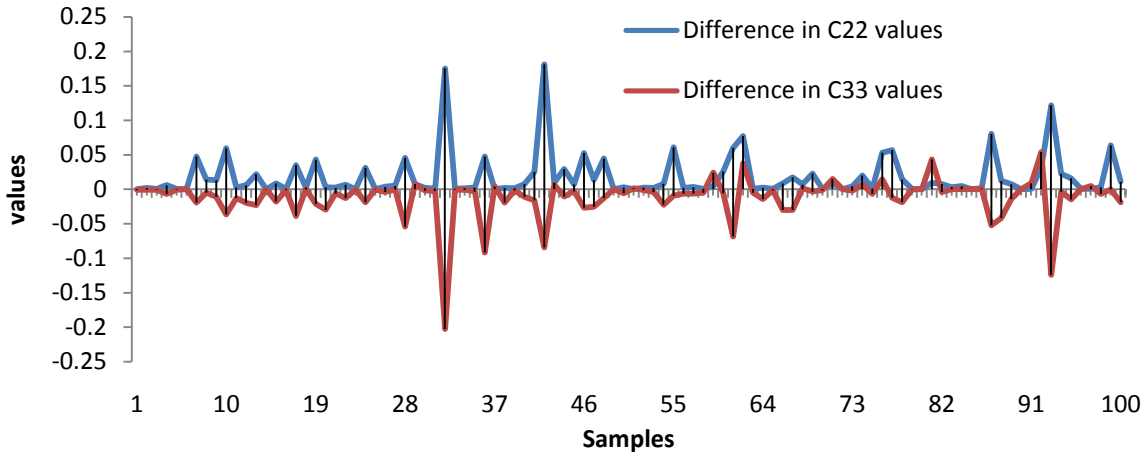

Figure 5-11: Difference in values of C22 and C33 elements before and after polarization orientation compensation

As a concluding remark from Figure 5-11 the increase in power is equal to that of decrease in power which leads to constant span.

5.3.3. Analysis of diagonal elements with cropped regions

Since the changes in diagonal element shows a reduction in the volume scattering power (C22) and increase in the double bounce power (C33), the areas in the images with only volume scattering power is dominant and areas possible of surface return is cropped and analysed for the changes in the diagonal elements. The Figure 5-12 (a) (b) shows thus selected regions. The main aim for selecting regions in Figure 5-12 (a) is that they are with volume scattering and also terrain is rugged

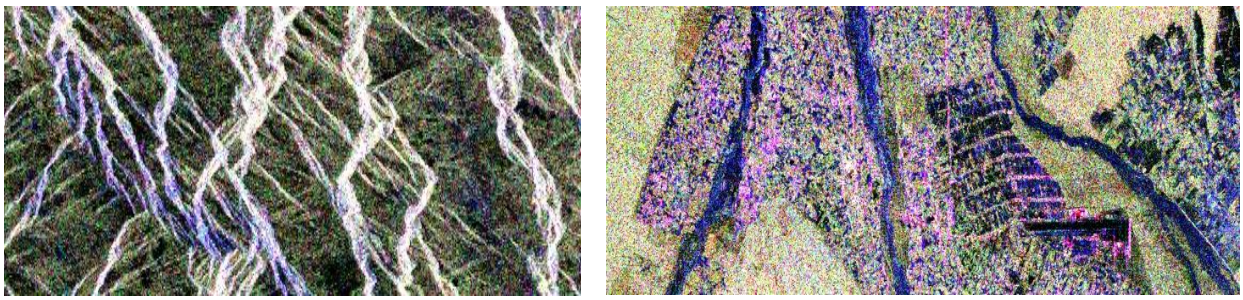

(a) (b)

Figure 5-12: (a) Region for volume scattering area (b) region for direct ground return

5.3.4. Analysis on diagonal elements from volume scattering region

The matrix element C11 of the volume scattering zone shows bright patches enabling possible surface return in Figure 5-13 (a) at some points. For the purpose of analysing changes in the matrix elements 50 samples around the cropped region is plotted in figure 5-13(b). The blue colour line shows values before compensation and red colour line shows values after compensation of this element. The C11 representing horizontal polarization resulting plot shows no changes in redlines with respect to blue line. It shows no change in this element after compensation.

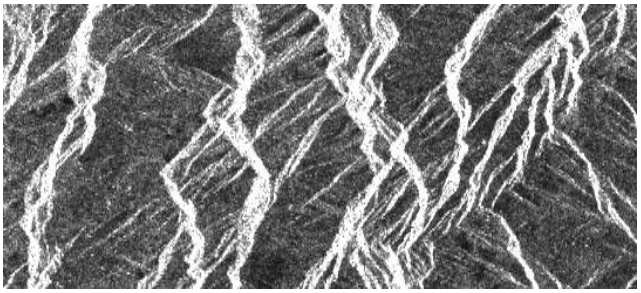

(a)

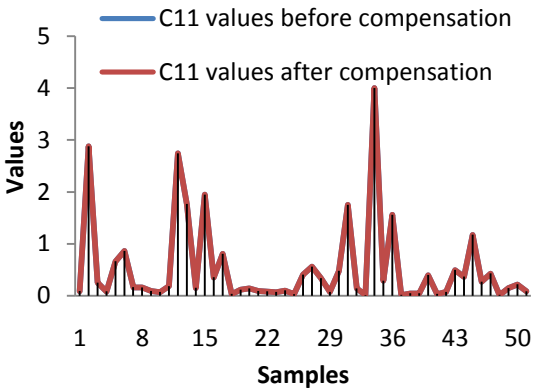

(b)

Figure 5-13: (a) Matrix element C11 (b) samples plot from C11

The Figure 5-14 (a) showing the matrix element C22 for the region considered as region with only volume scattering return. Since the element representing the volume scattering possible changes are expected. The main focus of selecting region is that they are with volume scattering and also terrain is rugged. 50 samples around this region are selected from this element before and after compensation. The blue colour and red colour representing sample values before and after compensation respectively. The decrease in values of red line with respect to blue line shows reduction in values of C22 element after compensation.

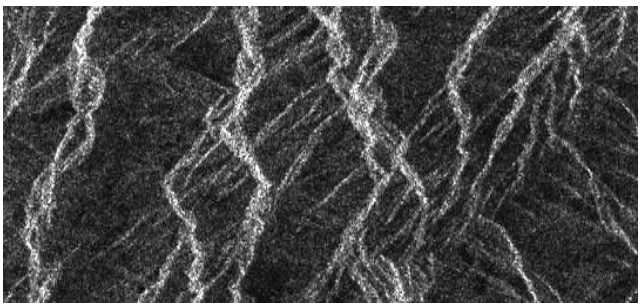

(a)

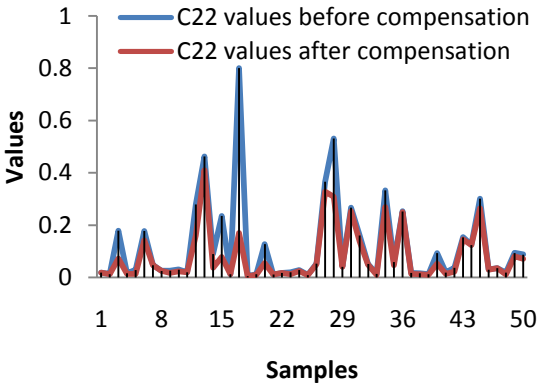

(b)

Figure 5-14: (a) matrix element C22 (b) samples plot from C22

The Figure 5-15 showing the matrix element C33 represent the double bounce scattering. Regions along terrain relief show bright patches. The bright regions representing the double bounce scattering. These regions show possible return from the ground trunk interaction. 50 samples around this region are selected from this element before and after compensation with blue colour line and red colour line representing sample values respectively. The Figure 5-15 (b) shows no changes in red colour lines with respect to blue colour lines. It shows the double bounce power remains unchanged for this region.

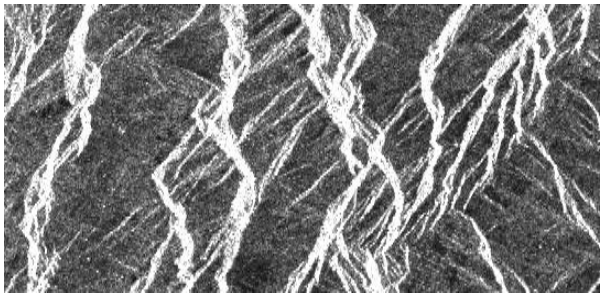

(a)

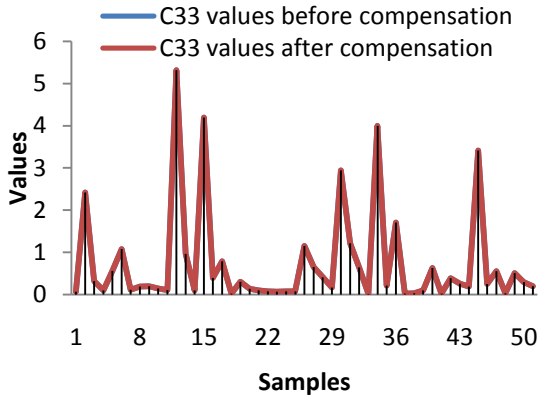

(b)

Figure 5-15: (a) Matrix element C33 (b) samples plot from C33

As a concluding remark the changes occurring with the cross-polarized term (C22 element) is reduction in values.

5.3.5. Analysis on diagonal elements from direct surface return region

The area in Figure 5-12(b) is considered for analysis in order to understand the influence of polarization orientation angle shift compensation where surface return is dominant. With the dominant surface return the possibility of over estimation of volume scattering power can be easily identified from this region. In Figure 5-16(a) the areas with surface return are clearly visible in bright patches. The straight white line is from the roads in selected region. 50 samples over these regions are considered for the analysis of orientation angle shift compensation. The blue colour lines in Figure 5-16(b) shows values from these regions before compensation and red colour line show values after compensation. Same as the earlier cases the values of the element C11 remains the same after the compensation with red lines showing no changes with respect to blue lines.

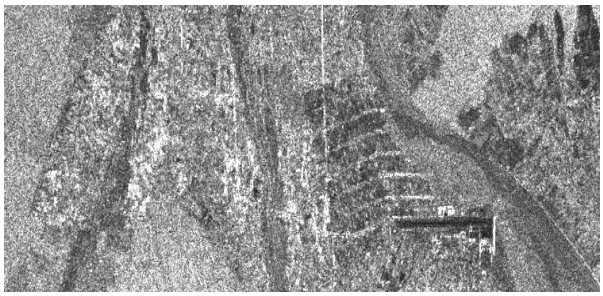

(a)

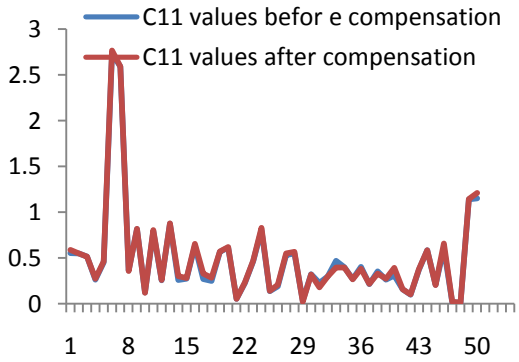

(b)

Figure 5-16: (a) Matrix element C11 (b) samples plot from C11

The Figure 5-17 (a) showing the matrix element C22 which is cross polarized power. Regions which looked bright in Figure 5-16(a) are appearing dark showing low volume scattering return. 50 samples over these regions are considered for analysis of orientation angle shift compensation. The blue colour lines in Figure 5-16(b) shows values from these regions before compensation and red colour line show values after compensation. Compensation of orientation angle shows a reduction in the volume scattering power by changes in red colour lines with respect to blue colour lines in Figure 5-16(b). The reduction in volume scatter power from this region shows a possible over estimation of the cross polarized power where there is dominant surface return or the double bounce.

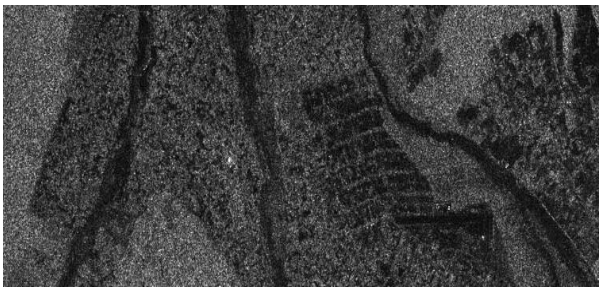

(a)

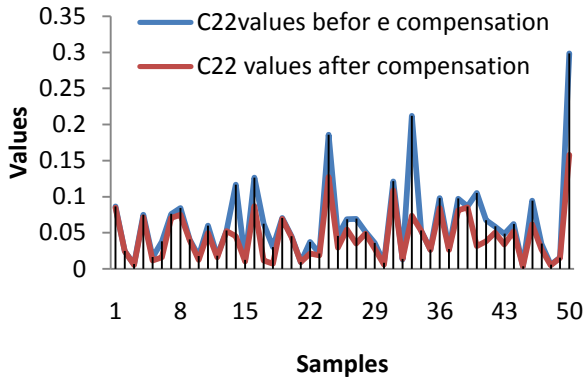

(b)

Figure 5-17: (a) Matrix element C22 (b) samples plot from C22

The Figure 5-18(a) shows the C33 element of the matrix which is vertical polarization and more sensitive to double bounce or corner reflectors. Some regions show the presence of double bounce with brighter appearance. 50 samples over these regions where the double bounce are dominant are selected from element before and after compensation. In Figure 5-18(b) the plots of these values are shown. The blue colour line and red colour line representing the values from the element before and after compensation respectively. Small amount of increase in values has been seen at points in this element by changes in red line with respect to blue line.

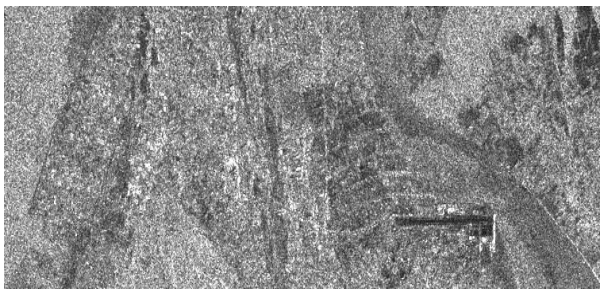

(a)

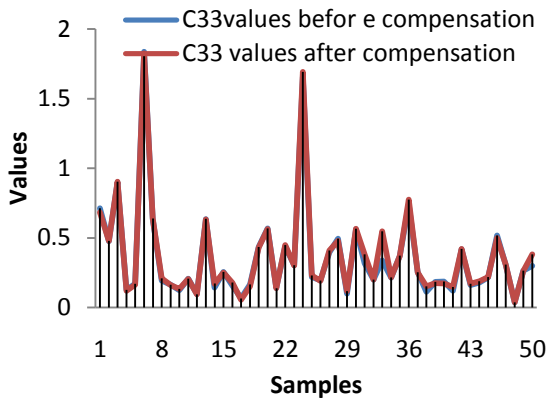

(b)

Figure 5-18: (a) Matrix element C33 (b) samples plot from C33

As a concluding remark, decrease in volume scattering power in places where surface return is dominant shows a clear over estimation of volume scattering power from that region due to orientation angle shift. Thereby the over estimation of volume scattering power can be reduced after compensation for the polarization orientation angle shift and helps in getting intrinsic quantity from these regions.

5.4. Analysis on off-diagonal elements of covariance matrix

The results in section 5.3 discusses about diagonal elements of matrix and the changes that can happen to the elements after the compensation for polarization orientation angle shift. The Freeman-II decomposition technique utilizes various other matrix elements as well. In the section 3.4.3 the components of various models shows the utilization. Hence it is mandatory to analyze the changes that can happen in rest of the matrix elements also.

The Figure 5-19(a) represents the real part of element C12. With Freeman-II models basic assumption of reflection symmetry it assumes the response from this element is zero as shown in section 4.2. Hundred (100) samples were randomly selected and plotted in order to analyse the changes in those element. The blue colour line in Figure 5-19(b) shows values from real part of this element before compensation and red colour line show values from real part of this element after compensation. This resulting plot shows no proper increase or decrease in values from this element by changes in red line with respect to blue line.

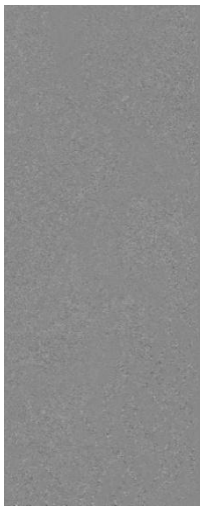

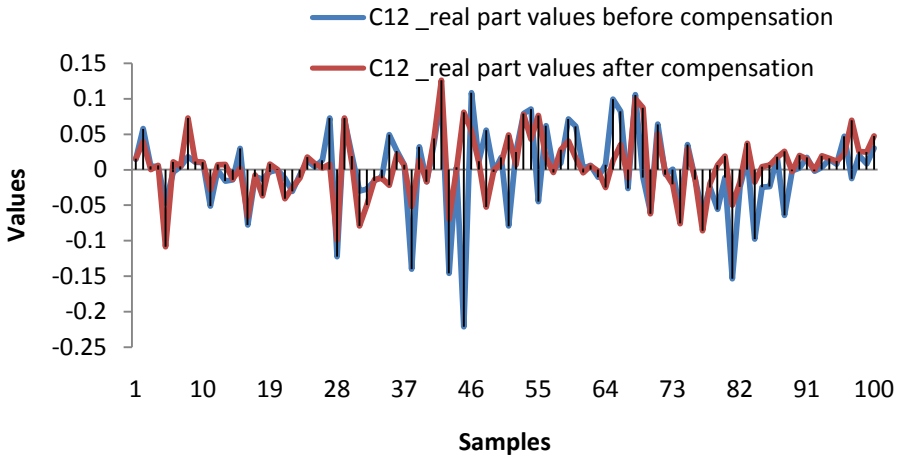

(a) (b)

Figure 5-19: (a) Real part of matrix element C12 (b) sample plots from the element

In the Figure 5-20(a) the imaginary part of the element is shown. 100 random samples have been selected from the element before and after compensation of polarization orientation angle shift. Blue colour line in Figure 5-20 (b) represents the values before compensation and red colour line represent the values after compensation for polarization orientation angle shift. This resulting plot also shows no proper increase or decrease in values after compensation with no proper changes in red line with respect to blue line.

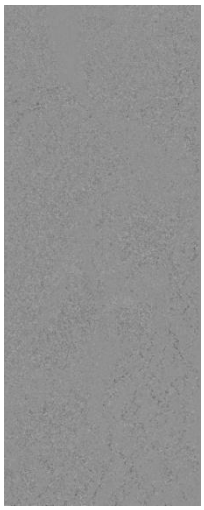

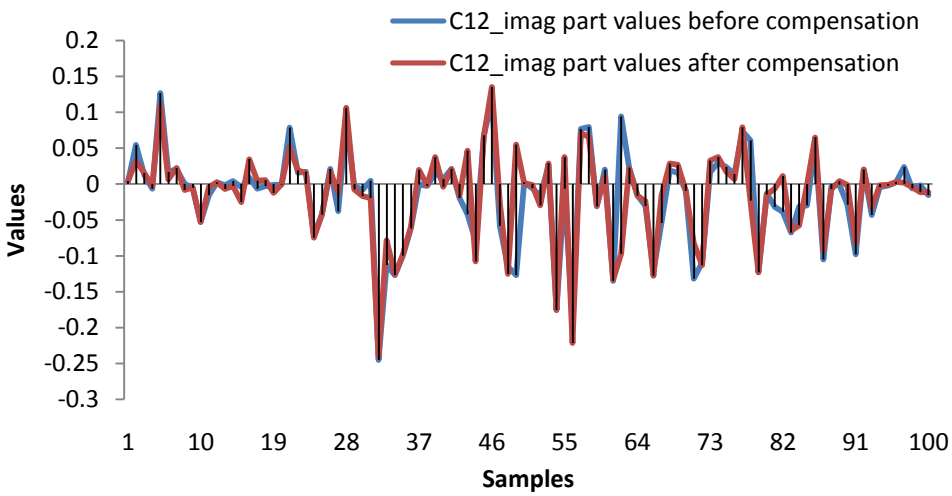

(a) (b)

Figure 5-20: (a) imaginary part of matrix element C12 (b) samples plots from the element

The Figure 5-21 (a) represents the real part of the element C13. This element is equal to $S_{HH} S^*_{VV}$ in the covariance matrix. In the Freeman-II model real part of this element is used for the calculation of equation (4-6), the imaginary part in calculation of equation (4-7). Hence change in this element will affect the model output. The plot in the Figure 5-21(b) shows little changes in real part of this element after

orientation angle shift compensation. The blue colour line and red colour line from same figure is showing values of this element before compensation and values of this element after compensation. With respect to blue line, red line showing some changes at places. The changes are little reduction in values at points.

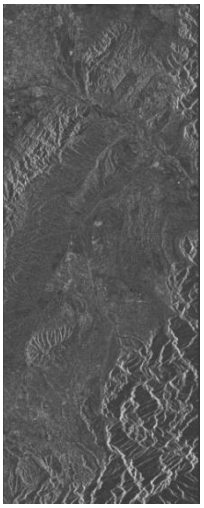

(a)

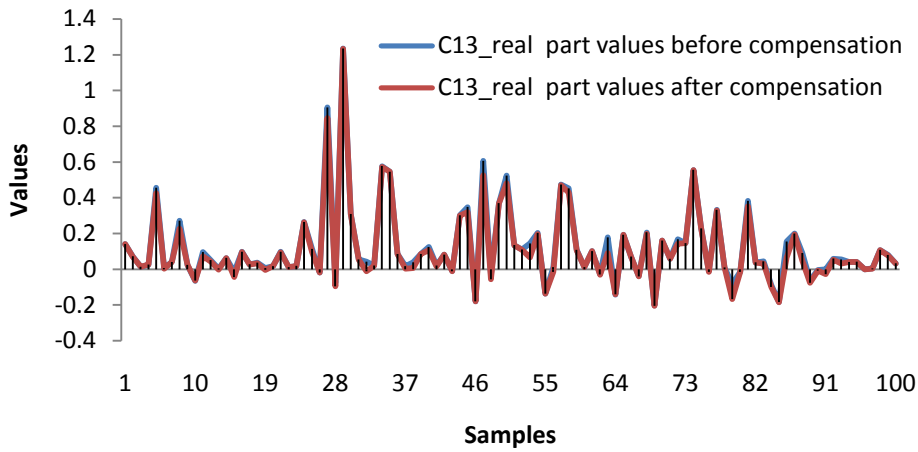

(b)

Figure 5-21: (a) real part of matrix element C13 (b) samples plots from the element

The Figure 5-22 (a) shows the imaginary part of element C13. Imaginary part of this element is used as the direct measure for imaginary part of the equation (4-6). Later this imaginary part will be used in the calculation of the imaginary part of the equation (4-7). Hence changes in this element will directly contribute to the model output. 100 samples were selected from this element before and after compensation to analyse the changes. The blue colour line in the Figure 5-22(b) shows the values from this element before compensation and the red colour line shows the values from this element after compensation. The graph from these values remains same at many points, at few points it shows some increase in values and decrease at some other points. The increase in values will be useful in calculating the model outputs by avoiding the assumption in the model mentioned in section 4.1.

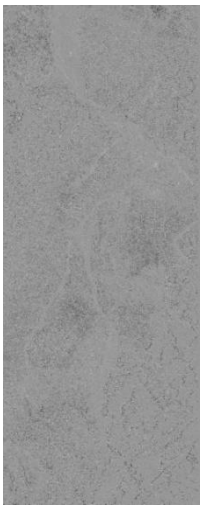

(a)

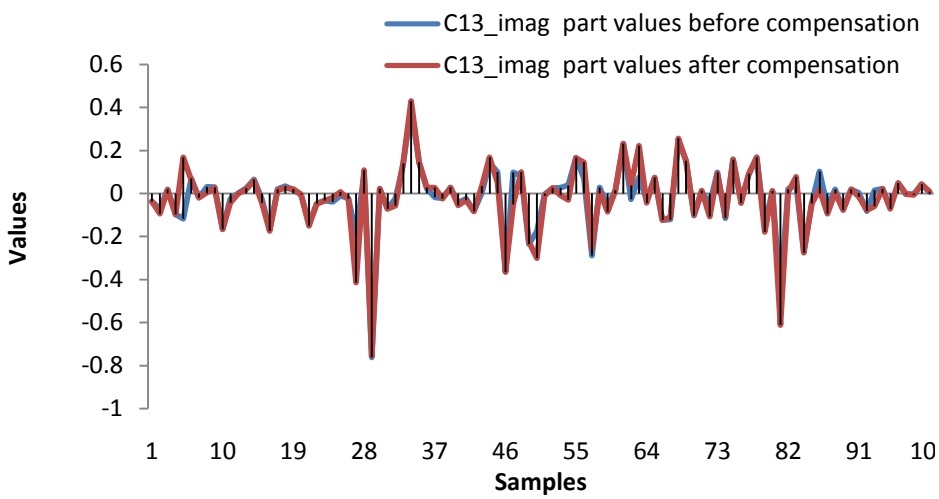

(b)

Figure 5-22: imaginary part of matrix element C13 (b) samples plots from the element

The Figure 5-23 (a) shows the real part of the element C23. This element is also assumed to be zero with the models basic assumption reflection symmetry. 100 samples were selected from element before and after the compensation of the matrix. The blue colour line in the Figure 5-23(b) shows the values of this

element before compensation and the red colour line in the same plot showing values of this element after compensation. Same as element C12 real part this element also showing no proper increase or decrease in values after compensation for polarization orientation angle shift compensation by analysing changes in red line with respect to blue line.

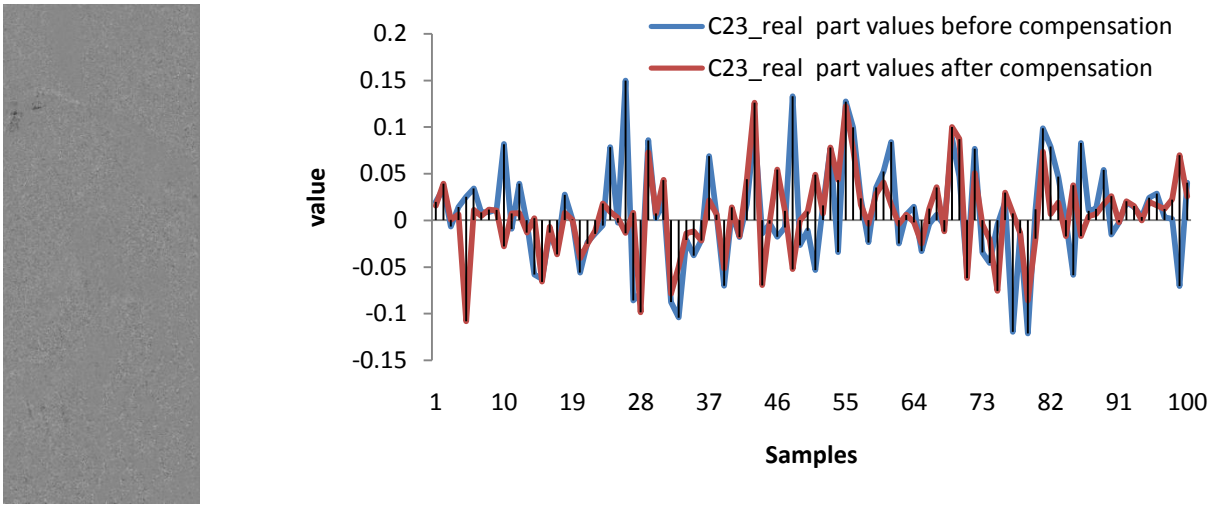

(a) (b)

Figure 5-23: (a) Real part of matrix element C23 (b) samples plots from the element

The same procedure of selecting 100 samples from the matrix before and after compensation was done. The Figure 5-24 (a), (b) shows the image of imaginary part of this element C23 and plots of values from this element respectively. This element also shows no proper values changes in values after the compensation by analysing changes in red line with respect to blue line.

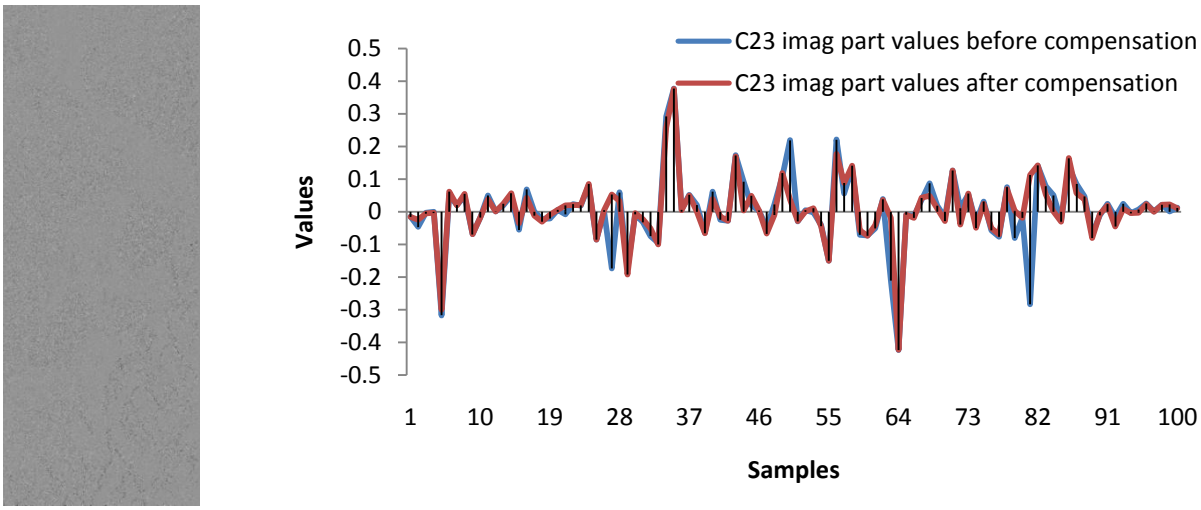

(a) (b)

Figure 5-24: (a) imaginary part of matrix element C23 (b) samples plots from the element

As a concluding remark, elements C12, C23 real and imaginary parts and C13 imaginary part are having changes after the compensation but they are not consistent as shown in Figures 5-19,5-20, 5-22, 5-23, and 5-24 (at some points there are increase and at some points there are decrease). The element C13 real part is relatively unchanged is shown in Figure in 5-21.

The average increase in values between the selected 100 samples shows 1.508539 db and average decrease is -0.4028063 db in C22 and C33 elements when their magnitudes are considered. Overall the OA shift compensation leads to reduction in volume scattering power and increase in the double bounce and

relatively unchanged surface return. Any results that can be obtained from the uncompensated data can produce the erroneous scattering characteristics which lead to misinterpretation. The Freeman-II decomposition technique which totally depends on the data for modeling different scatters could possibly over estimates the volume scattering contribution if the data is not compensated.

5.5. Analysis on the coherency matrix diagonal elements

The calculation of the OA shift was done using the coherency matrix by converting the covariance matrix into coherency matrix. It is needed to analyse the changes in the coherency matrix element also. The Figure 5-25 shows the coherency matrix diagonal elements.

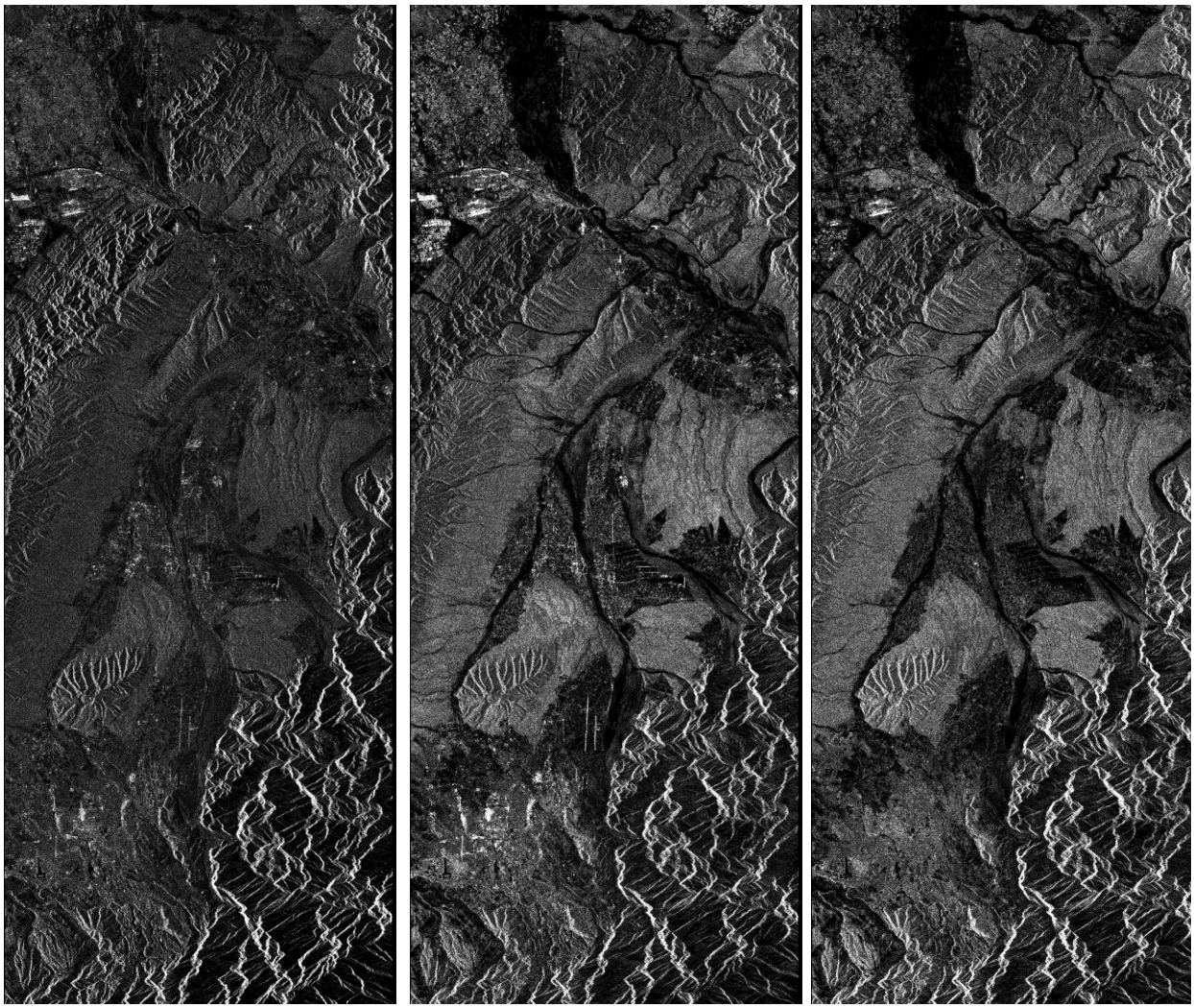

(a) (b) (c)

Figure 5-25: (a) Coherency matrix element T11 (b) coherency matrix element T22 (c) coherency matrix element T33

Unlike the covariance matrix, the coherency matrix is generated by expressing the data in Pauli basis as given in the equation (3-13). The coherency matrix element $T11 = \langle|S_{HH} + S_{VV}|^2\rangle$ shows the response from the surface return, the matrix element $T22 = \langle|S_{HH} - S_{VV}|^2\rangle$ represents the double bounces present in the data and the element $T33 = 4\langle|S_{HV}|^2\rangle$ represent cross polarized power which is more sensible to volume scattering and is equivalent to C22 element of covariance matrix. A sample of 100 points has been selected throughout the matrix element to find the effect of OA shift compensation.

5.5.1. Results of analysis on diagonal elements of matrix

Hundred (100) samples from each diagonal element T11, T22 and T33 of coherency matrix created before and after compensation were selected. The selected samples from element T11 is plotted in Figure 5-26 with blue and red colour lines representing values of samples before and after polarization orientation angle shift compensation respectively. The results of the coherency matrix are more promising when compared with the results of covariance matrix. After the compensation, the red line is showing no changes with respect to blue line. It shows coherency matrix element T11 remains constant and shows roll invariant property.

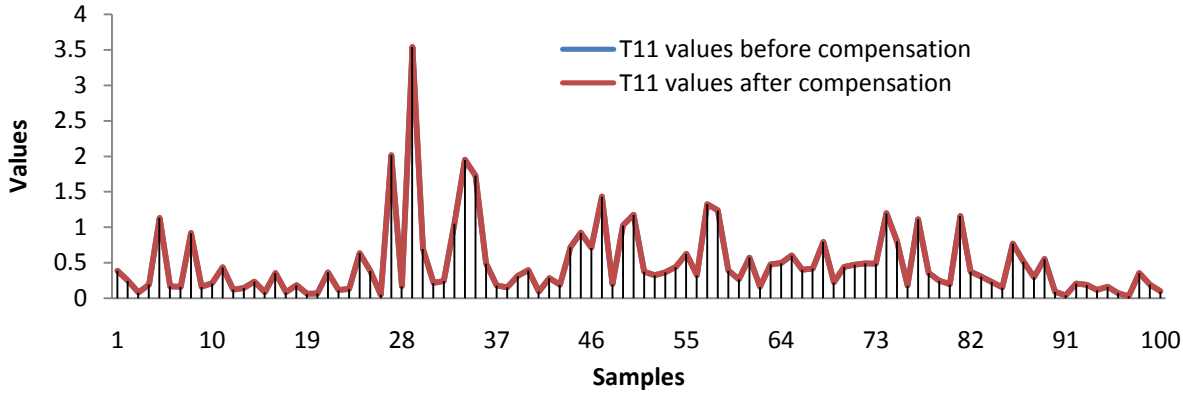

Figure 5-26: Samples plot of element T11

The element T22 represents the double bounce present in the data unlike covariance matrix element C22 which represents the volume scattering. 100 samples were selected from the element before and after compensation. The Figure 5-27 represents the graphs of the selected samples. The blue colour line in the graph represents the values from the element before compensation and the red colour line represents the values from element after polarization orientation angle shift compensation. There is increase in values of the red lines with respect to blue line. It shows a clear increase in the values of double bounce power after compensation.

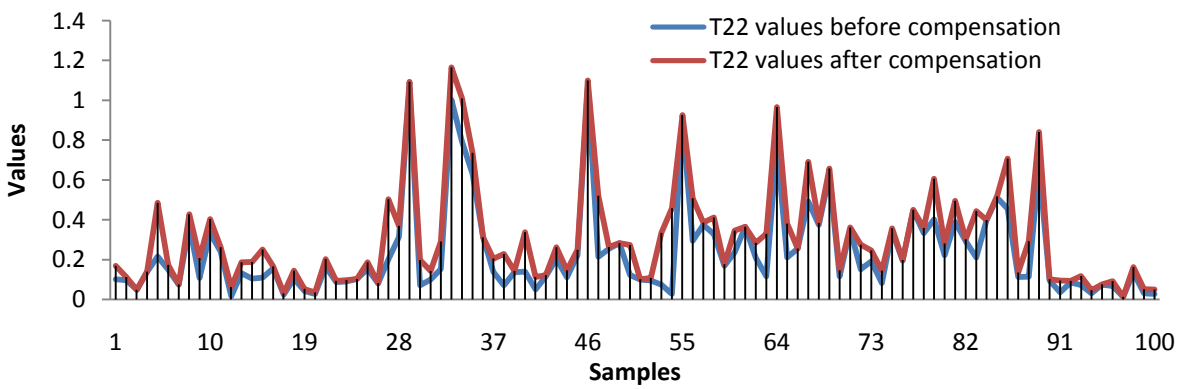

Figure 5-27: Samples plot of element T22

The T33 element represents the volume scattering present in the data. 100 samples were selected in order to analyse the results in the matrix element after compensation. Figure 5-28 shows the result obtained from this element. The blue colour line in this figure represent the values of element before compensation and the red colour line represents the values of element after compensation. The red line shows reduction in values with respect to blue line. The same phenomenon like covariance matrix the coherency matrix element also shows reduction in volume scattering values after compensation.

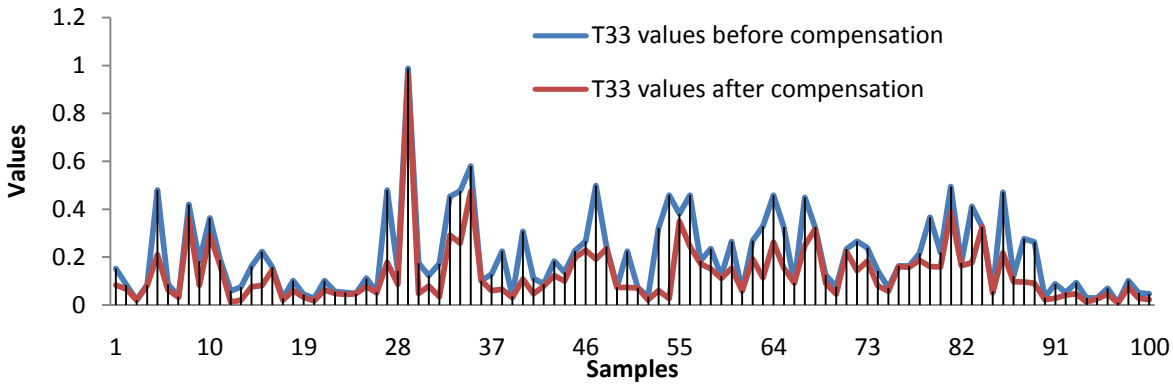

Figure 5-28: Samples plot of element T33

As a concluding remark the coherency matrix diagonal elements shows clear results for double bounce element than the covariance matrix. It shows a constant surface scattering power in element T11, increase in double bounce power in element T22 and reduction in volume scattering power in element T33.

5.5.2. Span of coherency matrix

The coherency matrix diagonal elements maintain the total power. The total power of this matrix is the addition of diagonal elements and called as span. To analyse changes in total power of coherency matrix 100 samples been selected from the span of the coherency matrix. The Figure 5-29 shows the plot of selected samples. The blue colour line represents span values before compensation and red lines showing span values after compensation. With no change in red lines with respect to blue line shows span of the coherency matrix also remains unchanged.

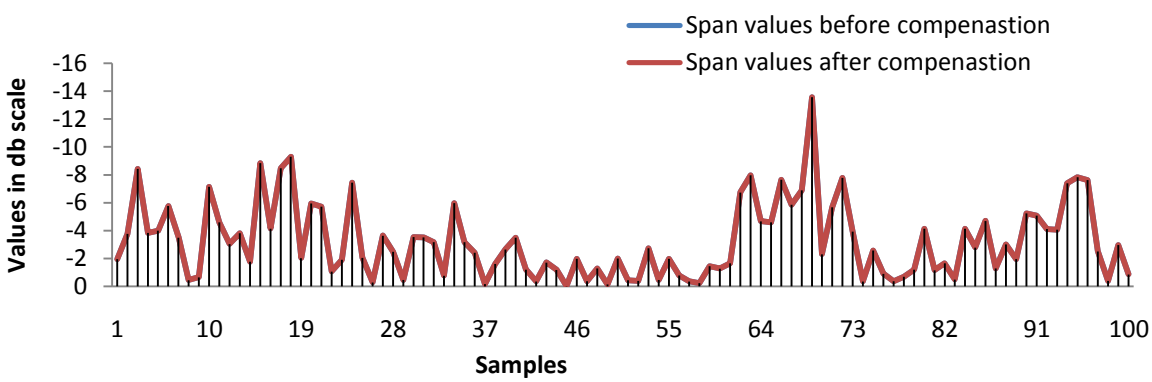

Figure 5-29: Span of coherency matrix

As a concluding remark, span of matrix represents the total power and it is the sum of all diagonal elements. With the element T11 remains constant after compensation and changes being occurring in between elements T22 and T33 the relationship between these changes can be analysed. Covariance matrix also shows the same phenomenon. The relationship between power increased in double bounce and power decreased in the volume scattering component was analyzed using the difference in values calculated for the same pixels before and after orientation angle shift compensation and it is shown in Figure 5-30. The blue colour line in the same figure shows a same amount of increase in values with the amount of decrease in values shown in red colour.

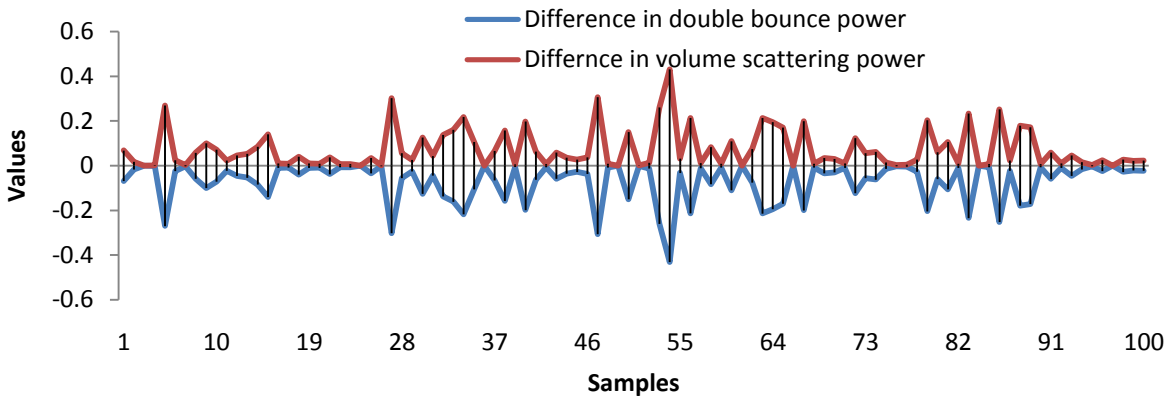

Figure 5-30: Difference in values of T22 and T33 elements before and after polarization orientation angle shift compensation

5.6. Analysis on off-diagonal elements of coherency matrix

The equation (3-15) for the calculation of orientation angle utilises the off diagonal elements also. The effect on various other elements of coherency matrix needs to be considered since compensation was performed in coherency matrix. Same procedure of collecting samples over the various matrix elements and plotting them to identify the difference is adopted. The Figure 5-31and 5-32 is showing the image and samples plot form the real and imaginary part of the element T12. 100 samples were selected throughout the image before and after compensation. The blue lines in the Figure 5-31 and 5-32 (b) representing the values from this elements real part and imaginary part before compensation and red colour lines representing the values from this elements real part and imaginary part after compensation. Changes happening in red line with respect to blue line show no proper increase or decrease in values. The compensation is not having any proper effect in these matrix elements. They tend to increase at some points and decrease at some other point.

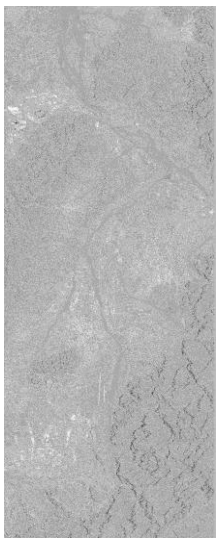

(a)

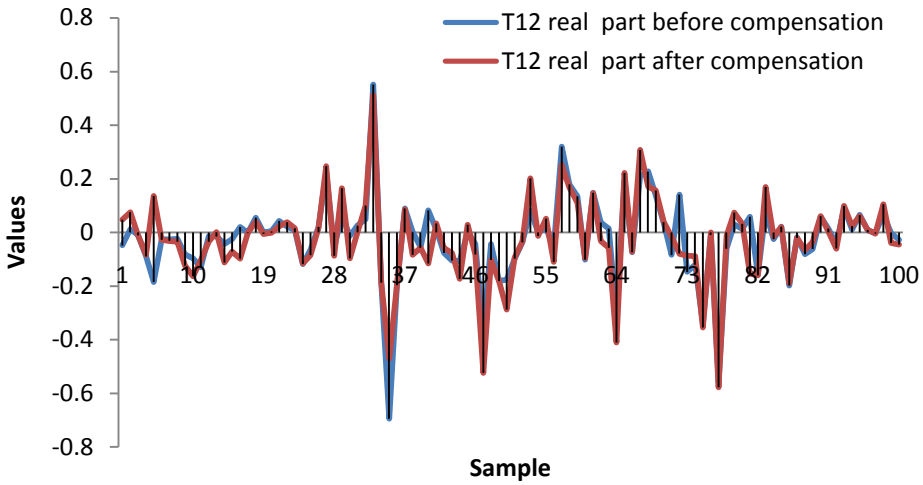

(b)

Figure 5-31: (a) Real part of matrix element T12 (b) samples plot from the element

(a)

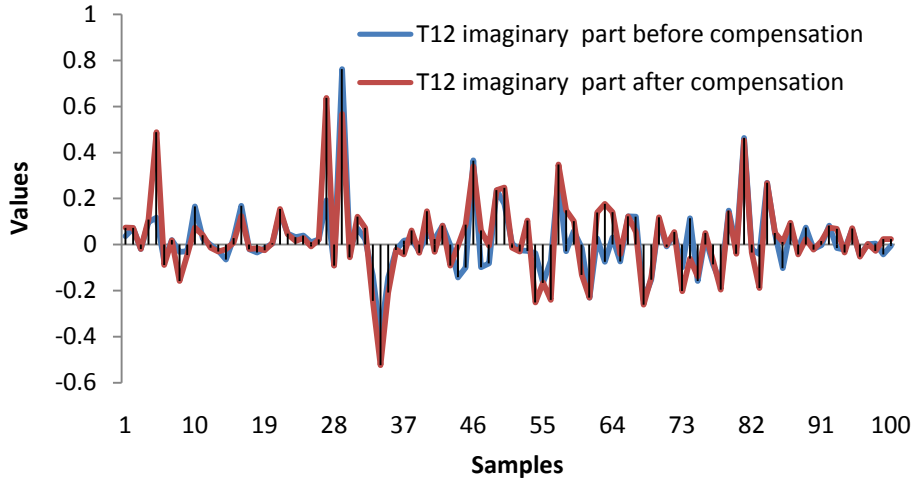

(b)

Figure 5-32: (a) imaginary part of matrix element T12 (b) samples plot from the element

The Figure 5-33 and 5-34 (a) shows the image of real and imaginary parts of element T13. 100 samples been selected from this element before and after the compensation. The blue colour lines in the Figure 5-33 and 5-34 (b) show the values before compensation and red colour line show the values after compensation. These elements are not showing any proper effects by the compensation. Same as the element T12 in Figure 5-31and 5-32 the element T13 also shows no proper increase or decrease in the values after compensation.

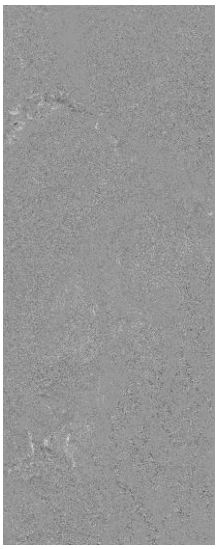

(a)

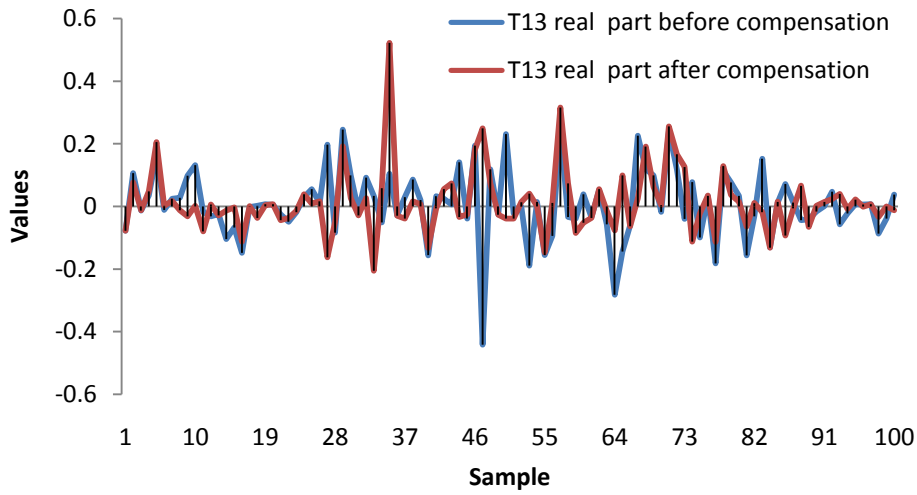

(b)

Figure 5-33 (a) real part of matrix element T13 (b) sample plots from the element

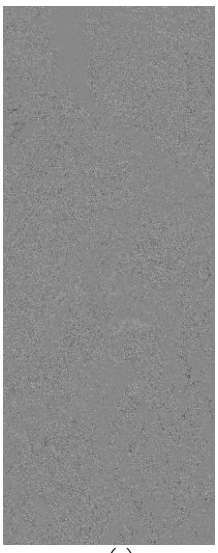

(a)

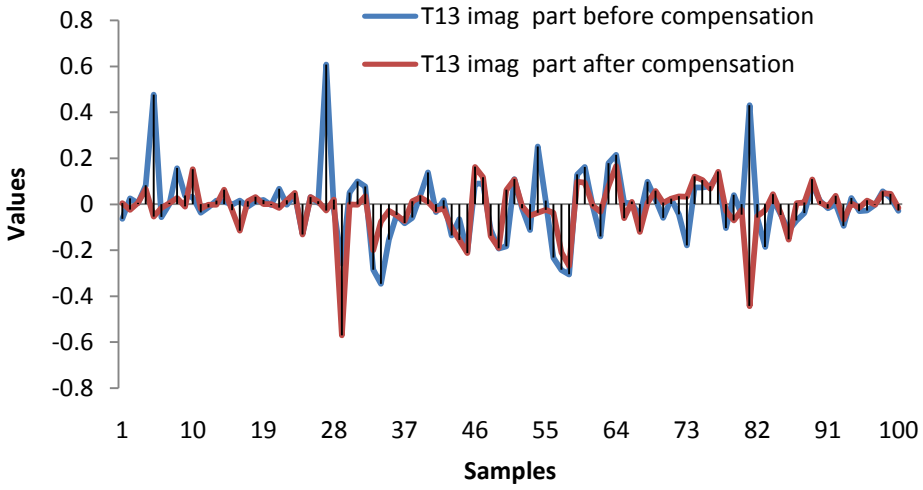

(b)

Figure 5-34: (a) imaginary part of matrix element T13 (b) samples plots from the element

Same procedure has been adopted in element T23. The Figures 5-35 and 5-36 (a) shows the image of real part and imaginary part of this element. The blue line in Figures 5-35 and 5-36 (b) shows values before compensation and redline shows value after compensation. In contrast to any element of the covariance matrix, the real part of the element T23 reduces to zero after compensation and it is shown in Figure 5-35(b) in red line. The imaginary part of the element T23 remains the same after compensation and shows its roll invariant property in Figure 5-36 (b).

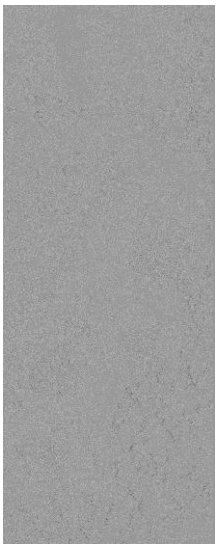

(a)

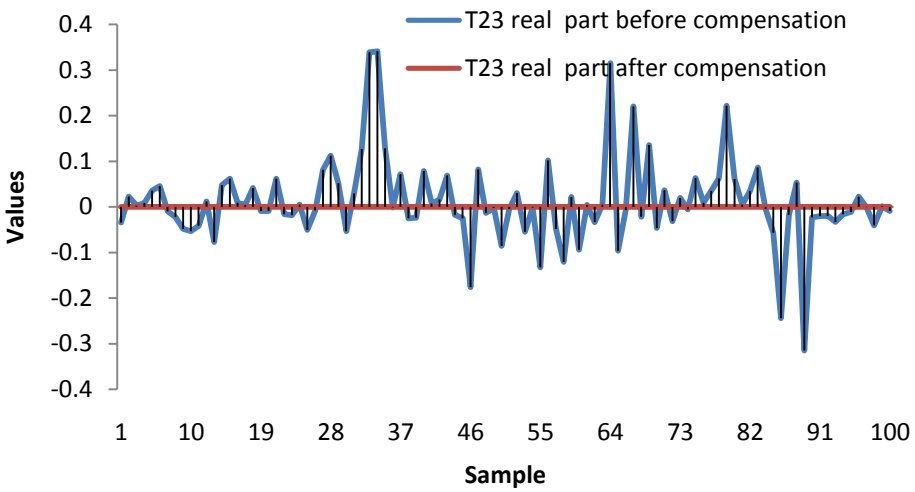

(b)

Figure 5-35: (a) Real part of matrix element T23 (b) samples plots from the element

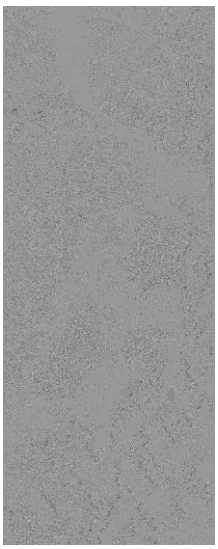

(a)

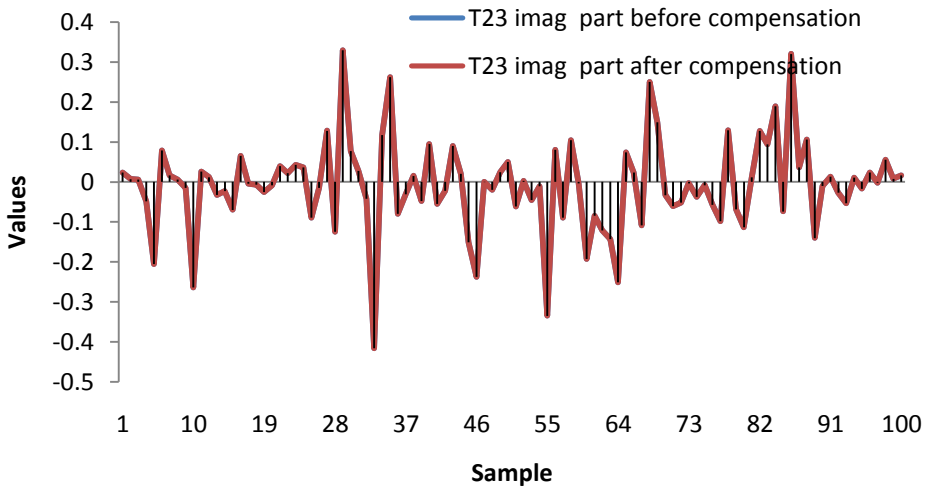

(b)

Figure 5-36: (a) imaginary part of matrix element T23 (b) samples plots from the element

As a concluding remark, coherency matrix shows some kind of difference from covariance matrix. The real part and imaginary parts of the matrix element T12 and T13 shows no pattern of change (either increase or decrease). The real part of the element T23 has been reduced to zero after compensation which is different from any of the covariance matrix element and also the imaginary part remains the same after compensation. Overall decrease in the average amplitude values of T22 element between the collected 100 samples is -1.50593 db and the increase in the amplitude values between the same samples are 2.054384 db which is greater when compared to the decrease and increase in power of covariance matrix. From the analysis of the various elements of both matrices, surface return is not been affected by the shift in the orientation angle and it is roll invariant and double bounce power and the volume scattering power has been affected by increase and decrease in power of equal amounts respectively.

5.7. Freeman – II Decomposition – surface scattering

In order to analyse the effect of polarization orientation angle shift in Freeman-II model, it has been applied in data before and after compensation. The effect of orientation angle shift compensation was analysed by selecting the area for particular scattering mechanism, in general related to the double bounces in surface output generated by the model for surface scattering. Two bridges have been selected since it is a perfect location for doubles bounce. The Figure 5-37(a) is showing the location of brides in the image. The Figure 5-37 (b) and (d) is showing the modelled response from the bridge. Due to over estimation of volume scattering, response from the bridge is not properly modelled and is clearly visible in same figure.

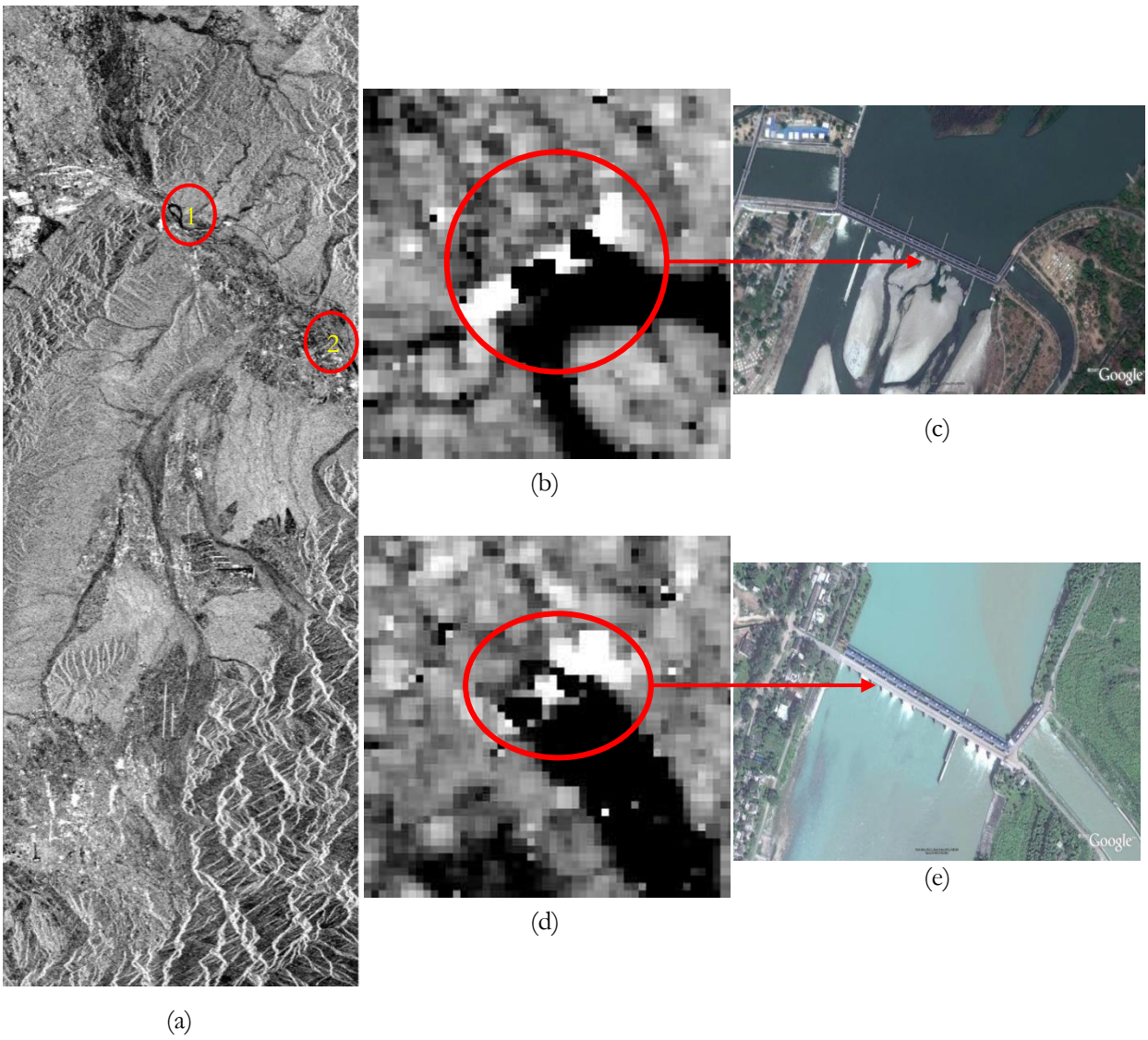

(a) (b) (c) (d) (e)

Figure 5-37: (a) Freeman-II model output for direct ground return before OA shift compensation (b) bridge at Rishikesh (c) Google image of bridge at Rishikesh (d) Bridge Laxman jhoola (e) Google image of the bridge Laxman jhoola.

The effect of changes on the matrix elements shows that the volume scattering power which has been generated without the compensation is erroneous. The areas selected in the surface scattering image generated by the Freeman-II model is the barrage at Rishikesh and the other is the bridge Laxman jhoola, the reference Google image of these bridges has been shown in Figure 5-37 (c) and (e). Due to alignment of bridges, orientation angle shift is clearly possible. Hence power from these regions has been over estimated as volume scattering power.

5.7.1. Freeman-II decomposition after orientation angle shift compensation

After compensation for orientation angle shift ,the reduction in the volume scattering power was shown in Figure 5-8 and Figure 5-28 and the consequent increase in double bounce power was shown in Figure 5-9 and Figure 5-27. This increase and reduction leads to correct estimation of response from these bridges as double bounce area is shown in output generated by the Freeman-II model after compensation for orientation angle shift in Figure 5-38 (b) and (d).

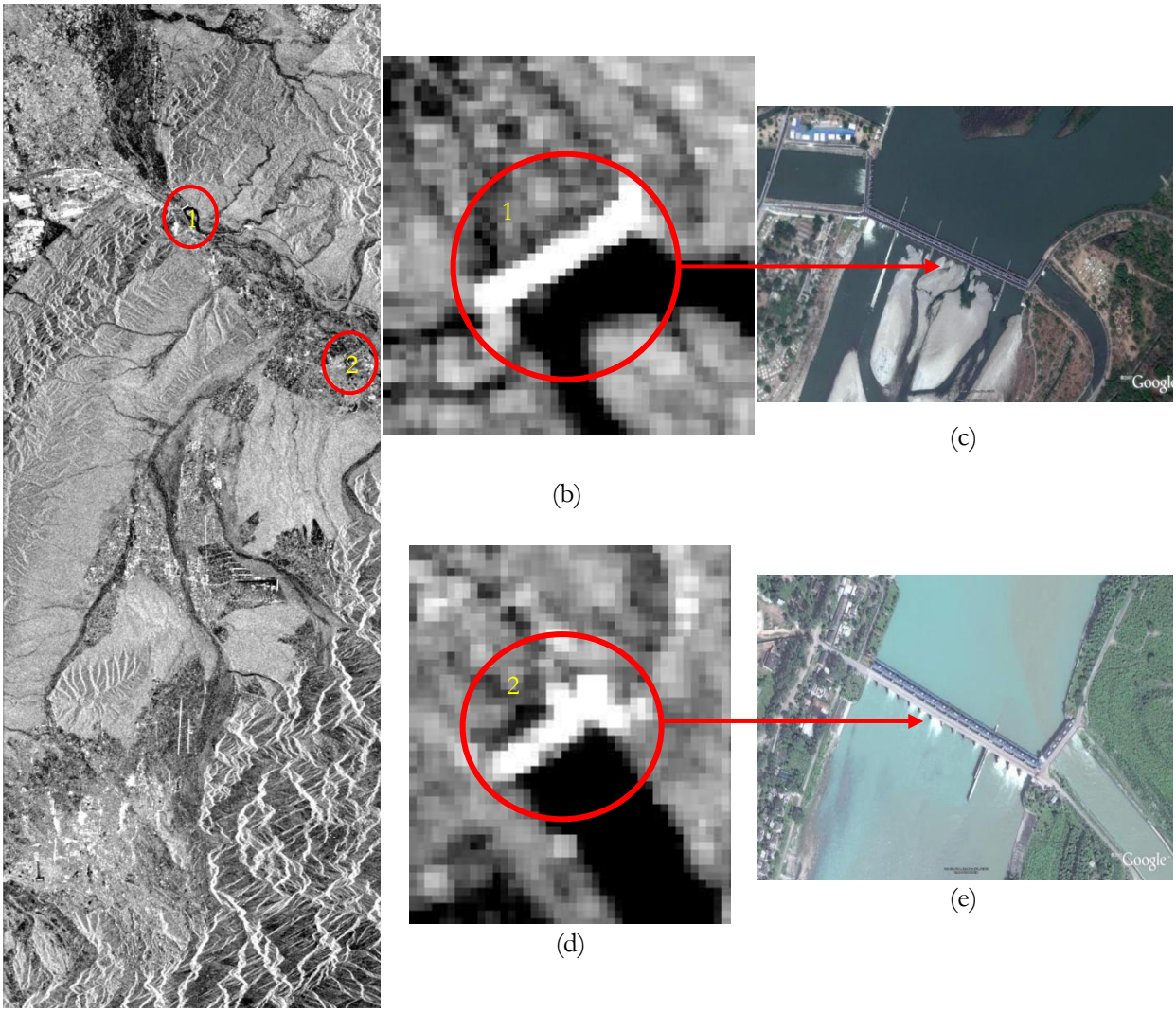

(a) (b) (c) (d) (e)

Figure 5-38: (a) Freeman-II model output for direct ground return after OA shift compensation (b) Zoomed area showing Bridge at Rishikesh in location 1 (c) Google image of bridge at Rishikesh (d) Zoomed area showing Bridge Laxman jhoola in location 2 (e) Google image of the bridge Laxman jhoola.

For understanding of increase and decrease in power of volume scattering and surface return at points, same samples has been collected from outputs of Freeman-II decomposition before and after compensation for orientation angle compensation. In Figure 5-39 the plot of samples collected over both sides of two above mentioned bridges from volume scattering and surface return outputs before and after orientation angle shift compensation has been shown. The plot shows a clear increase in surface return values and reduction in volume scattering values for the same pixel. Hence the orientation angle shift compensation removes the effect of randomly oriented tagets.

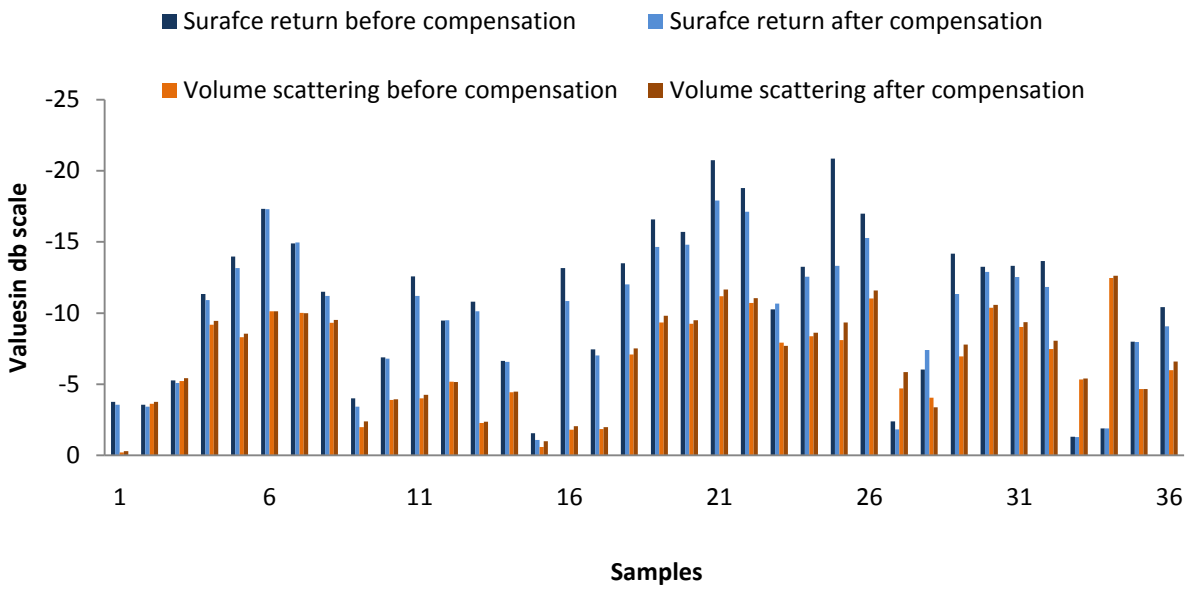

Figure 5-39: Plots showing increase in surface return values and reduction in volume bounce values for the same pixel after orientation angle shift compensation around the corner of the bridges.

The same phenomenon has been analysed with 100 random samples throughout the image. From the plots of the samples collected over the image a clear increase in the double bounce power has been evidenced as shown in Figure 5-40. The model over estimates some surface scattering regions as a volume scattering regions which lead to misinterpretation of features due to orientation angle shift. The orientation angle shift compensation reduces that effect and helps in the estimation of intrinsic vales from different scatter.

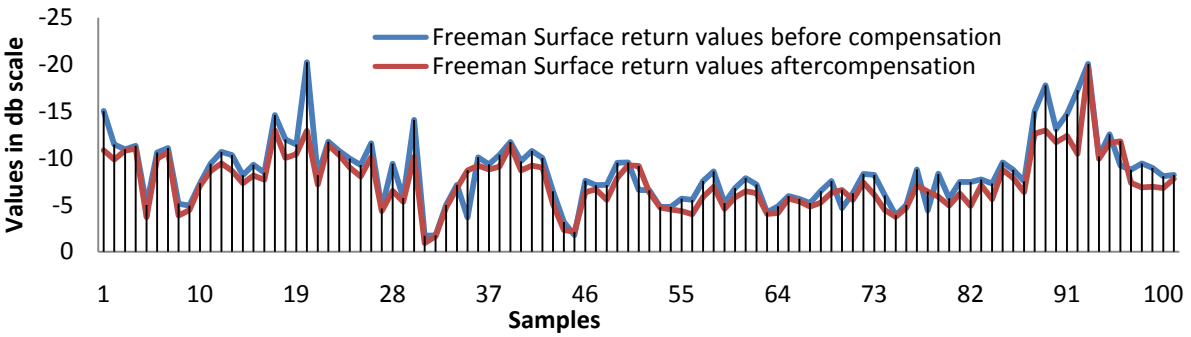

Figure 5-40: Samples plot from surface return of Freeman-II model.

The results of the model estimation are the direct contribution of the results in the Figure 5-8. The compensation helps in yielding same result from two identical targets with different orientation angle. Thus orientation angle shift compensation helps to identifying actual quantity of backscatter power from different scattering mechanism.

5.8. Freeman – II Decomposition–volume scattering

The changes in the volume scattering power has been analysed by selecting the dense forest area present in data which is shown in Figure 5-41. Fifty (50) samples from each of two forest patches has been collected and plotted. The blue colour line shows the value of volume scattering estimated by the model before compensation for orientation angle shift and the red line shows values estimated by model after compensation. The reduction in values of red line with respect to blue line shows reduction in the volume scattering power in Figure 5-41 and the over estimation has been avoided.

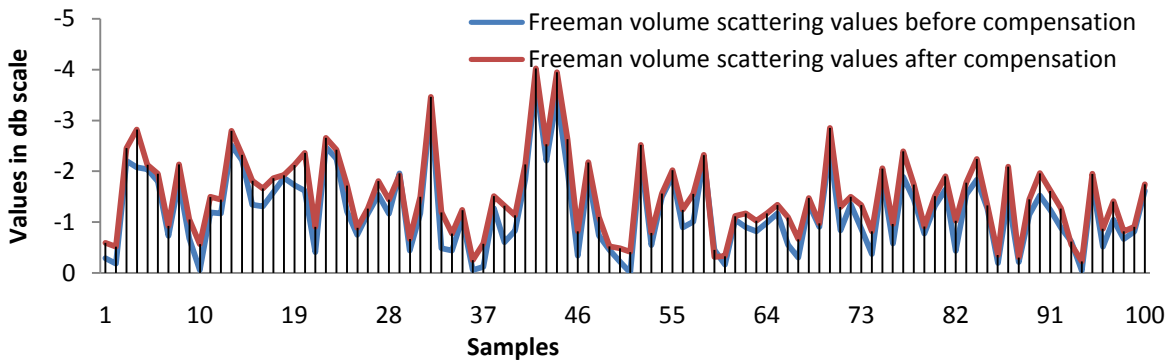

Figure 5-41: Sample plot from volume scattering of Freeman-II model in the selected forest region

Since the model uses the depolarization for the estimation of the volume scattering power compensation of orientation angle shift reduces the effect of de-polarization. With the reduction in effect of de-polarization estimation of volume scattering power and area with over estimation of the volume scattering power been reduced and intrinsic scattering mechanism is revealed. The Figure 5-43(a) shows the area selected for samples to analyse the effect of orientation angle shift compensation in volume scattering power.

Sample of 100 values over entire image also been selected and Figure 5-42 shows the plot. The reduction is happening in values estimated as volume scattering contribution.

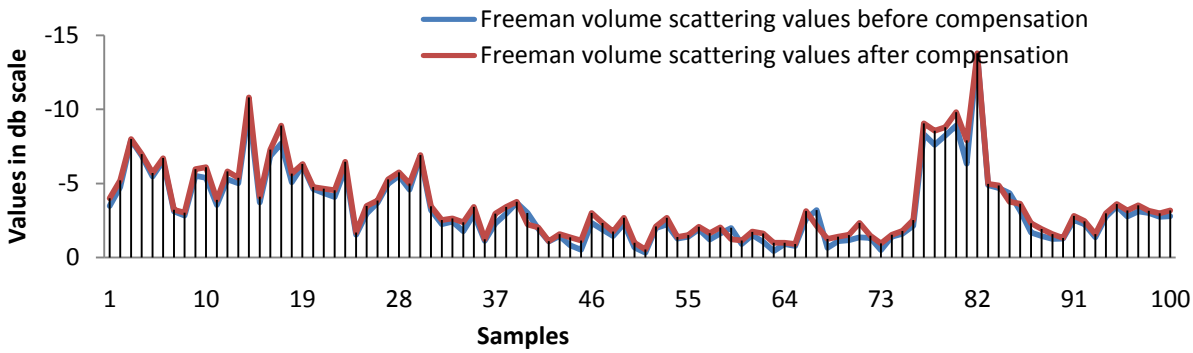

Figure 5-42: Sample plot from volume scattering of Freeman-II model collected throughout the image

As concluding remark, changes in values of volume scattering element C22 of covariance matrix before and after compensation show a large amount of reduction in values in Figure 5-8. This reduction directly contributes to model for estimation of volume scattering power and results in avoiding over estimation.

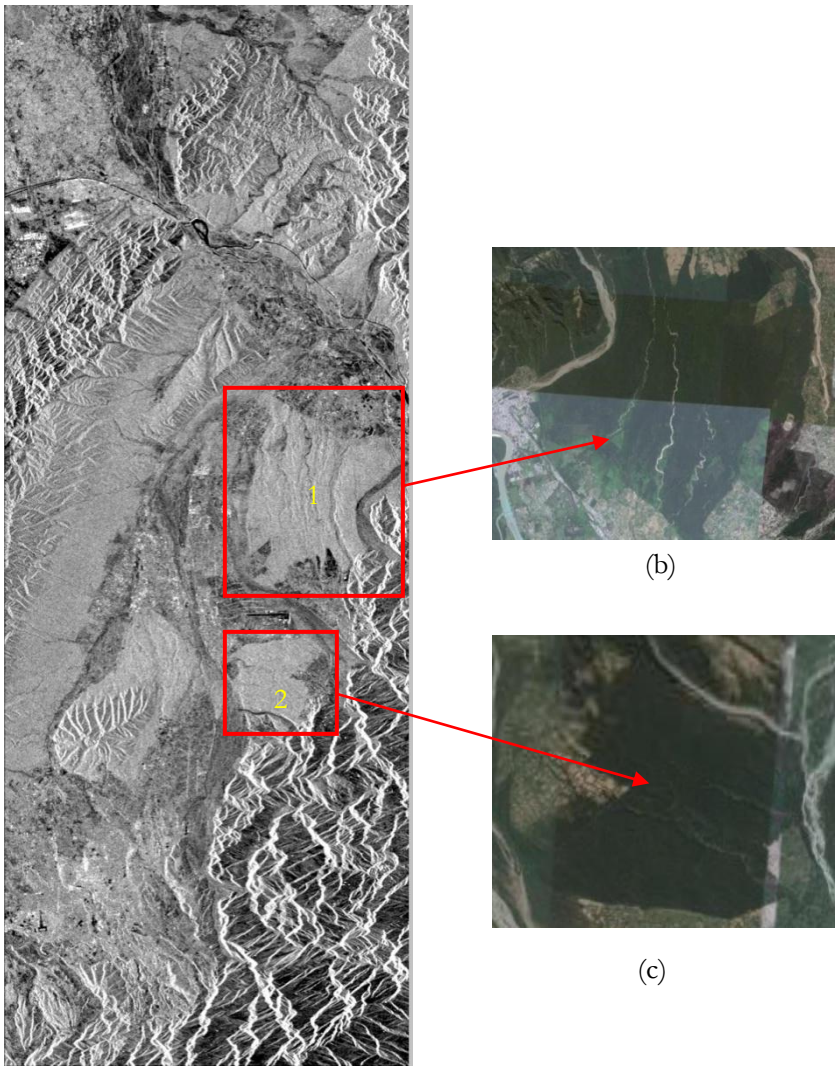

(b)

(c)

a)

Figure 5-43: (a) volume scattering power image generated by Freeman-II model (b) Reference Google image of marked area 1 (c) reference Google image of marked area 2.

Over all the estimation of volume scattering contribution and surface return contribution using Freeman-II model based decomposition technique results shows a clear influence of polarization orientation angle shift in estimation of different scattering mechanism. The compensation results in revealing exact quantity of different scattering mechanism. This has been shown in Figure 5-38 (b) and (d). As the model preserves the total power as shown in equation (4-13), and the span remains constant after orientation angle sift compensation the analysis for relationship between total reduction in power from surface scattering values and volume scattering values was carried out. The sample values selected throughout model output before and after compensation were used for this analysis. The difference in between values selected from surface return and difference in between values from volume return was plotted in Figure 5-44. The blue colour line shows difference in values from surface return and red colour line shows difference in values from volume scattering.

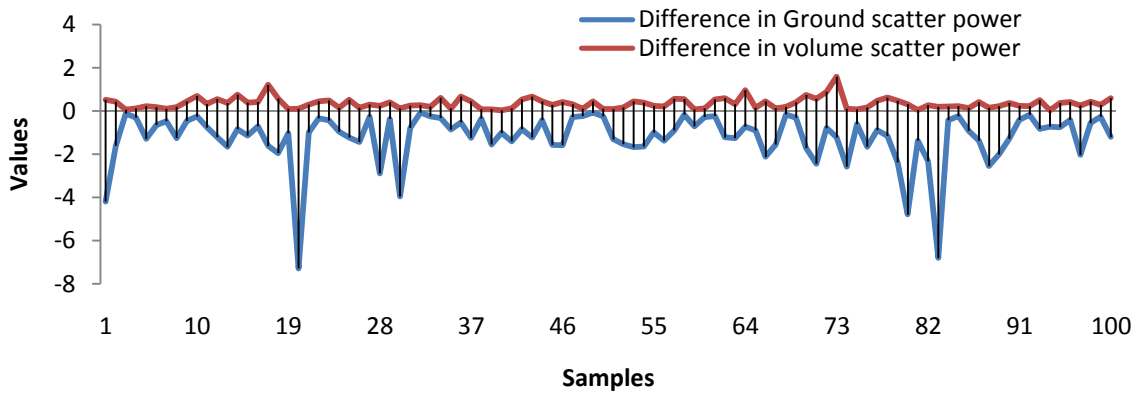

Figure 5-44: Difference in power generated for volume scattering and ground scattering power

The plot shows a clear representation of decrease in volume scattering power is not equal to the increase in the direct surface return power since the model utilises elements other than the cross-polarization component. Since the model has been shown to preserve the total power, the compensation of OA shift takes the modelled power close to total power is show in Figure 5-45. The figure shows plots between 20 samples for easy visualisation same result was obtained between all the 100 selected samples.

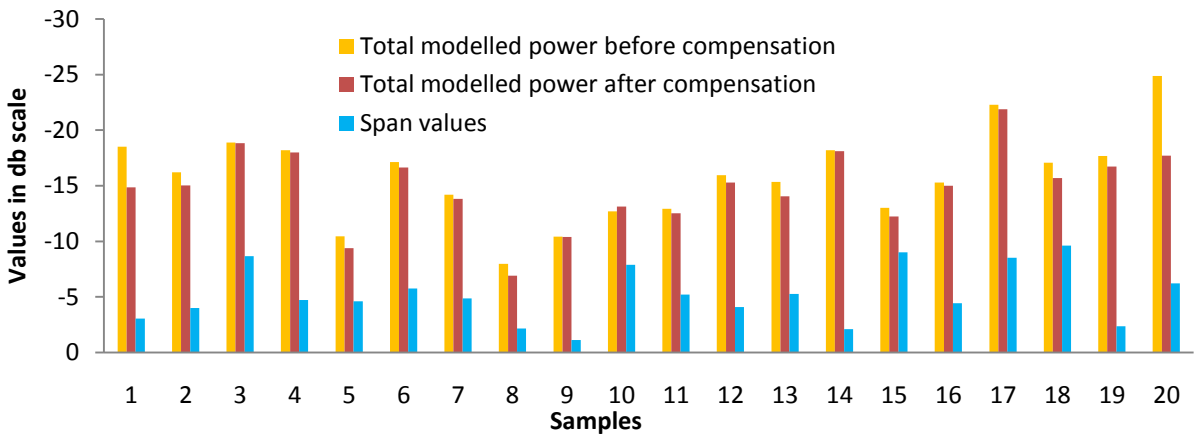

Figure 5-45: Plots between total modelled power before and after compensation and Span

This result shows a valid application of the de-orientation technique and its importance for the model based Freeman-II decomposition technique for calculating different scattering mechanisms.

5.9. Results from dataset one

5.9.1. Freeman – II Decomposition – surface scattering

The results under this section cover the results obtained from the remaining two data sets. The results produced form the dataset one as shown in section 3.1 is shown in the Figure 5-46(a).

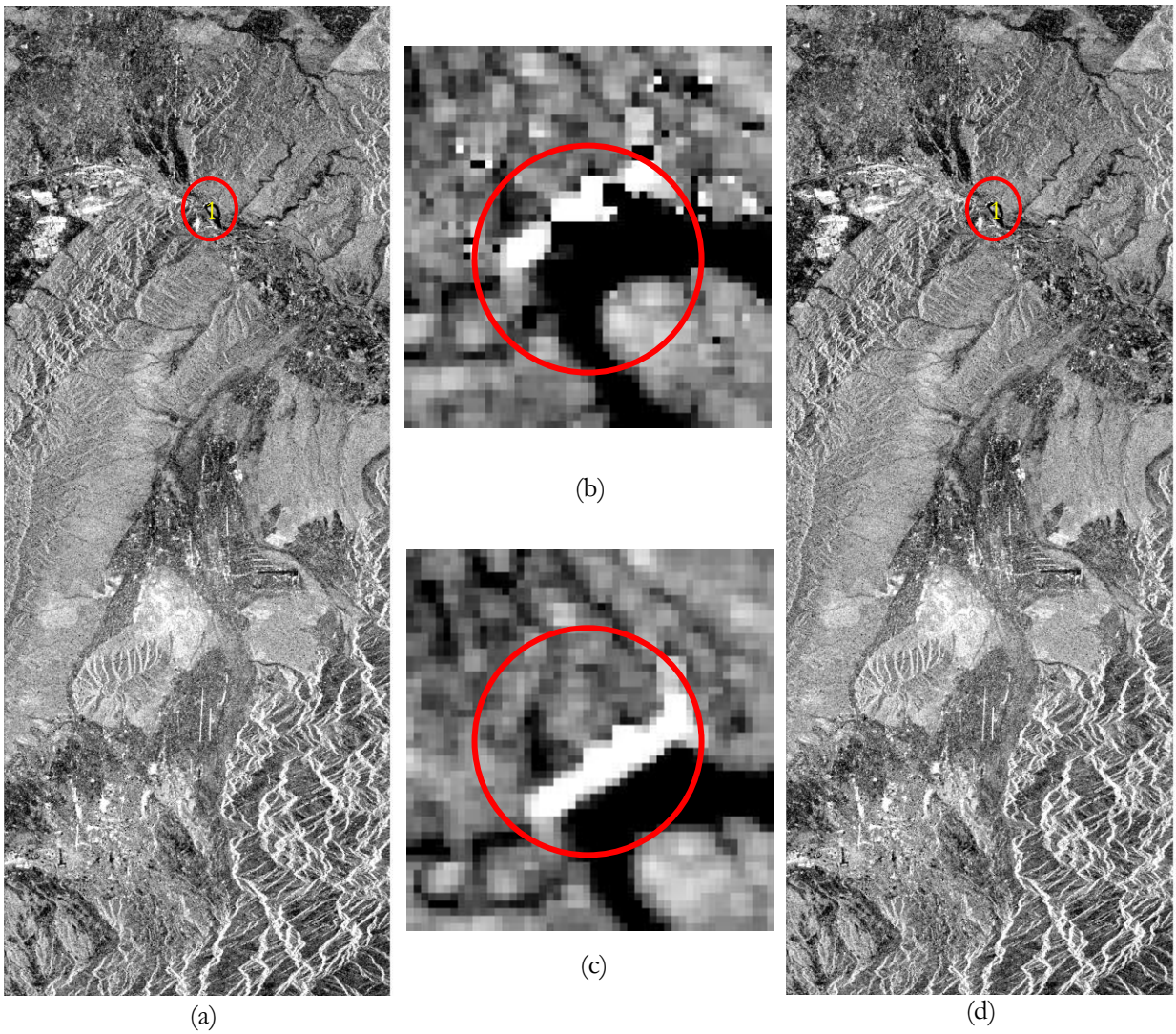

Figure 5-46: (a) Freeman-II model output for direct ground return before OA shift compensation (b) Zoomed area showing Bridge at Rishikesh in location 1 before OA shift compensation (c) Zoomed area showing Bridge at Rishikesh in location 1 after OA shift compensation (d)) Freeman-II model output for direct ground return after OA shift compensation

The dataset one used in the analysis has slight shift from the area covered by dataset two. Due to the shift the data was not covering both the bridges so only one bridge has been taken into consideration and is shown in Figure5-46(b) and(c). The pixels on the both corners of the bridge were selected from the output produced for Freeman-II ground return and volume scattering before and after orientation angle shift compensation. The plot in Figure 5-47 is showing results of these values. Same kind of results of reduction in volume scattering power and increase in surface return power was evidenced in this output also. The effect of the orientation shift compensation in identifying different scatters proved to be effective.

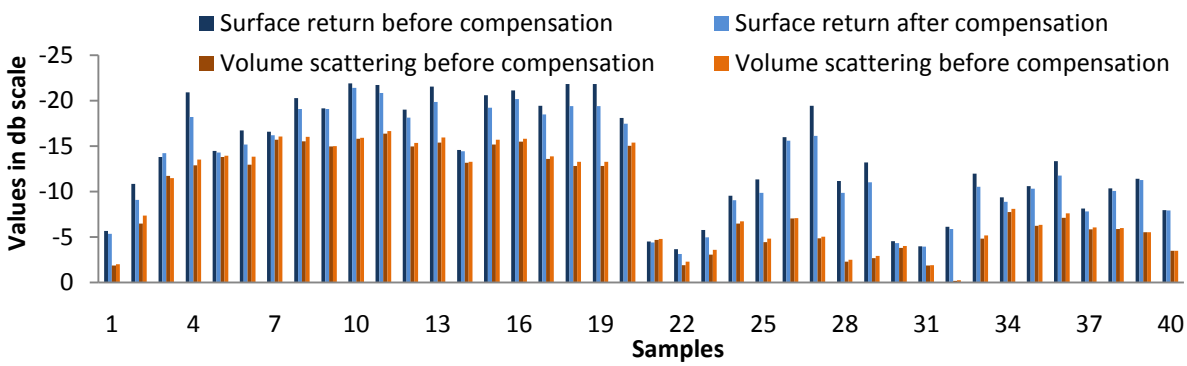

Figure 5-47: Plots showing increase in ground return values and reduction in volume bounce values for the same pixel after OA compensation around the corner of the bridge.

5.10. Results from data set three

These results are from data set three given in section 3.1. The locations considered in the data contain road strip at the bottom of the image and a bridge at the top of image.

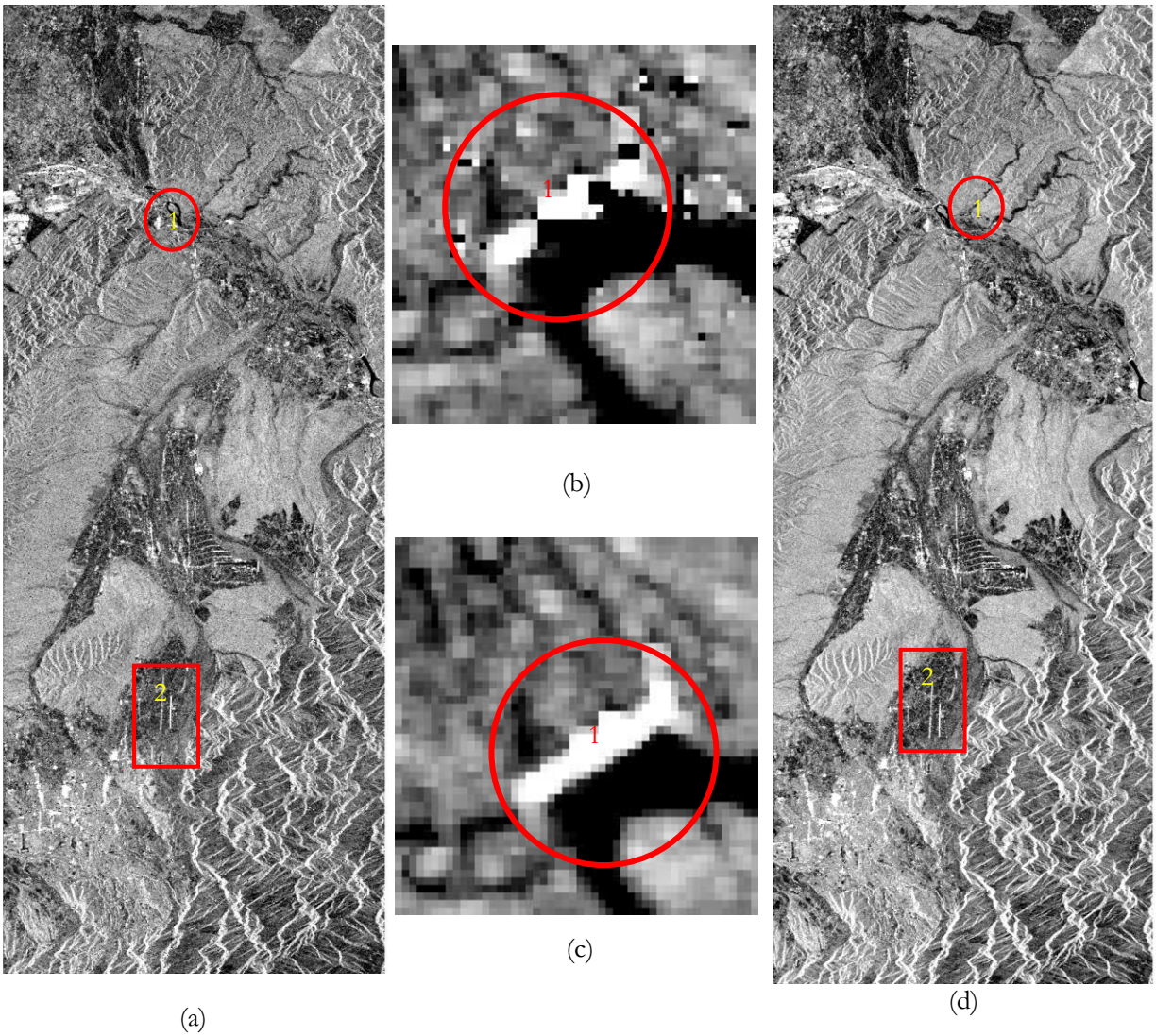

Figure 5-48: : (a) Freeman-II model output for direct ground return before OA shift compensation (b) Zoomed area showing Bridge at Rishikesh in location 1 before OA shift compensation (c) Zoomed area showing Bridge at Rishikesh in location 1 after OA shift compensation (d)) Freeman-II model output for direct ground return after OA shift compensation

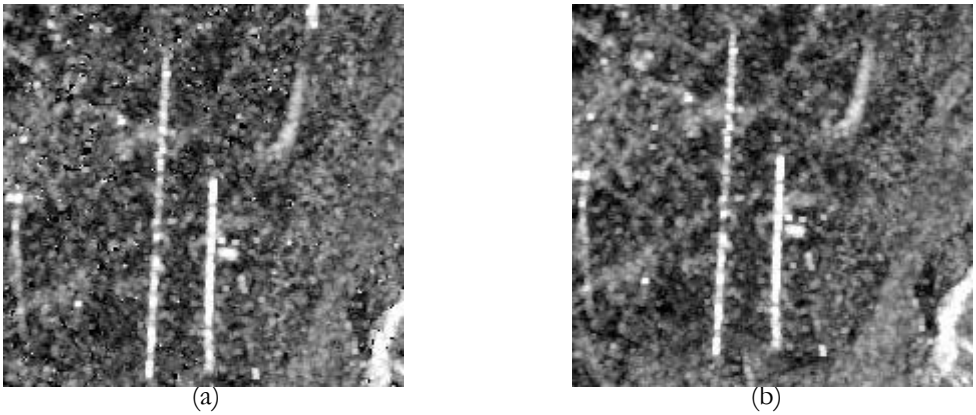

(a) (b)

Figure 5-49: (a) Zoomed area showing road strip in location 1 before OA shift compensation (b) Zoomed area showing road strip in location 1 after OA shift compensation

The area selected at the bottom is a strip of road which accounts for the direct surface return. The results below show increase in values of direct ground return and decrease in values of volume scattering in Figure 5-50 for the considered bridge at location 1 shown in Figure 5-48(a).

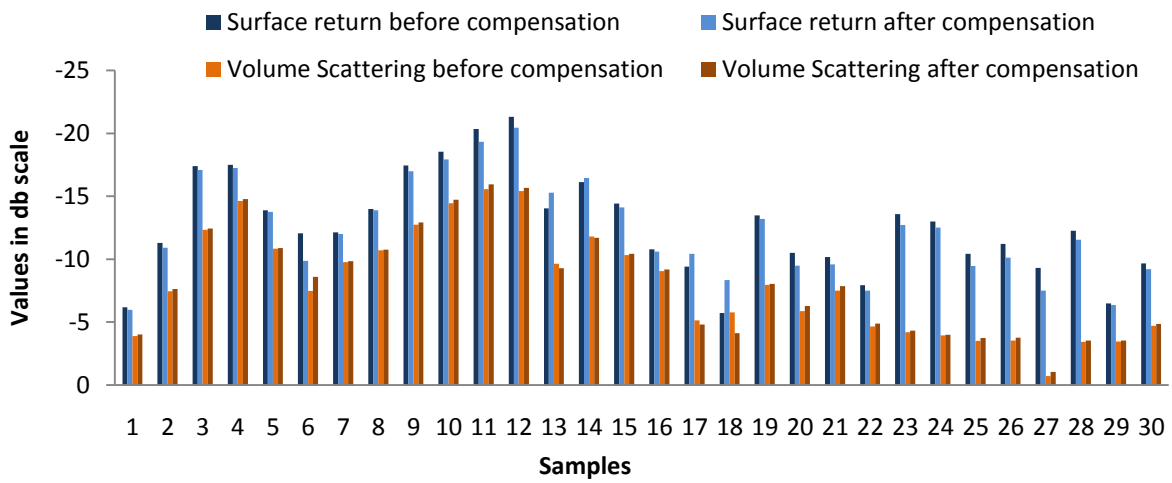

Figure 5-50: Plots showing increase in surface return values and reduction in volume scattering values for the same pixel after orientation angle shift compensation around the corner of the bridge.

Samples around the road strip shown at location 2 in Figure 5-48(a) was collected from the outputs by Freeman-II model after and before compensation. The result in Figure 5-51 shows increase in surface return values and decrease in volume scattering values for same pixel. This result holds with results of dataset one and two. These results are added validation for the results produced by the dataset two. It confirms that orientation angle shift in data leads to over estimation of volume scattering power. The compensation bring the

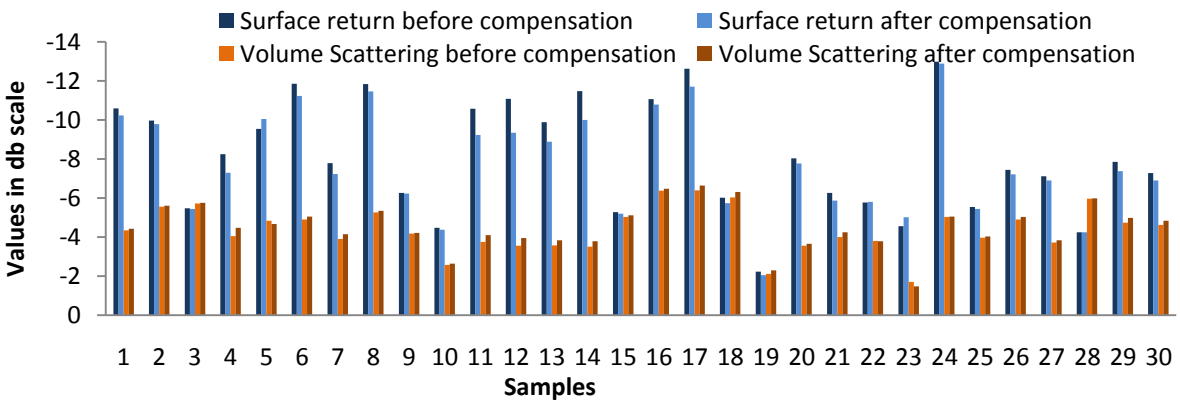

Figure 5-51: Plots showing increase in ground return values and reduction in volume bounce values for the same pixel after OA compensation in the road strip.

The results produced by different dataset shows the need for orientation angle shift compensation which helps in producing same results from two identical targets of different orientation. Hence the valid compensation of orientation angle shift helps to identify intrinsic scattering mechanisms.

6. CONCLUSIONS

This chapter concludes results of the method discussed in section 3.3. This chapter is outlined to give answers to each research question from the section 1.3.

The prime focus of this study was to analyse the effect of the OA shift effect in identifying different scatterers in ALOS PALSAR L-band fully polarimetric data.

6.1. Which polarimetric SAR element is used to represent the polarization orientation shift of tree trunks and surface scatterer?

The prime focus of this study is to calculate polarization orientation angle shift produced by under lying terrain. Without using any external data and from the polarization information this analysis was carried out. Hence identification of PolSAR element to calculate the polarization orientation angle shift is mandatory. The equation (3-15) used for calculation of polarization orientation angle shift. This equation uses only the elements of PolSAR data which are represented using coherency matrix. Thus the elements used to represent or calculate the orientation angle shift are Real part of the element T23, T22 and T33. In the same equation, real part of the element T23 is dividend so this element is the measure of orientation angle shift. And after compensation for orientation angle shift as shown in Figure 5-35(b) it reduces to zero proves there is no more shift present in the data after compensation.

6.2. What could be the effect of Signal to noise (SNR) in identifying different scatter?

The effect of SNR was analysed between total power of single look complex image and the Multilook complex image. The result from section 5.1 proved as a validatory analysis for this research question. The Figures 5-1 and 5-2 shows analysis for standard error in calculating span of matrix from a single look complex image and Multilook complex image. The standard error is the estimation of influence of noise. The Multilook image is generated by averaging adjacent pixels as explained in section 3.3.1. The results produced for standard error in multi look image drops to 0.2 db after averaging 40 pixels, where as a single look complex needs to average 130 pixels to bring standard error to 0.2 db (level showed in [11]). Hence in Multilook image the influence of noise is minimised. This research used Multilook image for application of Freeman-II decomposition technique. Hence in identifying different scatter the effect of noise is minimised by Multilooksetup.

6.3. What could be the improvement in the results produced by Freeman-II model after orientation angle shift compensation?

The Freeman-II model based decomposition technique for PolSAR data uses polarization property for estimating different scattering mechanism. Due to the polarization orientation angle shift the de-polarization measure increases. This results in over estimation of response from objects by the model before compensation. At locations shown in Figure 5-37, the model over estimates the response as volume scattering. As shown in Figure 5-8 the compensation leads to reduction in of volume scattering power of matrix element. This reduction directly contributes for model output. The output from the model after compensation shows the proper response from those objects in Figure 5-38. Since the polarization orientation angle shift compensation leads to the calculation of same response from objects with different orientation the model output in identifying different scattering mechanism is improved by increase in direct surface return and a reduction in volume scattering power in regions prone to surface returns. Also this compensation leads to reduction in power estimated from pure volume scattering zones also.

6.4. What will be the effect of de-orientation in volume scattering?

The volume scattering is measure of cross polarised power. This power will be measured using the de-polarization of wave. The polarization orientation angle shift can happen if the objects are not aligned in the line of sight of sensor. These shifts tend to de-polarize the wave and results in over estimation of volume scattering power. The de-orientation technique results in reduction of volume scattering power It also reduces the over estimation of volume scattering power in regions where surface scattering is dominant with reference to Figure5-8, 5-14(b) and 5-17(b).

6.5. How to validate the improvement in the result after modification in Freeman-II model?

The decomposition techniques are developed in order to identify different scattering mechanism. Hence these techniques need to identify intrinsic scattering response. From the results produced before and after compensation shown in Figure5-37 and 5-38, the ability of the Freeman-II model has increased to model responses from different objects. These zones where identified using a Google image as reference image. Also from the Figure 5-45, it shows that compensation takes the modelled power close to total power.

As a concluding remark to the thesis, since PolSAR data are sensitive to terrain slopes, proper estimation of terrain induced orientation angle shift is needed. The polarization orientation angle shift compensation will helps in identifying intrinsic quantity of responses from different object. Hence the covariance matrix needs to be compensated for terrain induced shift before applying the decomposition technique.

6.6. Recomendations

The study addressed the need for polarization orientation angle shift compensation in model based Freeman-II decomposition technique. This model decomposes the data to identify different scattering mechanisms. After compensation the effectiveness of model in revealing different scattering mechanism was improved.

The output generated by Freeman-II decomposition can be used as input for semi-empirical models like water cloud model to predict biomass. It can be taken as further step of this research.

With the reflection symmetry assumption the Freeman-II model utilises only five elements of the covariance matrix. The understanding and utilising remaining matrix element for the model based decomposition technique can improve the results produced by this model.

The Multilooksetup used in this research preserves resolution of scanning system of ALOS PALSAR quad-PolSAR data. Since results shows effect of noise in Multilooksetup is minimised, it can be generated to show one pixel representing one hectare which is 10000 m^2 and with reference to [28] the volume scattering power generated by Freeman-II model can be related to the calculated biomass per hectare using field observation. This work will predict the use of PolSAR data and decomposition technique for the purpose of calculating biomass.

REFERENCES

[1] Yunjin Kim and J. van Zyl, "Comparison of forest parameter estimation techniques using SAR data," *IGARSS 2001. Scanning the Present and Resolving the Future. Proceedings. IEEE 2001 International Geoscience and Remote Sensing Symposium (Cat. No.01CH37217)*, Sydney, NSW, Australia: , pp. 1395-1397.

[2] D.P. Lusch, "Intoduction to Microwave Remote Sensing," Center for Remote Sensing and Geographic Information Science Michigan State University, 1999.

[3] H. Maître, "Processing of Synthetic Aperture Radar Images," London,UK: ISTE Ltd, 2008.

[4] Pan Liang, M. Moghaddam, L. Pierce, and R. Lucas, "Radar backscattering model for multilayer mixed-species forests," *Geoscience and Remote Sensing, IEEE Transactions on*, vol. 43, 2005, pp. 2612-2626.

[5] D. Schuler, J. Lee, and G. de Grandi, "Measurement of topographic surface slopes using polarimetric SAR images," *Geoscience and Remote Sensing Symposium, 1994. IGARSS '94. Surface and Atmospheric Remote Sensing: Technologies, Data Analysis and Interpretation., International*, 1994, pp. 1467-1469 vol.3.

[6] D. L. Schuler T. L. Ainsworth J. S. Le, "Topographic mapping using polarimetric SAR data," *International Journal of Remote Sensing*, vol. 19, 1998, pp. 141-160.

[7] F. Holecz, A. Freeman, and J. van Zyl, "Topographic effects on the antenna gain pattern correction," *1995 International Geoscience and Remote Sensing Symposium, IGARSS '95. Quantitative Remote Sensing for Science and Applications*, Firenze, Italy: , pp. 587-589.

[8] J. Lee and T.L. Ainsworth, "The Effect of Orientation Angle Compensation on Coherency Matrix and Polarimetric Target Decompositions," *Geoscience and Remote Sensing, IEEE Transactions on*, vol. PP, 2010, pp. 1-12.

[9] S. Cloude and E. Pottier, "A review of target decomposition theorems in radar polarimetry," *Geoscience and Remote Sensing, IEEE Transactions on*, vol. 34, 1996, pp. 498-518.

[10] A. Freeman and S. Durden, "A three-component scattering model for polarimetric SAR data," *Geoscience and Remote Sensing, IEEE Transactions on*, vol. 36, 1998, pp. 963-973.

[11] A. Freeman, "Fitting a Two-Component Scattering Model to Polarimetric SAR Data From Forests," *Geoscience and Remote Sensing, IEEE Transactions on*, vol. 45, 2007, pp. 2583-2592.

[12] J. van Zyl, "Unsupervised classification of scattering behavior using radar polarimetry data," *Geoscience and Remote Sensing, IEEE Transactions on*, vol. 27, 1989, pp. 36-45.

[13] S. Durden, J. van Zyl, and H. Zebker, "Modeling and observation of the radar polarization signature of forested areas," *Geoscience and Remote Sensing, IEEE Transactions on*, vol. 27, 1989, pp. 290-301.

[14] S. Durden, J. Klein, and H. Zebker, "Polarimetric radar measurements of a forested area near Mt. Shasta," *Geoscience and Remote Sensing, IEEE Transactions on*, vol. 29, 1991, pp. 444-450.

[15] S.V. Nghiem, S.H. Yueh, R. Kwok, and F.K. Li, "Symmetry properties in polarimetric remote sensing," *Radio Science*, vol. 27, 1992, pp. 693-711.

[16] J. Lee, D. Schuler, T. Ainsworth, and W. Boerner, "Polarization orientation estimation and applications: a review," *IGARSS 2003. 2003 IEEE International Geoscience and Remote Sensing Symposium. Proceedings (IEEE Cat. No.03CH37477)*, Toulouse, France: , pp. 428-430.

[17] H. Kimura, "Radar Polarization Orientation Shifts in Built-Up Areas," *IEEE Geoscience and Remote Sensing Letters*, vol. 5, 2008, pp. 217-221.

[18] Yun Shao, Huaze Gong, Guojun Wang, and Aimin Cai, "Applications of polarimetric decomposition technology in a dried up lake evolution," *Geoscience and Remote Sensing Symposium (IGARSS), 2010 IEEE International*, 2010, pp. 4499-4502.

[19] Y. Yamaguchi, T. Moriyama, M. Ishido, and H. Yamada, "Four-component scattering model for polarimetric SAR image decomposition," *Geoscience and Remote Sensing, IEEE Transactions on*, vol. 43, 2005, pp. 1699-1706.

[20] Jong-Sen Lee, D. Schuler, and T. Ainsworth, "Polarimetric SAR data compensation for terrain azimuth slope variation," *Geoscience and Remote Sensing, IEEE Transactions on*, vol. 38, 2000, pp. 2153-2163.

[21] J. Lee, E. Krogager, D. Schuler, T. Ainsworth, and W. Boerner, "On the estimation of polarization orientation angles induced from azimuth slopes using polarimetric SAR data," *Geoscience and Remote Sensing Symposium, 2000. Proceedings. IGARSS 2000. IEEE 2000 International*, 2000, pp. 1310-1312 vol.3.

[22] I.H. Woodhouse, "Introduction to Microwave Remote Sensing," CRC press,Boca Raton, 2006.
[23] A. Andreou and Z. Kalayjian, "Polarization imaging: principles and integrated polarimeters," *Sensors Journal, IEEE*, vol. 2, 2002, pp. 566-576.
[24] R. Touzi, W. Boerner, J. Lee, and E. Lueneburg, "A review of polarimetry in the context of synthetic aperture radar: concepts and information extraction," *Canadian Journal of Remote Sensing*, vol. 30, 2004, pp. 380-407.
[25] C.Putignano,"PolSOM and TexSOM in Polarimetric SAR Classification," Ph.d thesis, Tor Vergata University, Rome, Italy, 2009.
[26] S. Quegan and I. Rhodes, "Statistical models for polarimetric data: consequences, testing and validity," *International Journal of Remote Sensing*, vol. 16, 1995, pp. 1183 - 1210.
[27] M.D.C.G. Sanpedro, "Optical And Radar Remote Sensing Applied To Agricultural Areas In Europe," Ph.d thesis, University of Valencia,Department of Earth Physics and Thermodynamics, 2008.
[28] T. Le Toan, A. Beaudoin, J. Riom, and D. Guyon, "Relating forest biomass to SAR data," *Geoscience and Remote Sensing, IEEE Transactions on*, vol. 30, 1992, pp. 403-411.
[29] S. Anfinsen, A. Doulgeris, and T. Eltoft, "Estimation of the Equivalent Number of Looks in Polarimetric SAR Imagery," *Geoscience and Remote Sensing Symposium, 2008. IGARSS 2008. IEEE International*, 2008, pp. IV - 487-IV - 490.
[30] W. Holm and R. Barnes, "On radar polarization mixed target state decomposition techniques," *Radar Conference, 1988., Proceedings of the 1988 IEEE National*, 1988, pp. 249-254.
[31] T. Zou, W. Yang, D. Dai, and H. Sun, "Polarimetric SAR Image Classification Using Multifeatures Combination and Extremely Randomized Clustering Forests," *EURASIP Journal on Advances in Signal Processing*, vol. 2010, 2010, pp. 1-10.
[32] L. Zhang, J. Zhang, B. Zou, and Y. Zhang, "Comparison of Methods for Target Detection and Applications Using Polarimetric SAR Image," *PIERS Online No. 1 2008 pp: 140-145*, vol. 4, 2008, pp. 140-145.
[33] M. Karam and A. Fung, "Radiative Transfer Theory For Active Remote Sensing Of A Forested Canopy," *Geoscience and Remote Sensing Symposium, 1989. IGARSS'89. 12th Canadian Symposium on Remote Sensing., 1989 International*, 1989, pp. 2493-2496.
[34] L. Tsang, J.A. Kong, K. Ding, and C.O. Ao, "Scattering of Electromagnetic Waves: Numerical Simulations, " New York: A Wiley-lnterscience Publication.John Wiley & Sons, Inc., 2001.
[35] L. Zuberbuhler and E. Meier, "The dependence of polarimetric decomposition parameters on biophysical forest parameters, frequency and methodology," *Geoscience and Remote Sensing Symposium, 2007. IGARSS 2007. IEEE International*, 2007, pp. 4148-4151.
[36] E. Krogager, "New decomposition of the radar target scattering matrix," *Electronics Letters*, vol. 26, 1990, pp. 1525-1527.
[37] E. Pottier, J. Lee, and L. Ferro-Famil, "PolSARpro_v4.2.0-Tutorial-Part1 RadarPolarimetry-4 Polarimetric Decompositions," 2007.
[38] R. Touzi, "Target Scattering Decomposition in Terms of Roll-Invariant Target Parameters," *Geoscience and Remote Sensing, IEEE Transactions on*, vol. 45, 2007, pp. 73-84.
[39] S. Cloude and E. Pottier, "An entropy based classification scheme for land applications of polarimetric SAR," *Geoscience and Remote Sensing, IEEE Transactions on*, vol. 35, 1997, pp. 68-78.
[40] Jong-Sen Lee, M. Grunes, E. Pottier, and L. Ferro-Famil, "Unsupervised terrain classification preserving polarimetric scattering characteristics," *Geoscience and Remote Sensing, IEEE Transactions on*, vol. 42, 2004, pp. 722-731.
[41] Yi-Cheng Lin and K. Sarabandi, "A Monte Carlo coherent scattering model for forest canopies using fractal-generated trees," *Geoscience and Remote Sensing, IEEE Transactions on*, vol. 37, 1999, pp. 440-451.
[42] Pan Liang, M. Moghaddam, and L. Pierce, "Backscattering simulation for nonuniform forest canopies using multilayer MIMICS," *Geoscience and Remote Sensing Symposium, 2004. IGARSS '04. Proceedings. 2004 IEEE International*, 2004, pp. 1021-1024 vol.2.
[43] M. Moghaddam and S. Saatchi, "Analysis of scattering mechanisms in SAR imagery over boreal forest: results from BOREAS '93," *Geoscience and Remote Sensing, IEEE Transactions on*, vol. 33, 1995, pp. 1290-1296.
[44] M. Karam, A. Fung, R. Lang, and N. Chauhan, "A microwave scattering model for layered vegetation," *Geoscience and Remote Sensing, IEEE Transactions on*, vol. 30, 1992, pp. 767-784.

[45] M. Dobson, F. Ulaby, T. LeToan, A. Beaudoin, E. Kasischke, and N. Christensen, "Dependence of radar backscatter on coniferous forest biomass," *Geoscience and Remote Sensing, IEEE Transactions on*, vol. 30, 1992, pp. 412-415.
[46] Yun Shao, Huaze Gong, Chou Xie, and Aimin Cai, "Detection subsurface hyper-saline soil in Lop Nur using full-polarimetric SAR data," *Geoscience and Remote Sensing Symposium,2009 IEEE International,IGARSS 2009*, 2009, pp. III-550-III-553.
[47] Huaze Gong, Yun Shao, Aimin Cai, and Chou Xie, "Subsurface microwave remote sensing and scattering modelling on hyper-saline soil: Example of Lop Nur," *Geoscience and Remote Sensing Symposium,2009 IEEE International,IGARSS 2009*, 2009, pp. III-546-III-549.
[48] J. Toomay, "Principles of radar," New Delhi: Prentice-Hall of India Private limited, 2008.
[49] Y. Yamaguchi, Y. Yajima, and H. Yamada, "A four-component decomposition of POLSAR images based on the coherency matrix," *Geoscience and Remote Sensing Letters, IEEE*, vol. 3, 2006, pp. 292-296.
[50] S. Anfinsen, A. Doulgeris, and T. Eltoft, "Estimation of the Equivalent Number of Looks in Polarimetric Synthetic Aperture Radar Imagery," *Geoscience and Remote Sensing, IEEE Transactions on*, vol. 47, 2009, pp. 3795-3809.
[51] C. Oliver and S. Quegan, "Understanding Synthetic Aperture Radar Images," Raleigh, NC 27613, US: SciTech Publishing, 2004.
[52] Jong-Sen Lee, D. Schuler, T. Ainsworth, E. Krogager, D. Kasilingam, and W. Boerner, "On the estimation of radar polarization orientation shifts induced by terrain slopes," *Geoscience and Remote Sensing, IEEE Transactions on*, vol. 40, 2002, pp. 30-41.
[53] D. Schuler, Jong-Sen Lee, and G. De Grandi, "Measurement of topography using polarimetric SAR images," *Geoscience and Remote Sensing, IEEE Transactions on*, vol. 34, 1996, pp. 1266-1277.
[54] D. Schuler, J. Lee, and G. De Grandi, "Topographic measurements using polarimetric SAR data," *IGARSS '96. 1996 International Geoscience and Remote Sensing Symposium*, Lincoln, NE, USA: , pp. 2086-2088.
[55] D.L. Schuler, J. Lee, and T.L. Ainsworth, "Compensation of Terrain Azimuthal Slope Effects in Geophysical Parameter Studies Using Polarimetric SAR Data," *Remote Sensing of Environment*, vol. 69, Aug. 1999, pp. 139-155.
[56] D. Schuler, Jong-Sen Lee, T. Ainsworth, and W. Boerner, "Correction for terrain azimuthal slope effects in polarimetric SAR images," *Geoscience and Remote Sensing Symposium, 2000. Proceedings. IGARSS 2000. IEEE 2000 International*, 2000, pp. 1304-1306 vol.3.
[57] Feng Xu and Ya-Qiu Jin, "Deorientation theory of polarimetric scattering targets and application to terrain surface classification," *Geoscience and Remote Sensing, IEEE Transactions on*, vol. 43, 2005, pp. 2351-2364.
[58] H. Kimura, "Calibration of Spaceborne Polarimetric SAR Data using Polarization Orientation," *Geoscience and Remote Sensing Symposium, 2006. IGARSS 2006. IEEE International Conference on*, 2006, pp. 344-347.
[59] T. Ainsworth, L. Ferro-Famil, and Jong-Sen Lee, "Orientation angle preserving a posteriori polarimetric SAR calibration," *IEEE Transactions on Geoscience and Remote Sensing*, vol. 44, 2006, pp. 994-1003.
[60] M. Molinier, J. Laaksonen, Y. Rauste, and T. Hame, "Detecting changes in polarimetric SAR data with content-based image retrieval," *Geoscience and Remote Sensing Symposium, 2007. IGARSS 2007. IEEE International*, 2007, pp. 2390-2393.
[61] S. Quegan, T.L. Toan, H. Skriver, J. Gomez-Dans, M.C. Gonzalez- Sampedro, and D.H. Hoekman, "Crop Classification with Multitemporal Polarimetric SAR Data," *in Workshop on POLinSAR - Applications of SAR Polarimetry and Polarimetric Interferometry (ESA SP-529)*, Jan. 2003.
[62] S. Cloude, K.P. Papathanassiou, and E. Pottier, "Radar Polarimetry and Polarimetric Interferometry," *IEICE Transactions on Electronics*, vol. E84-C, 2001, pp. 1814-1822.
[63] R. Touzi, A. Lopes, J. Bruniquel, and P. Vachon, "Coherence estimation for SAR imagery," *Geoscience and Remote Sensing, IEEE Transactions on*, vol. 37, 1999, pp. 135-149.

Appendix A
List of Acronyms

PolSAR	Polarimetric Synthetic Aperture Radar
[C]	Covariance matrix
[T]	Coherency matrix
ALOS	Advanced Land Observing Satellite
db	decibel
DEM	Digital Elevation Model
HH	Horizontal Horizontal (Polarization)
HV	Horizontal Vertical (Polarization)
MLC	Multi Look Complex
OA	Orientation Angle
PALSAR	Phased Array L-band Synthetic Aperture Radar
radar	Radio detection and ranging
SLC	Single Look Complex
SNR	Signal to Noise ratio
VV	Vertical Vertical (Polarization)